The Dissertation Committee for Fei Yan Certifies that this is the approved version of the following dissertation:

PAH Degradation and Redox Control in an Electrode Enhanced Sediment Cap

Committee:

Danny Reible, Supervisor

Philip Bennett

Randall Charbeneau

Robert Gilbert

Howard Liljestrand

PAH Degradation and Redox Control in an Electrode Enhanced Sediment Cap

by

Fei Yan, B.E.;M.E.;M.E.

Dissertation

Presented to the Faculty of the Graduate School of

The University of Texas at Austin

in Partial Fulfillment

of the Requirements

for the Degree of

Doctor of Philosophy

The University of Texas at Austin

August 2012

Dedication

To all who love me.

Acknowledgements

First and foremost, I would like to express my sincere gratitude to my PhD advisor, Dr. Danny Reible, for his guidance, advice, encouragement and support throughout my PhD study. His creative ideas, broad and in-depth knowledge have inspired me and broadened my vision; his encouragement and support have been invaluable to me as I pursue my PhD. It has been an incredible journey learning from and working with him.

Moreover, I would like to thank the members of my committee: Dr. Philip Bennett, Dr. Randall Charbeneau, Dr. Robert Gilbert, and Dr. Howard Liljestrand for their support, guidance, and suggestions. I would also like to give my thanks to Dr. Mary Jo Kirisits for her valuable advice on biodegradation and microbiology. I am always grateful for her kindness, encouragement and willingness to help. I would like to thank Dr. Kerry Kinney, Dr. Lynn Katz, Dr. Desmond Lawler, Dr. David Maidment, Dr. Jeremy Meyers, and Dr. Allen Bard for their help at various stages of my PhD study. Also, thanks to Dr. Gregory Lowry and Dr. Kelvin Gregory at Carnegie Mellon University, and Dr. Joseph Hughes at Drexel University and Georgia Institute of Technology for our collaboration and discussions.

I would like to acknowledge everyone who graciously provided their expertise, time, and resources to my doctoral research including Dr. Xiaoxia Lu (general laboratory procedures, passive sampling, HPLC trouble shooting, etc.), Charles Perego and Chia-Chen Chen (technical supports), Tony Smith (biodegradation and microbiology), Yongseok Hong (pH and redox behaviors), Dave Lampert (passive sampling and model development), Nate Johnson (electrochemical application), Sungwoo Bae, Andy

Hoisington, Weiwei Wu and Liming Luo (microbiology), Wei Shi and Ling Huang (aquatic chemistry), Joaquin Rodriguez Lopez and Mei Shen (electrochemistry), Mei Sun and Ruiling Zhang (collaboration on electrochemical application), Wu Chen and Gabe Trejo (laboratory supports), Yachao Qi (analytical method), and every member in Dr. Reible's group.

Last but not the least, I would like to thank my parents, brother, sister-in-law for their love and support; I would also like to express my gratitude to my girlfriend, Yiyi Chu, for her love, support, patience and understanding.

PAH Degradation and Redox Control in an Electrode Enhanced Sediment Cap

Fei Yan, Ph.D

The University of Texas at Austin, 2012

Supervisor: Danny Reible

Capping is typically used to control contaminant release from the underlying sediments. However, the presence of conventional caps often eliminates or slows natural degradation that might otherwise occur at the surface sediment. This is primarily due to the development of reducing conditions within the sediment that discourage hydrocarbon degradation. The objective of this study was to develop a novel active capping method, an electrode enhanced cap, to manipulate the redox potential to produce conditions more favorable for hydrocarbon degradation and evaluate the approach for the remediation of PAH contaminated sediment.

A preliminary study of electrode enhanced biodegradation of PAH in sediment slurries showed that naphthalene and phenanthrene concentration decreased significantly within 4 days, and PAH degrading genes increased by almost 2 orders of magnitude.

In a sediment microcosm more representative of expected field conditions, graphite cloth was used to form an anode at the sediment-cap interface and a similar cathode was placed a few centimeters above within a thin sand layer. With the application of 2V voltage, ORP increased and pH dropped around the anode reflecting water electrolysis. Various cap amendments (buffers) were employed to moderate pH changes. Bicarbonate was found to be the most effective in laboratory experiments but a

slower dissolving buffer, e.g. siderite, may be more effective under field conditions. Phenanthrene concentration was found to decrease slowly with time in the vicinity of the anode. In the sediment at 0-1 cm below the anode, phenanthrene concentrations decreased to ~70% of initial concentration with no bicarbonate, and to ~50% with bicarbonate over ~70 days, whereas those in the control remained relatively constant. PAH degrading gene increased compared with control, providing microbial evidence of PAH biodegradation

A voltage-current relationship, which incorporated separation distance and the area of the electrodes, was established to predict current. A coupled reactive transport model was developed to simulate pH profiles and model results showed that pH is neutralized at the anode with upflowing groundwater seepage.

This study demonstrated that electrode enhanced capping can be used to control redox potential in a sediment cap, provide microbial electron acceptors, and stimulate PAH degradation.

Table of Contents

List of Tables

List of Figures

Chapter 1: Introduction

1.1 BACKGROUND

Contaminated sediment has become a major concern at many sites throughout the United States and the world. A variety of organic and inorganic contaminants such as chlorinated solvents, aromatic hydrocarbons and heavy metals have been found in contaminated sediment and pose a risk to ecology and human health. Therefore, an effective remediation method is needed for the management of contaminated sediment.

Generally, contaminated sediment can be treated by ex-situ or in-situ approaches. Ex-situ approaches are based on dredging and disposal of the contaminated sediment. Because of its high cost and limited effectiveness (Palermo et al., 1998; Reible et al., 2003), dredging is sometimes not applicable for the treatment of contaminated sediment.

An alternative for the management of contaminated sediment is in-situ capping - the placement of clean material (usually sand) on the sediment to isolate the contaminants into the overlying water (Palermo et al., 1998; Wang et al., 1991). In-situ capping can be a relatively cost-effective and noninvasive approach compared to dredging. However, capping doesn't necessary provide detoxification, and the risk to ecological and human health may recur if the contaminant can migrate through the caps. Furthermore, conventional capping usually drives the entire sediment anaerobic, hindering natural degradation processes for some contaminants. For example, reducing conditions that develop beneath the cap hinders the biodegradation of polycyclic aromatic hydrocarbons (PAHs).

The use of an active capping technology has been proposed to enhance contaminant degradation in capping layers. Unlike conventional capping, active caps can facilitate transformations that can detoxify migrating contaminants. The primary

difficulty in active capping is maintaining conditions conducive to transformations, e.g. redox conditions, sufficient nutrient or electron donor levels.

Electrochemical remediation is among the processes being investigated for their potential application in soil and sediment remediation. Laboratory experiments and limited field work (Renaud and Probstein, 1987; Shapiro et al., 1989; Hamed et al., 1991; Shapiro and Probstein, 1993; Acar and Alshawabkeh, 1993; Hicks and Tondorf, 1994; Acar at al., 1995; Lageman, 1993; Gent et al., 2009) have shown the effectiveness of this novel approach. In most of these reported cases, decontamination of organic contaminant was achieved by direct electrochemical oxidation and/or reduction. Some other successful electro-remediation includes sequestration of heavy metals at the electrode and collection of contaminants by electrokinetic process for further treatment. However, almost all these processes are not cost-effective due to the requirement of high voltage input, and they do not utilize the biodegradation potential of indigenous microorganisms in soil/sediment.

In this study, electrode enhanced capping is proposed and investigated for the bioremediation of contaminated sediment. In contrast to other electrode based remediation technologies, this approach uses low power, and integrates biodegradation into electrochemical process. The application of the electrodes is designed to modify redox conditions in a thin layer in the immediate vicinity of the electrode to encourage biodegradation of contaminants migrating through the cap (as opposed to trying to control redox conditions in the entire contaminated sediment layer). This hybrid remediation technology could provide an inexpensive and effective means for the management of contaminated sediment.

In this study, PAHs were selected as typical contaminants for remediation because of their occurrence in sediment and toxicity to ecology. Furthermore, natural attenuation

processes of PAHs are hindered under conventional caps. The electrode enhanced capping technology will overcome the limitation of conventional caps for remediation of PAH contaminated sediments.

The proposed biodegradation of PAHs by electrode enhanced caps is shown in Figure 1.1. Two graphite electrodes are placed perpendicular to contaminant transport in the cap and polarized at low potential. By water electrolysis, oxygen is produced at the anode, making the local sediment environment more oxidizing. Consequently, these redox conditions changes and/or produced oxygen are expected to stimulate the activity of PAH degrading microbes, and accelerate contaminant biodegradation.

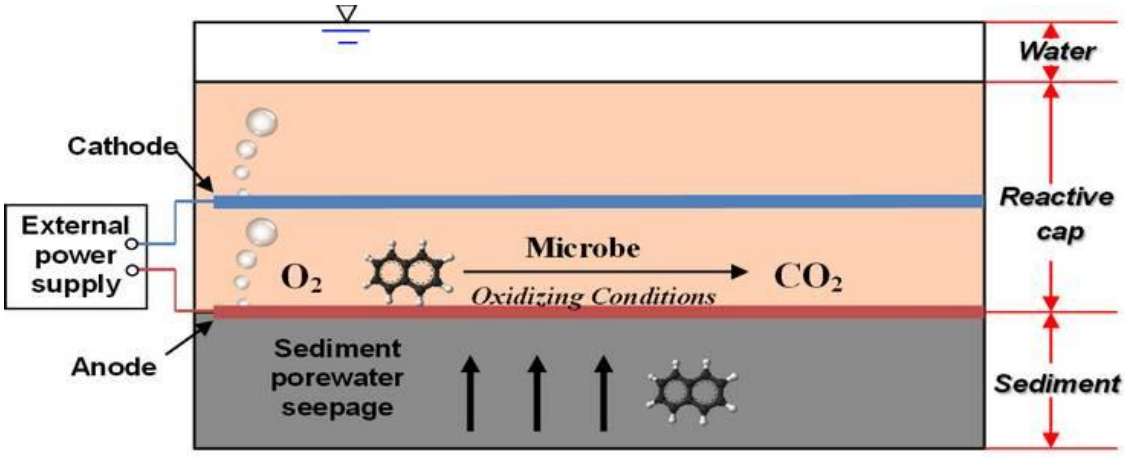

Figure 1.1 Conceptual model for an electrode enhanced cap for PAH remediation

1.2 RESEARCH OBJECTIVES AND DISSERTATION OUTLINE

The research objective of this study is to demonstrate the feasibility of electrode enhanced caps for the remediation of PAH contaminated sediment. To achieve the stated goal, two types of laboratory scale experiments were conducted. The potential for this approach was first assessed in slurry reactors under idealized conditions to demonstrate effective enhancement of biodegradation. When success was confirmed in slurry phase,

the hybrid technology was then extended to microcosms to simulate capping under a more realistic field-like condition. A mathematical model was also developed to describe the complex physical and chemical processes for electrode enhanced capping. Based on these specific research objectives, this dissertation is divided into the following chapters:

1) Literature review on PAH contamination and degradation, electrochemical remediation of soil and sediment and remediation of contaminated sediments (Chapter 2).

2) Electrode enhanced biodegradation of PAH in sediment slurry. This proof of concept experiment examined the feasibility of electrode enhanced biodegradation of PAH in slurry phase. In a slurry reactor, mass transfer resistances can be overcome and conditions conducive to the biological processes can be maintained (Chapter 3).

3) Electro-biodegradation of PAH and redox control in sediment/cap microcosms. Laboratory scale reactors were used to simulate field conditions for the application of electrode enhanced caps. The potential to accelerate biodegradation was evaluated in simulated sediment and cap environments with electrodes, and redox conditions were characterized (Chapter 4).

4) Model of electrode enhanced capping. A voltage-current relationship was developed and a coupled reactive transport model was presented to describe the processes involved in electrode enhanced capping (Chapter 5).

5) Conclusions and recommendations for future work (Chapter 6).

Chapter 2: Literature Review

2.1 PAH CONTAMINATION AND DEGRADATION

2.1.1 PAH contamination

Polycyclic aromatic hydrocarbons (PAHs) are chemical compounds that consist of fused aromatic rings and do not contain heteroatoms or carry substituents. In addition to their presence in fossil fuels, PAHs are formed by incomplete combustion of organic materials such as wood, coal, diesel, fat, or tobacco (Page et al., 1999). They may come from such natural sources as forest fires and volcanic eruptions or from variety of other anthropogenic sources including fuel combustion, pyrolytic processes, spillage of petroleum products, waste incinerators and domestic heaters (Juhasz and Naidu, 2000). Some PAHs (e.g. naphthalene and phenanthrene) have been used for the synthesis of organic compounds in pesticides, fungicides, mothballs, etc. (Shennan, 1984).

Many PAHs may pose a health risk to ecology and humans because of their toxic, mutagenic and carcinogenic properties (Goldman et al., 2001; Mastrangelo et al., 1996). The structure of many PAHs makes them highly lipid soluble and thus they can be easily absorbed by the lungs, gut, and skin of mammals. Therefore, many PAHs are considered to be environmental pollutants that can have a detrimental effect on the flora and fauna of affected habitats, resulting in the uptake and accumulation of toxic chemicals in food chains. Consequently, the US Environmental Protection Agency (US EPA) listed 16 PAHs as priority pollutants, and determined that benz[a]anthracene, benzo[a]pyrene, benzo[b]fluoranthene, benzo[k]fluoranthene, chrysene, dibenz[a,h]anthracene, and indeno[1,2,3-c,d]pyrene are probable human carcinogens.

PAHs can be classified into two groups: low molecular weight PAHs (2-3 rings) and high molecular weight PAHs (4 or more rings). Low molecular weight PAHs (2-3

rings) are more soluble and reactive in environment. As molecular weight and ring number increase, aqueous solubility decreases but hydrophobicity, lipophilicity and environmental persistence increase. The genotoxicity also increases as the number of rings increase up to 4 or 5. In addition, volatility decreases with an increasing number of fused rings (Wilson and Jones, 1993).

The release of PAHs into the environment is widespread and PAHs have been detected in a wide variety of environmental samples including air, soil, sediments, water, oils, tars and food (Juhasz and Naidu, 2000). PAH contamination is frequently associated with industrial activities such as processing, combustion and disposal of fuel/oil products (Wilson and Jones, 1993). PAHs are found at many Superfund sites, and other petroleum-impacted sites (Johnston et al., 1993; Menzie et al., 1992). Because creosote, a compound containing 85% PAHs by weight, was commonly used in the wood-preserving industry, PAHs are frequently detected in wood treatment areas (Mueller et al., 1989). Significant levels of PAHs have been reported in sediments from many industrialized areas throughout the world.

Due to their hydrophobicity and low solubility, PAHs concentrations in water are very low. However, PAHs tend to accumulate in soil and sediment, especially those with high organic carbon fraction. So in aquatic environment, most PAH contamination is concentrated in sediment, which is considered as a reservoir for PAH accumulation.

2.1.2 PAH degradation

Microbial research in the past several decades has demonstrated that a wide variety of bacteria, fungi and algae have the ability to metabolize PAHs. A large number of microorganisms that can degrade PAH have been isolated from soil, sediment, sewage, and water and characterized (Cerniglia, 1992). Generally, the rate of PAH degradation is

inversely proportional to the number of rings. It is believed that 2-ring and 3-ring PAHs are readily biodegradable given optimal environmental conditions, while PAHs with more than three rings are more resistant to biodegradation.

The microbial degradation of low molecular PAHs such as naphthalene, phenanthrene, anthracene and acenaphthene has been well elucidated, and the pathways, enzymes and genetics have all been reported (Cerniglia, 1992; Davies and Evans, 1964; Gibson and Subramanian, 1984). However, less is known about the degradation of high molecular PAHs (Kanaly and Harayama, 2000). Of the four-ring PAHs, biodegradation of fluoranthene, pyrene, chyrsenene and benz[a]anthracene has been investigated to various degrees (Kanaly and Harayama, 2000; Juhasz et al., 2000). In general, lower molecular PAHs tend to oxidize completely to form CO_2 and H_2O while the high molecular PAHs will degrade partially to yield various oxygenated metabolites (e.g., various phenolic and acid metabolites, cis-dihydrodiol, etc.) (Kanaly and Harayama, 2000).

PAHs are more readily biodegradable under aerobic conditions than with any other terminal electron acceptor (TEA). Oxidation of aromatic ring is the principal mechanism involved during PAH biodegradation (Cerniglia, 1992). During the first step in the aerobic degradation of PAHs, dioxygenase incorporates oxygen atoms at two carbon atoms of a benzene ring of a PAH resulting in the formation of *cis*-dihydrodiol (Kanaly and Harayama, 2000). It undergoes rearomatization by dehydrogenases to form dihydroxylated intermediates. Subsequently dihydroxylated intermediates undergo ring cleavage and form tricarboxylic acid (TCA) cycle intermediates (Sabate et al., 1999).

PAH degradation in anaerobic conditions has also been reported but the rate is much slower compared to that in aerobic conditions (Chang et al.,2002; Rothermich et al.,2002; Rockne and Strand, 1998, 2001; Rockne et al., 2000; Johnson and Ghosh,

1998), and the details of metabolism pathways are very complicated and need further elucidation (Annweiler et al., 2002).

2.1.3 PAH degradation genes

The traditional culture-dependent methods have been used to enumerate PAH degrading bacterial population for years. However, only a small portion of microorganisms of interests can be cultivated under standard cultivation conditions (Amann et al., 1995). Cultivation-independent approaches have also been employed to quantifying PAH degrading microorganisms. Recent advances in molecular microbial technology have allowed for broader analysis of biodegradative organisms in the environment. Quantitative polymerase chain reaction (qPCR), using primers that target PAH ring-hydroxylating dioxygenase (PAH-RHD$_\alpha$) genes, has been used to estimate copy numbers of PAH degrading gene from environmental samples. The genes encoding PAH degradation include *nah*-like genes from *psedudomas* species (Lloyd Jones et al.,1999; Wilson et al.,1999), *phn*-like genes from *Burkholderia* species (Laurie and Lloyd Jones, 1999), *nag*-like genes from *Ralstonia* (Widada et al.,2002), *ndo*-like genes (Gomes et al., 2007), *nid*-like genes (Brezna et al.,2003), *pdo*-like genes (Johnsen et al.,2006), etc. Since genes coding for ring-hydroxylating dioxygenases are highly diverse, primers to amplify a wide range of PAH-RHD$_\alpha$ genes were developed and employed to target majority of PAH degrading genes (Ding et al., 2010; Cebron et al., 2008). All these primers can be employed in the study of PAH degrading genes by conventional polymerase chain reaction (PCR) or quantitative PCR (qPCR). qPCR have been proven to be a powerful tool to determine relative activity of PAH degrading genes. The gene abundance revealed by qPCR results can potentially be used as an indicator for PAH biodegradation.

2.2 ELECTROCHEMICAL REMEDIATION FOR SOIL AND SEDIMENT

Electrochemical remediation technology is an innovative method for in-situ remediation for contaminated soil and sediment. Contaminants that could be treated by this method include inorganic compounds, organic compounds and radionuclides (Acar et al., 1995; Reddy et al., 1997). It can be performed for different soil types and is particularly effective for fine-grained soils of low hydraulic conductivity, which are difficult by other methods.

A typical field electrochemical remediation system is shown in Figure 2.1 (Saichek and Reddy, 2005). Electrodes are inserted at different locations at the contaminated site and a voltage is applied across the electrodes. Several processes occur during the application of electric field at contaminated sites to facilitate the removal of contaminants. These processes will be discussed in more details in the following section.

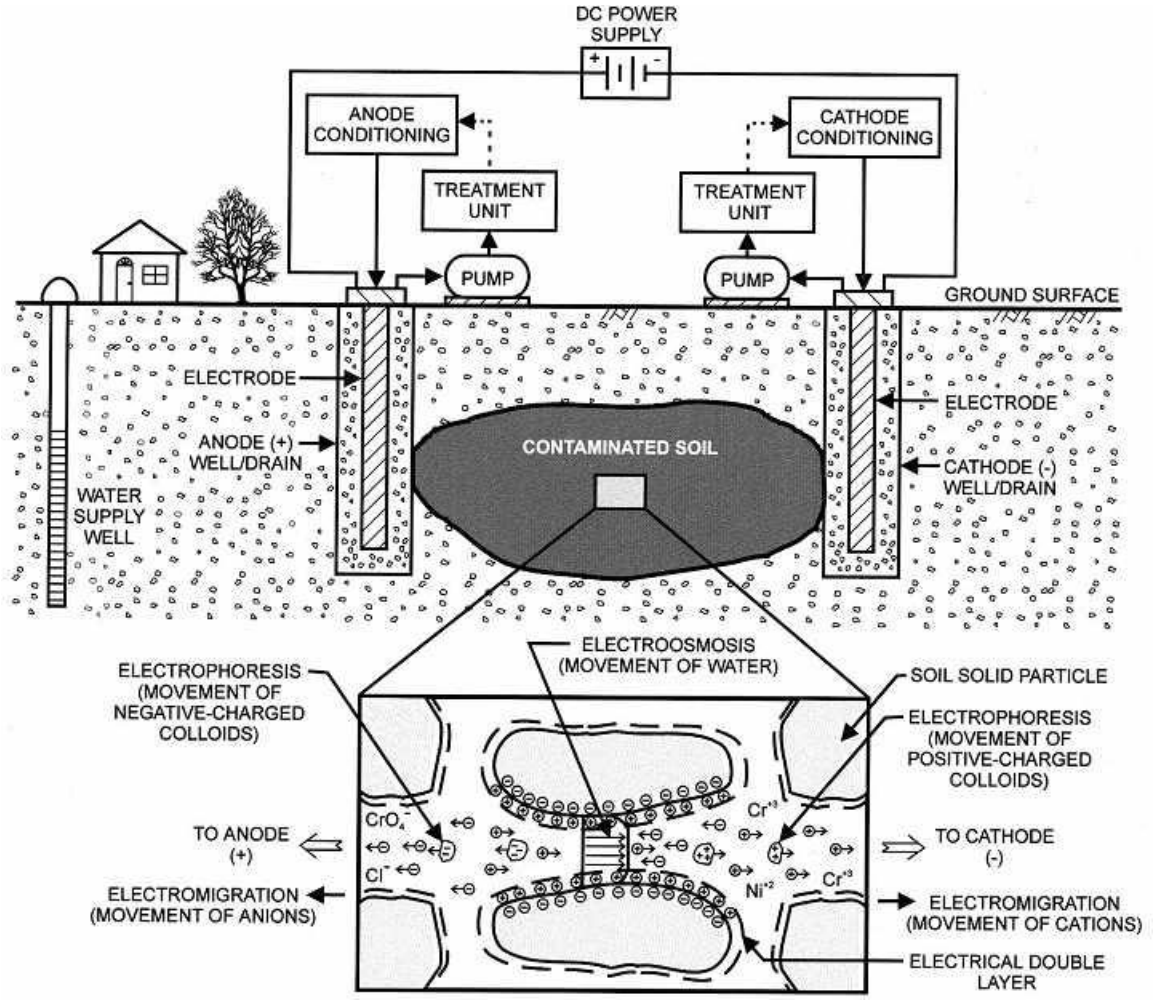

Figure 2.1 Schematic of electrochemical remediation of contaminated soil

2.2.1 Electrokinetic phenomena

Electrokinetics is defined as the physicochemical transport of charge, action of charged particles, and effects of applied electric potentials on formation and fluid transport in porous media. The presence of the diffuse double layer gives rise to several electrokinetic phenomena in soil, which may result from either the movement of different phases with respect to each other including transport of charge, or the movement of different phases relative to each other due to the application of an electric field (Acar and Alshawabkeh, 1993). The electrokinetic phenomena include electroosmosis,

electrophoresis, electromigration, streaming potential, sedimentation potential, etc. (Probstein and Hicks, 1993; Reddy et al., 1997). Electroosmosis is the fluid movement with respect to solid wall under the influence of an applied electric field. Electrophoresis is the motion of particles under influence of electric field. Electromigration refers to the migration of ionic species under an applied potential. Streaming potential, being the reverse of electroosmosis, is the generation of electric potential by fluid moving through porous medium. Sedimentation potential, similar to streaming potential, is an electric field generated by sedimenting colloid particles. Other transport processes, such as advection, dispersion and diffusion, sometimes play important roles in electrokinetic processes.

2.2.2 Water electrolysis

Water electrolysis can occur at the electrodes during the application of electrochemical remediation. The standard potential of a water electrolysis cell is 1.23 V at 25 °C based on the Nernst Equation. If the applied potential is large enough to overcome activation barriers, water electrolysis is usually the primary reaction at the electrodes. Protons and oxygen are produced at the anode, and hydroxyl anions and hydrogen gas are produced at the cathode.

$$\text{Anode: } 2H_2O = O_2 + 4H^+ + 4e \qquad E^0 = 1.229V \qquad (2\text{-}1)$$

$$\text{Cathode: } 2H_2O + 2e = H_2 + 2OH^- \qquad E^0 = -0.827V \qquad (2\text{-}2)$$

Other electrochemical reactions may occur depending on the concentration of species, their electrochemical potentials, and the reaction kinetics. For example, ferric iron may be reduced to ferrous iron at the cathode and chloride may be oxidized to chlorine at the anode.

Anode: $Fe^{3+} + e = Fe^{2+}$ $E^0 = 0.771V$ (2-3)

Cathode: $2Cl^- = Cl_2 + 2e$ $E^0 = 1.3583V$ (2-4)

These secondary reactions usually are not favored at the anode and/or cathode because of the low concentrations of reactants in environmental systems. So water electrolysis is most often the dominant electrolytic reaction. As a result of water electrolysis, oxidizing and acidic zone is developed at the anode, and reducing alkaline zone is developed at the cathode.

2.2.3 Electrochemical oxidation/reduction

During electrochemical remediation, organic contaminants may be destroyed or converted by either direct or indirect processes. Numerous studies have focused on the use of direct current (DC) to oxidize or reduce organic contaminants directly (Alshawabkeh et al., 2005; Goel et al., 2003; Petersen et al., 2007). A few studies explored the use of alternating current (AC) to degrade organic contaminants (Chin and Cheng, 1985; Nakamura et al., 2005). Sequential electrolytic reduction-oxidation system was also developed to degrade energetic compounds (Gilbert and Sale, 2005).

Indirect electrolysis also contributes to contaminants removal during electrochemical oxidation/reduction processes. During indirect anodic oxidation, strong oxidants such as ozone, hydrogen peroxide, chlorine, etc. are generated at the anode instead of oxygen. The contaminant is then oxidized by these strong oxidants (Goel et al. 2003).

2.2.4 Electrochemical stimulation of biodegradation

During biodegradation, microorganisms require an electron donor for reductive degradation or an electron acceptor for oxidation process. Generally, electron donors and

acceptors are applied as chemicals. Electron donors commonly used for in-situ remediation include hydrogen gas, zero valent iron and vegetable oil, and electron acceptors in bioremediation include oxygen, nitrate, iron (III), manganese (IV), and sulfate. A novel alternative is to supply electron donors and/or acceptors by direct application of electricity.

Electrolysis of water is the primary reaction during electrochemical remediation process. Hydrogen produced at the cathode can serve as an electron donor and be utilized by consortia of anaerobic bacteria for reductive degradation, such as dechlorination or denitrification (Sun et al., 2010; Thrash et al., 2007; Sakakibara and Nakayama, 2001). At the anode of the reaction of water electrolysis reaction, oxygen is generated and can serve as an electron acceptor. The produced oxygen has been proven to be effective in stimulating bacterial growth during nitrification (Watanabe et al., 2002).

Direct electron transfer from electrodes to a bacterial cell provides another means to stimulate microbial metabolism. *Geobacter* species and some other microorganisms were shown to be able to directly transfer electrons to electrodes (Lovley, 2008; Logan, 2009). Electrodes can serve as either an electron donor or acceptor directly. It was shown that graphite electrodes could serve as an electron acceptor for the degradation of toluene and benzene (Zhang et al., 2010). Another study has shown the evidence of graphite electrodes as an electron donor in anaerobic respiration (Gregory et al., 2004).

2.3 REMEDIATION OF CONTAMINATED SEDIMENTS

2.3.1 Contaminated sediments

Contaminated sediments are defined as aquatic sediments that contain chemical substances in excess of appropriate geochemical, toxicological, or sediment quality criteria, or are otherwise considered to pose a threat to human health or the environment

(US EPA, 1998). It has been estimated that approximately 10 percent of aquatic sediments underlying United States surface waters are sufficiently contaminated to pose potential risks to fish and to humans and wildlife that eat fish (US EPA, 1998).

Sediment is an environmental sink for many contaminants, since many pollutants originally introduced into the water column have affinities for sediment particles. The contaminants that introduced into the sediment are from various sources, including municipal sewage treatment plants, combined sewer overflows, storm water discharges, direct industrial discharges of process waste, runoff and leachate from hazardous and solid waste sites, agricultural operations, mining operations, industrial manufacturing and storage sites, atmospheric deposition and contaminated groundwater discharges to surface water (Baudo and Muntau, 1990). Contaminants detected in sediments include polychlorinated biphenyls (PCBs), heavy metals, chlorinated solvents, pesticides, PAHs, etc. Sediments can serve as contaminant sources for transport and exposure to aquatic biota particularly with bioaccumulative contaminants. Hydrophobic organic contaminants such as PAHs and PCBs typically bind strongly to organic matter in sediments and these sediment-bound pollutants serve as long-term exposure sources to aquatic ecosystems. For instance, fish and bottom-dwelling organisms can accumulate toxic compounds like PCBs that are passed up the food chain.

PAHs have been found to be a key contaminant at many contaminated sediment sites (Reible et al., 2007; Perelo, 2010; Baumard et al., 1998). Because they can be adsorbed strongly to organic matters in sediment, PAHs have been found to be particularly persistent in sediments. Since PAHs have been reduced in many wastewater effluents, the accumulated PAHs in the sediments will release slowly into water column as a long-term source and pose potential threat to water quality and aquatic ecosystem via bioaccumulation in food chains.

Despite the persistence of PAHs in sediments, it does not imply that PAHs may reside in the bottom sediments indefinitely. Microbial degradation of PAHs is one of the main processes to remove these contaminants from bottom sediments and the water column. Both aerobic and anaerobic degradation of PAHs occurs in aquatic sediments naturally, but anaerobic degradation occurs at a much slower rate than aerobic degradation. Sediments are generally anaerobic except in the upper layer adjacent to water, ranging from millimeters to centimeters. Therefore biodegradation of PAHs is greatly hindered by oxygen shortage in sediments.

2.3.2 Sediment remediation methods

Current remediation approaches to addressing contaminated sediments include monitored natural attenuation (MNA), dredging and excavation, and capping techniques.

2.3.2.1 Monitored natural attenuation

Monitored natural attenuation (MNA) is a technique used to monitor or test the progress of natural attenuation processes that can degrade contaminants in sediments (US EPA, 2005). It may be used with other remediation processes as a finishing option or as the only remediation process if the rate of contaminant degradation is fast enough to protect human health and the environment. Not all natural processes result in risk reduction; some may increase or shift risk to other locations or receptors. Therefore, to implement MNA successfully as a remedial option, those processes that contribute to risk reduction should be identified and evaluated. Appropriate monitoring are required to ensure acceptable risk management, and these monitoring methods include contaminant analyses and ecological and health effects assays.

The most common natural attenuation processes occurring in sediments are intrinsic biodegradation of the contaminants and the chemical transformation of the

contaminant to a less toxic form. Other important natural attenuation processes, from most to least preferable, include (1) sorption or other binding processes to the sediment matrix to reduce contaminant mobility and bioavailability; (2) a decrease in contaminant concentration levels in near-surface sediment zone through burial or mixing-in-place with cleaner sediment; (3) a decrease in contaminant concentration levels in the near-surface sediment zone through dispersion of particle-bound contaminants or diffusive or advective transport of contaminants to the water column. Exposure levels are reduced by the decrease of contaminant levels through the last two natural attenuation processes.

The two primary advantages of MNA are its relatively low cost and its non-invasive nature. The implementation cost includes monitoring, site characterization and modeling, among which monitoring is the major cost in most cases. MNA typically has no physical disruption to the current ecological conditions, which may be an important advantage for sensitive environments. One major limitation of MNA is that it leaves contaminants in place so that the risk of exposure remains. Another disadvantage of MNA is that the rate of reducing risk is relatively slow compared to active remediation technologies. MNA is widely considered to be the most effective remediation technique at those sites with a low exposure risk to ecology and/or human, otherwise active methods are required to reduce the risks posed by contaminated sediments.

2.3.2.2 Dredging and excavation

A more effective approach than MNA is preferred for contaminated sediments with a higher risk to natural environment and human. The most common method of remediating contaminated sediment to reduce risk is removal by dredging or excavation. Dredging is the removal of submerged material, while excavation refers to the sediment of which water has been diverted or drained. The processes involved in dredging of

contaminated sediments include sediment removal, transport, staging, treatment, and disposal.

If cleanup goals are achieved by dredging or excavation, it minimizes the uncertainty about long-term effectiveness by removal of contaminated sediments from the aquatic environment. Furthermore, removal of contaminated sediment requires less time to achieve remedial action objectives, and it has greater flexibility for future water body use. Because of these advantages, dredging or excavation has been used for remediation of contaminated sediment at more than 100 Superfund sites (US EPA, 2005).

The limitations of dredging or excavation compared to MNA or in-situ capping include complexity and high cost considering the dredging itself and the processes of transport, staging, treatment and disposal of the dredged sediment. Furthermore, contaminant release from resuspension, and the potential risk of residual contamination following dredging/excavation give rise to uncertainties associated with dredging/excavation (Hong et al., 2011). Finally, the aquatic community and habitat within the remediation area is at least temporally destroyed with the long term effect being unknown. As a result of these limitations, Perelo (2010) examined the effectiveness of dredging and found that half of the 20 sites studied didn't achieve remedial goals by dredging.

2.3.2.3 In-situ capping

In-situ capping is the placement of a covering or cap made of clean isolating material over contaminated sediment, which remains in place. Capping materials include clean sediment, sand, gravel, geotextiles, liners, and other permeable or impermeable materials or the combination of above elements. In-situ capping can reduce the risk of contaminated sediment by physical isolation of sediment to reduce direct exposure,

stabilization of sediment to reduce resuspension and transport to other sites, and/or chemical isolation of sediment to reduce exposure from dissolved and colloidally bound contaminants transported into the water column (US EPA, 2005).

In-situ capping can quickly reduce the exposure risk, and it requires less capital cost and material handling. Also it reduced the risks of resuspension, dispersion and volatilization of contaminants in comparison to dredging. The cap may be less disruptive of local ecological communities, and provide clean substrate for recolonization by bottom-dwelling organisms. In comparison to MNA, capping is considered to be a more aggressive and effective approach.

Laboratory and field studies of capping have shown that even a simple sand cap can reduce the risks of contaminants from contaminated sediments. Thibodeaux and Bosworth (1990) used clean material as a capping layer to retard diffusion and reduce the flux from PCB-contaminated sediments. Wang et al. (1991) and Thoma et al. (1993) measured and modeled diffusion flux of some organic compounds from capped sediments and evaluated its migration through clean sediment. Lampert et al. (2011) demonstrated the effectiveness of thin-layer sand caps to reduce the bioaccumulation of PAHs provided the thickness of the cap layer exceeds the depth of organism interaction with the sediments, and contaminant migration is controlled by molecular diffusion.

Because contaminants remain in the aquatic environment, contaminants could become exposed or be dispersed if the cap is significantly disturbed or if contaminants move through the cap by diffusion or advection. Gidley et al. (2012) showed rapid breakthrough of lower molecular weight PAHs with groundwater seepage in coarse sand capping material.

To overcome the limitation that contaminants remain untreated with conventional sand capping, an alternative - active capping has been proposed. Active capping can be

broadly defined as capping with materials that encourage degradation or enhance sequestration of the contaminants. A variety of materials has been proposed and used for sequestration of the different contaminants. Apatite, a matrix of calcium phosphate and various other common anions, has been investigated for sequestration of metals in sediments (Reible et al., 2007; Kaplan and Knox, 2004). Zeolite was also evaluated for containment of metals as active barrier system (Jacobs and Forstner, 1999). Organoclay, a modified bentonite prepared by introducing organic molecules into the clay mineral structure, has been tested for control of non-aqueous phase liquids and other hydrophobic organic contaminants (Reible et al., 2005; Knox et al., 2012). Organic sorbents such as activated carbon, coke and biopolymer showed the ability to sequester hydrophobic organic contaminants (Zimmerman et al., 2004; Murphy et al., 2006; Knox et al., 2012). The effectiveness of a cap was greatly improved by adding an organic sorbent layer such as activated carbon, or by mixing sorbent directly with contaminated sediment. Commercially available active capping materials include AquaBlok™ (Adventus Americas, Inc., Toledo, OH), which is a bentonite clay material formed around a granular core, and organoclay materials, reactive core mat, liners, etc. from CETCO.

Being similar to conventional capping, the sequestration approach does not degrade contaminants; it only physically sequesters them. Slight changes in the capping environment can cause the erosion of the capping layer and resuspension of the sequestered contaminants at high concentration. Also, surface fouling of the sorptive materials may occur and lead to lower treatment efficiencies (Reible et al., 2007). So the sequestration approach may not be appropriate for all the contaminated sites. These limitations have stimulated the idea of an active capping in which contaminants are transformed to nontoxic products by chemical, biological and/or combined processes. Research on the application of active capping to enhance contaminant degradation has

not been addressed adequately and has very few successful cases. Choi et al. (2009) developed a "reactive" cap/barrier system composited of granular activated carbon impregnated with reactive iron/palladium (Fe/Pd) bimetallic nanoparticles (reactive activated carbon) for PCB-contaminated sediments. 2-chlorobiphenyl was chemically degraded via a combined process of adsorption and dechlorination with the reactive cap. Sun et al. (2010) proposed an integrated Fe(0)–sorbent–microorganism remediation system as an in-situ active capping technique to remediate nitrobenzene-contaminated sediment. In the integrated capping system, Fe(0) acted to reduce nitrobenzene to aniline, cinder served as the sorbent and support matrix, and nitrobenzene was biodegraded to aniline by microorganisms. Himmelheber et al. (2011) demonstrated that a laboratory-scale bioreactive in-situ sediment cap could completely dechlorinate dissolved-phase PCE for the treatment of PCE with the amendment of a mixed, anaerobic dechlorinating consortium and soluble electron donor. Now there is a pressing need to develop new cost-effective active capping technologies over the long time scales for in-situ sediment remediation.

2.4 RESEARCH NEEDS: ACTIVE CAPPING COUPLING ELECTROCHEMICAL PROCESSES WITH BIOREMEDIATION

During recent years, electrochemical technologies have been proposed for the remediation of soil and sediment. Numerous studies have demonstrated the effectiveness of electrokinetic remediation in the removal of soil contaminants. However, for hydrophobic organic compounds (HOCs) with a high tendency to be adsorbed onto soil and sediment, electrokinetic remediation was not applicable because of their low concentration in mobile phase. PAHs, a representative subset of HOCs, fall into this group. Bioremediation is a reasonable alternative to treat soil and sediment polluted by PAHs but the terminal electron acceptor in sediments even a few centimeters below the

sediment-water interface is typically iron or sulfate reflecting highly reduced conditions that are not conducive to PAH degradation. Successful implementation of in-situ bioremediation sometimes requires the presence or injection of electron acceptors into the porous medium. A technology for a continuous introduction of electron acceptors has been the principle bottleneck in the successful treatment for PAH contaminated soil and sediment. Application of an electric current may be an alternative option for providing more favorable electron acceptors. An electrode-based active capping has the potential as a continuous pollutant remediation method for PAH contaminated sediments. Research on active capping coupling electrochemical processes with bioremediation is needed for the management of PAH contamination.

Although both electrochemical remediation and bioremediation have been documented intensively for treatment of contaminated soil and sediment, the integration of electrochemical processes and bioremediation has not been addressed adequately. The proposed study will focus on coupling electrochemical processes with bioremediation within an active cap for PAH contaminated sediment. This novel technology will fill the gap between electrochemical processes and bioremediation for PAH contaminated soil and sediment. Also, an electrode enhanced capping will be one of the few active capping technologies that are able to enhance contaminant biodegradation.

Chapter 3: Electrode Enhanced Biodegradation of PAH in Sediment Slurry

3.1 INTRODUCTION

PAHs may be naturally removed in sediments by microbial degradation. Numerous bacterial species are capable of using PAHs as sole carbon and energy sources, and most of these organisms can metabolize a range of PAHs (Kastner et al., 1994; Chung and King, 2001; Hedlund and Staley, 2006; Dagher et al., 1997). The ability of aerobic microorganisms to degrade PAHs is well known and has been observed in laboratory and field studies with a variety of soils and sediments for many years (Bauer and Capone, 1985; Hambrick et al., 1980; Heitkamp and Cerniglia. 1987; Boyd et al., 2005). PAH degradation under anaerobic conditions has also been reported but it is relatively recent, and results on the extent of anaerobic biodegradation are controversial (Foght, 2008; Leduc et al., 1992; Johnson and Ghosh, 1998; Mihelcic and Luthy, 1988). In general, the rate of anaerobic biodegradation is much slower than the rate of aerobic conditions. However, the rate of PAH biodegradation in sediments is highly site specific and varies significantly (Shuttleworth and Cerniglia, 1995).

Sediments are often anaerobic because of the high biological oxygen demand of organic material, low solubility of oxygen, and mass transfer limitations of oxygen from the atmosphere into the sediment. The addition of oxygen has the potential to enhance PAH biodegradation in sediments. A novel technique to supply oxygen is by water electrolysis in the sediment. At the anode of the reaction of water electrolysis, oxygen is generated and it has been proven to be effective in stimulating bacterial growth (Watanabe et al., 2002).

In this dissertation, an electrode enhanced capping was proposed and investigated for the bioremediation of PAH contaminated sediment. In this Chapter, the potential for

this approach was assessed in slurry reactors under idealized conditions to demonstrate effective enhancement of biodegradation.

Anacostia River sediment was selected as model sediment in this study because of its historical contamination by PAHs (Lu et al., 2006). Degradation of two model PAHs (naphthalene and phenanthrene) were studied under aerobic and nitrate reducing conditions to evaluate PAH degradation potential in the Anacostia sediments. Electrode enhanced biodegradation in sediment slurry was conducted, and compared with biodegradation under aerobic and anaerobic conditions. To distinguish the effect of abiotic loss of PAH during electrochemical processes, PAH loss in a killed control reactor was also studied.

3.2 BIODEGRADATION OF PAH UNDER AEROBIC AND NITRATE REDUCING CONDITIONS

3.2.1 Materials and methods

3.2.1.1 Sediment and medium

PAH contaminated sediment was obtained from Anacostia River sediment and sieved through 2mm. It was stored at 4 °C until added to slurries for these studies. The water used to form the slurry was a low salt solution to simulate a typical freshwater environment. The minimal salt medium (MSM) to make sediment slurry contained 4 g of KH_2PO_4, 4 g of Na_2HPO_4, 0.5 g of NH_4Cl, 0.2 g of $MgCl_2 \cdot 6H_2O$, and 1 mL of trace element solution SL-4 per 1 L of DI water. SL-4 was composed of 0.5 g of EDTA, 0.2 g of $FeSO_4 \cdot 7H_2O$ and 100 mL of trace element solution SL-6 per 1 L of DI water. The composition of SL-6 was 0.3 g of H_3BO_3, 0.2 g of $CoCl_2 \cdot 6H_2O$, 0.1 g of $ZnSO_4 \cdot 7H_2O$, 0.03 g of $MnCl_2 \cdot 4H_2O$, 0.03 g of $Na_2MoO_4 \cdot H_2O$, 0.02 g of $NiCl \cdot 6H_2O$ and 0.01 g of $CuCl_2 \cdot 2H_2O$ per 1 L of DI water (Atlas, 2010). The pH of MSM is 6.8.

3.2.1.2 Biodegradation under aerobic conditions

Aerobic experiments were conducted in 250-mL amber bottles, each containing 100 mL sediment slurry (1 % solid content by weight), and 150 mL air. These bottles were sealed with a Teflon-lined septum and secured with a screw cap.

The total oxygen demand for 100 mL sediment slurry with a solid content of 1 % was about 5-10 mg because the biochemical oxygen demand (BOD) of sediment was estimated as 5-10 mg/g. In each bottle, 150 mL air had 45 mg oxygen, keeping the slurry in aerobic condition during the course of the experiment.

0.45 mg of naphthalene and 0.08 mg of phenanthrene were spiked to each bottle at the beginning of the experiment. After establishing an appropriate gas headspace composition (21 % oxygen as in the ambient air), the bottles were sealed and incubated in a tumbler at room temperature. Periodically, a serum bottle from the batch samples was sacrificed for PAH analysis and DNA extraction. Measurement of dissolved oxygen (DO) concentration (YSI Incorporated, Model 50B) was made to assure that oxygen was not a limiting factor for biodegradation.

Control samples were run concurrently with the test samples. Control samples were treated by autoclaving the glassware and sediment slurry at 121 °C for 30 minutes and then adding sodium azide such that the concentration of sodium azide in the control samples was 10 mM. The experiments were conducted in a batch mode with test samples and controls being prepared simultaneously.

3.2.1.3 Biodegradation under nitrate reducing conditions

Amber glass tubes of 40 mL were used for anaerobic experiment. Each tube was filled with sediment slurry (2.5 % solid content) to zero headspace, and sealed with a Teflon-lined septum and secured with a screw cap.

Nitrate reducing conditions have been generated with the addition of external nitrate (Leduc et al., 1992; Johnson and Ghosh, 1998; Mihelcic and Luthy, 1988). In this study, $NaNO_3$ was added to MSM so that the initial nitrate concentration in each tube was 5.88 mM.

0.27 mg of naphthalene and 0.074 mg of phenanthrene were spiked to each tube at the beginning of the experiment. Strict anaerobic procedures were followed during system setup. The medium was purged with nitrogen gas immediately after autoclaving and stored in an anaerobic chamber overnight prior to the experiment. All the sediment slurry was prepared in an anaerobic chamber. After the setup, all the bottles were sealed and incubated in a tumbler at room temperature. Periodically, a serum bottle from the batch samples was sacrificed for PAH analysis and DNA extraction. Dissolved oxygen concentration was measured at each sampling event to assure no oxygen was detected in the sediment slurry. Control samples were prepared under anaerobic condition by autoclaving the glassware and sediment slurry at 121 °C for 30 minutes and then adding sodium azide at a final concentration of 10 mM.

3.2.1.4 Sampling procedures

Bottles and tubes were unloaded from tumbler and sediment slurry was allowed to settle down for 1 hour before sampling. Triplicate supernatant samples were collected and extracted using liquid-liquid extraction by hexane for PAH analysis.

The procedures of liquid-liquid extraction by hexane include the following steps:

1) 5 mL or 10 mL hexane was added to glass sample vials and weighed;
2) An aliquot of supernatant was collected and added to the hexane sample vials, and weighed again. The difference of weight was used to calculate the volume of supernatant;

3) The mixture was sonicated (Branson 2200 ultrasonic cleaner) for about 30 minutes in a water bath and then stored in 4 °C before the next step;
4) 2 mL hexane sample was added to a 2 mL graduated vial and concentrated under nitrogen flow to 0.1~0.3 mL;
5) 2 mL acetonitrile was added to the graduated vial and concentrated under nitrogen flow to a total volume of 2 mL. The graduated vial was weighed before adding the hexane sample and after this step, and the difference was used to calculate the final acetonitrile volume. The acetonitrile sample was ready for PAH analysis by HPLC.

Sediment slurry was centrifuged at 3500 RPM for 30 minutes by centrifuge (International Equipment Company, Model Size 2). The supernatant and solid were collected and stored in 4 °C and -20 °C until further analysis, respectively.

3.2.1.5 PAH analysis

PAH concentration was measured by HPLC with a 250×4.6 mm column (Phenomenex Luna 5u C18(2) 100A) using a mobile phase composed of 15 % water and 85 % acetonitrile at 1 mL/min. Detection was made by a fluorescence detector (Waters 2475) with an excitation wave length of 270 nm and an emission wave length of 360 nm.

3.2.1.6 DNA extraction

Solids were collected for each sacrificed sample and the solid was stored at -20 °C until DNA extraction. DNA from an aliquot of sediment solid was extracted using FastDNA SPIN Kit for Soil (MP Biomedicals) according to the instructions of the manufacturer with minor changes. The water content was also measured in order to determine the DNA concentration per weight of dry sediment.

Pseudomonas putida G7 (DSMZ 4476) carrying the naphthalene dioxygenase (*nah*A) gene was used as a reference strain for primer test and qPCR calibration. It was pre-grown in DSMZ medium 444, and harvested in log-phase. DNA from *Pseudomonas putida* G7 (ppG7) was extracted using DNeasy Blood & Tissue Kit (Qiagen).

DNA concentrations in extracts were determined by Nanodrop ND-1000 spectrophotometer (NanoDrop Technologies, Inc). The absorbance at 260 nm was read and converted to DNA concentration. DNA extract was diluted to a final concentration of 10 ng/μL, 1 ng/μL, 0.1 ng/μL, 0.01 ng/μL, and 0.001 ng/μL as stock solution.

3.2.1.7 PCR and qPCR for PAH degrading genes

The primer set used in PCR and qPCR targets aromatic ring-hydroxylating-dioxygenase (RHD_{α}) for gram negative PAH-degrading bacteria, which covers a large range of functional genes including *bph*A1, *phn*Ac, *nag*Ac, *nah*Ac, *nah*A3, etc. (Cebron et al., 2008).

Table 3.1 Characteristics of gram negative PAH-RHD_{α} primer

	Sequence 5'-3'	Amplicon size(bp)	Annealing temperature(C)
Forward primer	GAG ATG CAT ACC ACG TKG GTT GGA	306	57
Reverse primer	AGC TGT TGT TCG GGA AGA YWG TGC MGT T		

Conventional PCR was performed in a reaction volume of 25 μL containing 12.5 μL of DreamTaq Green PCR Master Mix (2X) (Fermentas), 2 μL of mixed forward and reverse primer (5 μM), 2.5 μL DNA extract (2.5 μL water for negative control), 2.5 μL of

20X bovine serum albumin (BSA) and 5.5 μL water. It was conducted in a PTC-200 Peltier thermal cycler (MJ Research).

PCR thermal cycling includes the following steps:

Step 1: Initial dissociation: 95 °C for 5 min;

Step 2: 35 cycles of the following three steps:

Step 2.1 Denaturation: 95 °C for 30 s;

Step 2.2 Primer annealing: 57 °C for 30 s;

Step 2.3 Elongation: 72 °C for 30 s;

Step 3: 72 °C for 7 min.

qPCR was performed in 25 μL reaction volume containing 12.5 uL of Power SYBR green PCR master mix(Applied Biosystems), 2 μL of mixed forward and reverse primer (5 μM), 2.5 μL DNA extract (2.5 μL water for negative control), 2.5 μL of 20X BSA and 5.5 μL water. All DNA samples were analyzed in duplicate or triplicate. qPCR was performed in Applied Biosystems 7900HT sequence Detection System machine.

qPCR thermal cycling includes the following steps:

Step 1: Initial dissociation: 95 °C for 5 min;

Step 2: 40 cycles of the following three steps:

Step 2.1 Denaturation: 95 °C for 30 s;

Step 2.2 Primer annealing: 57 °C for 30 s;

Step 2.3 Elongation: 72 °C for 30 s;

Step 2.4 Dissociation of the primer's dimers: 80 °C for 10 s;

Step 3: 72 °C for 7 min;

Step 4: Melting curve analysis: 0.5 °C temperature increment from 51 °C to 95°C.

Two major changes for qPCR from conventional PCR were: 1) dissociation of primer's dimmers at 80 °C for 10 s; 2) melting curve analysis at the end of the regular

thermal cycling. Both steps were added to avoid the formation of primer's dimmers, whose signal will interfere with PCR products. Dissociation step was to dissociate any primer dimers during each polymerase chain reaction, and in the final step by viewing a melting curve, it was ensured that the desired amplicon was detected and no primer dimers were formed.

3.2.2 Results and discussion

Figure 3.1 shows the time varying concentration of naphthalene and phenanthrene under aerobic conditions. Maintenance of aerobic conditions throughout the experiment was confirmed with the measurement of dissolved oxygen at the end of the experiment. Triplicate experimental samples showed an average DO of 83.1 % with a standard deviation of 3.1 %, while DO of control samples was 96.6 % with a standard deviation of 1.0 %. Over a period of two days, considerable degradation of naphthalene and phenanthrene was observed, while the concentration of PAH in the control sample remained relatively constant. Naphthalene concentration decreased from ~1500 µg/L to ~10 µg/L within the first 24 hours and to no detection level (<1 µg/L) in the next 24 hours. Phenanthrene biodegradation rate was slower than naphthalene but complete disappearance still happened within 48 hours. Phenanthrene concentration decreased from 65 µg/L to 20 µg/L within the first 24 hours and to no detection level (<1 µg/L) in the next 24 hours.

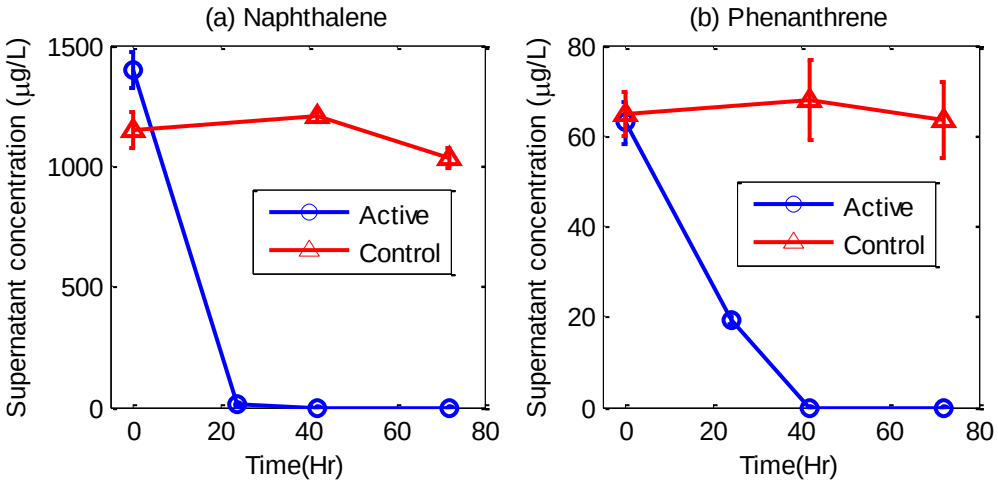

Figure 3.1 Naphthalene (a) and phenanthrene (b) biodegradation under aerobic condition. Points represent the mean of triplicate supernatant samples and error bars indicate standard deviation of triplicate data. Active means biological active samples, and control represents killed control samples.

Figure 3.2 shows the supernatant concentration of naphthalene and phenanthrene under nitrate reducing conditions. Significant reduction of both PAH was observed within one month, though the degradation rates were much slower than those observed under aerobic conditions. Under this ideal conditions, i.e. no mass transfer limitation and no nutrient limitation, the half life time of naphthalene and phenanthrene were about 3 and 5 days, respectively.

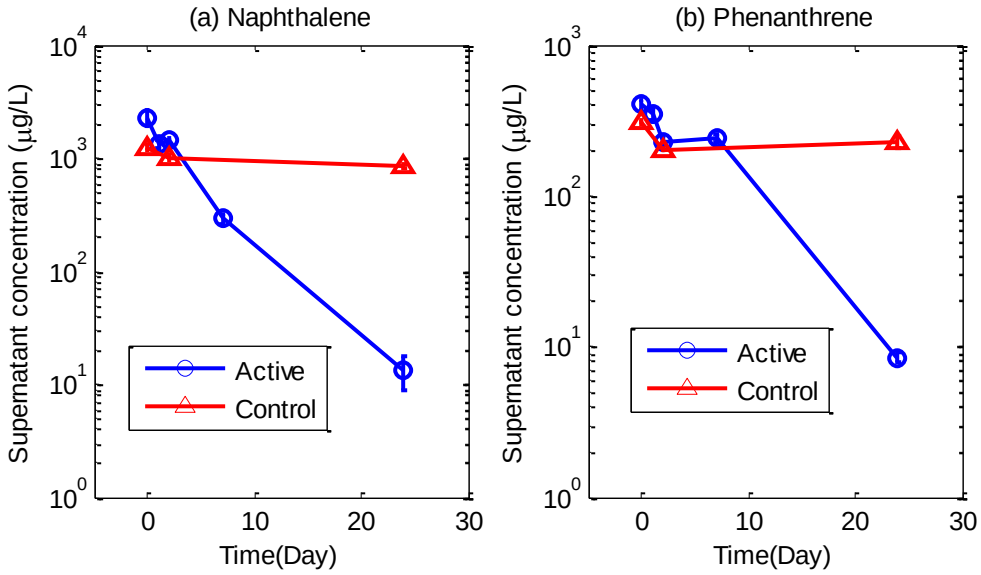

Figure 3.2 Naphthalene (a) and phenanthrene (b) biodegradation under nitrate reducing condition. Points represent the mean of triplicate supernatant samples and error bars indicate standard deviation of triplicate data. Active means biological active samples, and control represents killed control samples.

Extraction of ppG7 DNA from 10 fold serial dilution was used for qPCR calibration and efficiency estimation. The final concentration of ppG7 DNA for qPCR was 1, 10^{-1}, 10^{-2}, 10^{-3}, and 10^{-4} ng/µL. It was assumed that the qPCR tube with a DNA concentration of 1 ng/µL had an arbitrary 10^{8} unit gene, and subsequent samples had 10 fold decrease gene copies. Threshold cycle (Ct) reflects the cycle number at which the fluorescence generated within a reaction crosses the threshold, and it is inversely correlated to the initial gene copy number. A linear relationship between Ct and the logarithm of the initial gene copy number was used to estimate the gene copy number in all the sediment samples.

The relationship of Log(gene copy number) and Ct by the standard curve was estimated as

$$\text{Log(gene copy numbers)} = k * Ct + b \quad (3\text{-}1)$$

Ct value of environmental samples was estimated from amplification plot and then converted to gene copy number by this linear relationship.

For easier comparison of PAH degrading gene populations among environmental samples, the PAH-RHD$_\alpha$ GN gene levels were normalized by total DNA or weight of dry sediment. Gene copy number per DNA was an indicator of relative percentage of PAH degrading bacteria among the entire community, while gene copy per dry sediment reflected the absolute quantity of PAH degrading bacteria.

All values were reported as an increase from unincubated sediment, which was stored in 4 °C until DNA extraction.

Figure 3.3 shows that under aerobic condition PAH degrading gene concentration in the PAH spiking sediment slurry increased by two orders of magnitude at t = 4 hr compared to unincubated sediment (t = 0), and the increase was three orders of magnitude at t = 28 hr. After one day, the gene copies reached the plateau phase, where gene copy number neither increased nor decreased. The killed control sampled at t = 72 hr didn't show any changes of gene copy number compared to the unincubated sediment.

The results of two normalization methods didn't show significant difference in terms of gene copy increase. However, it was observed that total DNA per dry sediment increased by 2-3 times after the incubation, which implied that the total bacterial population increased under aerobic condition. Consequently, the increase of gene copy number per DNA was less than the increase of gene per dry sediment.

Similarly, Figure 3.4 shows the PAH degrading gene concentration under nitrate reducing condition. The PAH degrading gene concentration in sediment slurry increased by one orders of magnitude after two days, and the increase was two orders of magnitude

at the seventh day, after which the gene copies reached the plateau phase. Although increased gene copy numbers was observed under both aerobic and nitrate reducing condition, the maximum increase under nitrate reducing condition was one order magnitude less than that under aerobic condition.

The increase of gene copy number was believed to be associated with PAH biodegradation. In the first 24 hours, it was observed that the fast growth of dioxygenase gene and PAH disappearance occurred simultaneously. However, after all the PAH was depleted, gene copies stopped increasing, which implied the PAH degrading bacteria went into stationary phase.

qPCR analysis provided the evidence of PAH biodegradation under aerobic and nitrate reducing condition, indicating that the indigenous microbial community in Anacostia River sediment has the potential to biodegrade naphthalene and phenanthrene in suitable environmental conditions. It was demonstrated that the occurrence of the biodegradation process can be determined by monitoring the number of catabolic genes. PAH-RHD$_{\alpha}$ Gram Negative primer could be used for accurate qPCR quantification of PAH degrading bacteria directly on DNA from sediment samples.

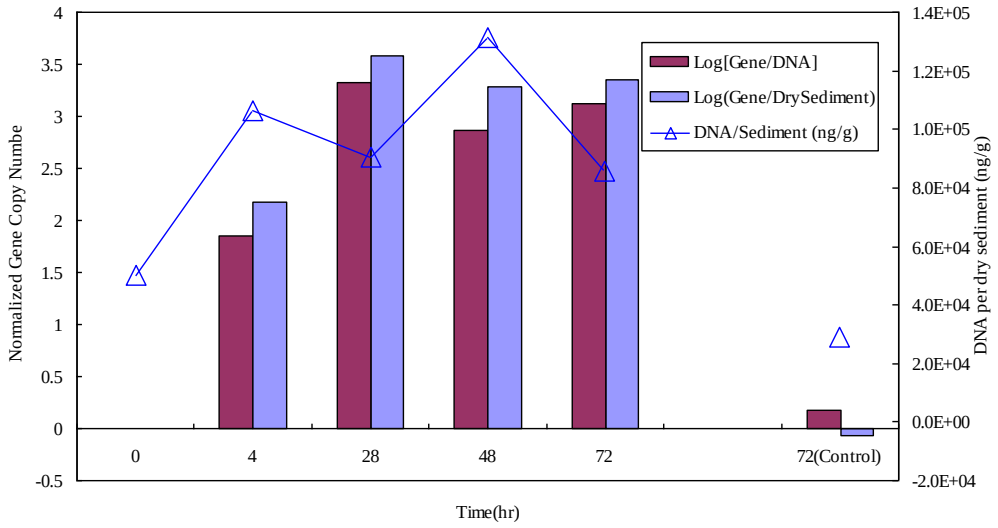

Figure 3.3 qPCR quantification and DNA extraction results under aerobic condition: 1) Copy number of PAH degrading gene normalized by total DNA; 2) Copy number of PAH degrading gene normalized by dry sediment; 3) DNA concentration per dry sediment.

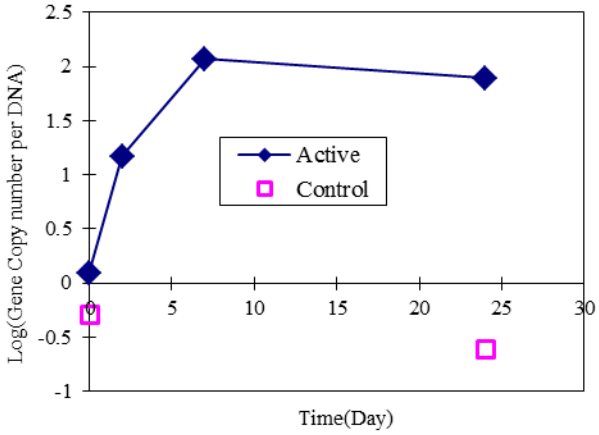

Figure 3.4 PAH degrading gene abundance by qPCR quantification under nitrate reducing condition. The PAH-RHD$_\alpha$ GN gene levels were normalized by the weight of dry sediment. All the values were reported as an increase from unincubated sediment control.

3.3 ELECTRODE ENHANCED BIODEGRADATION OF PAH IN SEDIMENT SLURRY

3.3.1 Materials and methods

3.3.1.1 Experiment design and instruments

The electrode enhanced biodegradation experiments were conducted using glass electrolysis reactors to minimize adsorption of PAH on the cell wall. Each reactor has a compartment of 500-600 mL volume and several ports for fitting the electrodes into the solution and for sampling (Figure 3.5).

Figure 3.5 The reactor for electrode enhanced biodegradation experiment

The electrode materials were 6.15 mm (0.242 in) diameter * 75 mm (3 in) long graphite rod (Alfa Aesar). Copper wires were soldered to alligator clips, and alligator

clips were connected to the graphite rods. The external power was connected only to the copper wires for power supply.

Four out of five ports in each reactor were sealed with Teflon lined rubber stopper. If external power was applied, copper wires went through rubber stoppers to connect to power. Screw-caps with Mininert valve were used at the sampling port of the reactor. By this setting, all the ports in each reactor were air tight and there was no leak to the atmosphere.

The following four sets of experiments were conducted:

1) ElectroBio reactor (RE): Power was applied to active sediment slurry that was initially anaerobic;

2) Killed control (KC): Power was applied to killed control sediment slurry (autoclaved) and also initially anaerobic;

3) Aerobic control (AE): No power was applied, but the sediment slurry was maintained in aerobic conditions during the course of the experiment. By maintaining aerobic conditions, the PAH degradation potential of the slurries could be determined;

4) Anaerobic control (AN): No power was applied, but anaerobic conditions were maintained. In this treatment the rate of degradation in an ineffective electrode cap could be determined (that is, one that was ineffective at creating oxidizing conditions).

The copper wires at the electrodes were connected to Extech 382202 DC power supply (Extech Intruments Corp, Waltham, MA). The applied power was about 3.5 V and the current was about 15 mA.

The experiments were conducted in a period of 4 days, constantly stirred by a stir bar, and sediment slurry were samples periodically for PAH analysis. GASTIGHT syringe and needle (Hamilton Company) were used for sampling at each sampling time.

After the experiment, the slurry was centrifuged at 3500 RPM for 30 minutes and solids were collected and store in -20 °C.

3.3.1.2 Sediment slurry preparation

PAH contaminated sediment was obtained from Anacostia River sediment and sieved through 2 mm. It was stored at 4 °C until used.

The minimal salt medium (MSM) was used to make sediment slurry. 2 L of anaerobic MSM was made by autoclave, deoxygenation, and stored in anaerobic chamber (Coy Laboratories) filled with 95 % nitrogen and 5 % hydrogen. 1 L of aerobic medium was made by oxygenation with air, and stored under atmosphere conditions.

43.3 mg naphthalene and 8.1 mg phenanthrene were dissolved in 20 mL hexane as stock solution for spiking the sediment slurry.

To prepare the sediment slurry for RE, AE and AN, naphthalene and phenanthrene were initially coated onto the insides of a jar by hexane delivery. 3.14 mL PAH stock in hexane (6.79 mg naphthalene and 1.27 mg phenanthrene) was added to a jar and distributed evenly around the bottom and sides of the jar. The hexane was allowed to evaporate under nitrogen gas flow, leaving the PAH coated on the inside wall of the jar. 30.20 g wet Anacostia River sediment (water content = ~50 %) was added to the jar and diluted with 150 mL of anaerobic MSM in anaerobic chamber. The solid content of this sediment slurry was 10 %. The sediment slurry was sealed and tumbled overnight to make PAH dissolved and partitioned into solid phase. The next day, 45 mL of 10 % solid slurry with PAH and 405 mL of anaerobic MSM were added to RE reactor in anaerobic chamber, making a final sediment slurry of 450 mL with a solid content of 1 % by weight. Similarly, 55 mL of 10 % solid slurry and 545 mL of anaerobic MSM made 600 mL final sediment slurry for AN in anaerobic condition, and 40 mL of 10 % solid slurry

and 360 mL of aerobic MSM made 400 mL of aerobic sediment slurry for AE in aerobic condition. The total volume of AE reactor was 600 mL, leaving 200 mL space for air. 200 mL air had about 60 mg oxygen, which was enough to keep AE reactor in aerobic condition during a period of several days.

To prepare the sediment slurry for KC, 11.30 g wet sediment was added to a jar (jar-1) and diluted to 50 mL using MSM, and autoclaved at 121 °C for 30 minutes three times. Another jar (jar-2) was autoclaved and then coated with 1.18 mL PAH stock (6.79 mg naphthalene and 1.27 mg phenanthrene). Sediment slurry in jar-1 was transferred to jar-2 in anaerobic chamber, sealed and tumbled overnight. The next day, all the 50 mL slurry and 450 mL autoclaved anaerobic MSM was added to reactor in anaerobic chamber, making a final medium of 500 mL.

Following the above procedures, sediment slurry in each reactor had the same initial concentration and solid content(1 %), and sediment slurries in RE, KC and AN were initially oxygen free, which mimicked anaerobic condition of sediment under a capping layer.

3.3.1.3 Sampling procedures

Stirring in reactors were stopped and sediment slurry was allowed to settle down for 30 minutes before sampling. GASTIGHT syringe and needle were injected through Mininert valve to sample ~1 mL supernatant from slurry. Triplicate samples were obtained each time to minimize sampling uncertainty.

Liquid-liquid extraction by hexane was performed after the supernatant was collected as previously described.

PAH analysis, DNA extraction, and PCR and qPCR for PAH degrading genes followed the same procedures as previously described.

3.3.2 Results and discussion

Figure 3.6 represents naphthalene concentration in sediment slurry under ElectroBio reactor (RE), killed control (KC), aerobic (AE) and anaerobic (AN) conditions. At the end of the experiment, i.e. t= 96 hrs, naphthalene concentration under RE, KC, and AE conditions decreased to 20-60 µg/L from an initial concentration of about 1000 µg/L. The removal efficiency for RE, KC and AE were 96%, 93% and 97%, respectively. However, naphthalene concentration still remained 80% of initial concentration under anaerobic condition. These data suggested that the presence of oxygen was critical for the degradation of naphthalene. Naphthalene had a much smaller biodegradation rate under anaerobic conditions.

Although significant degradation of naphthalene was observed in all the three oxygen present conditions, the pattern of the degradation was different for all the three cases. In killed control sample, the logarithmic of naphthalene concentration decreases linearly with time, which was equivalent to an exponential decrease with time, i.e. $C=C_0*exp(-k*t)$. This first order reaction kinetics was consistent with the abiotic condition in the killed control. The abiotic loss of naphthalene in the electrolytic reactor may be a combined process of direct electrochemical oxidation at the anode, oxidation by hydrogen peroxide, Fenton's reagent and hydroxyl radicals (Goel et al., 2003).

Under aerobic condition, naphthalene biodegradation began several hours later after the incubation. So there was a lag phase in the order of 10 hours for the microbial community to degrade naphthalene. As soon as the biodegradation began, the rate of naphthalene disappearance was significantly fast. In a period of 20 hours, naphthalene was degraded from ~1000 µg/L to ~40 µg/L.

The degradation in the ElectroBio reactor was a combined process of abiotic degradation and biotic degradation. The rate in the first 24 hours was in the same order of

magnitude as the abiotic degradation, with a half-life about 10 hours. There was a longer lag phase (~20 hours) in this case. However, when the microbial activity started, the rate of degradation increased significantly. Naphthalene concentration decreased from ~400 µg/L to ~50 µg/L within only 10 hours. That was about the same rate as observed under fully aerobic conditions, suggesting that the presence of the electrodes was able to generate and maintain aerobic degradation processes despite the initial state of the slurry as being anaerobic.

Under both AE and RE conditions, naphthalene concentration reached a plateau phase after about t=30 hr. Though the concentration kept decreasing, the rate was very slow. It is implied that the bacteria in the sediment slurry stopped using naphthalene as the carbon source.

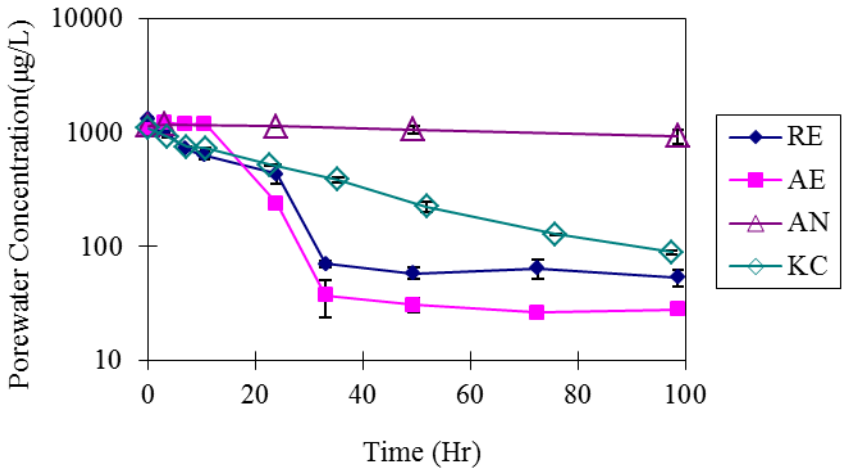

Figure 3.6 Degradation of naphthalene over time in ElectroBio reactor (RE), killed control (KC), aerobic (AE) and anaerobic (AN) conditions. Points represent the mean of triplicate supernatant samples and error bars indicate standard deviation of triplicate data.

Figure 3.7 represents phenanthrene concentration in sediment slurry under ElectroBio reactor (RE), killed control (KC), aerobic (AE) and anaerobic (AN) conditions. Phenanthrene degradation was not observed under killed control and anaerobic condition during 4 days. The abiotic loss of phenanthrene was not as much as naphthalene probably because of its high hydrophobicity and low aqueous concentration. Majority of phenanthrene was adsorbed in the solid phase, and only a small fraction was in aqueous phase and became available to direct electrochemical reaction and chemical oxidizing reagents.

Phenanthrene degradation occurred both in ElectroBio reactor and under aerobic condition, and the removal efficiency were 82% for RE and 86% for AE at the end of the experiment. The lag phase of RE and AE were about 50 and 30 hours, respectively. However, in both cases, phenanthrene degradation didn't start until naphthalene concentration reached the plateau phase. It is implied that the PAH degrading microbial consortium in the slurry have a priority of naphthalene over phenanthrene, and the bioavailability of naphthalene is higher than phenanthrene.

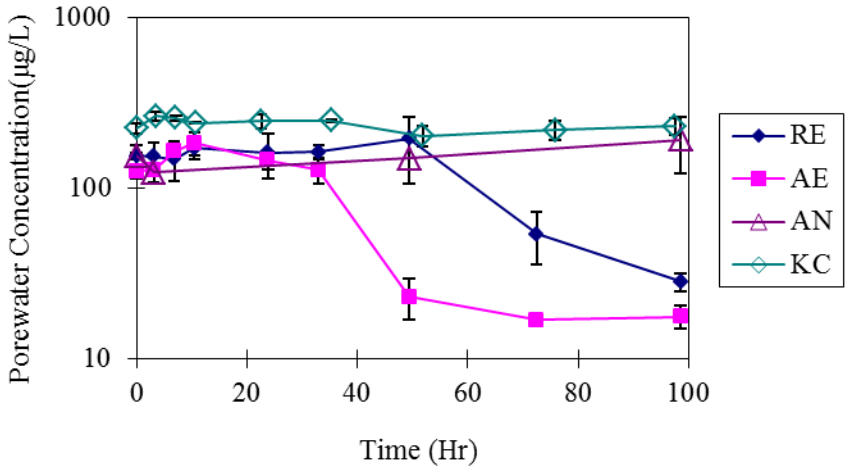

Figure 3.7 Degradation of phenanthrene over time in ElectroBio reactor (RE), killed control (KC), aerobic (AE) and anaerobic (AN) conditions. Points represent the mean of triplicate supernatant samples and error bars indicate standard deviation of triplicate data.

For easier comparison of PAH degrading gene populations among environmental samples, the PAH-RHD$_\alpha$ GN gene levels were normalized by the weight of dry sediment. All the values were reported as an increase from unincubated sediment, which was stored at 4 °C until DNA extraction. Figure 3.8 shows that PAH degrading gene concentration increased significantly in the ElectroBio reactor, in a manner similar to the aerobic reactor, which implied the growth of PAH degrading bacteria. The gene concentration under anaerobic condition was about the same level as that in unincubated control, and this phenomenon was consistent with the fact that PAH was not biodegraded under anaerobic conditions. In killed control, the PAH degrading gene was not detectable, so it was confirmed that the decrease of PAH in killed control was only due to electrochemical reaction and no biological activities was involved.

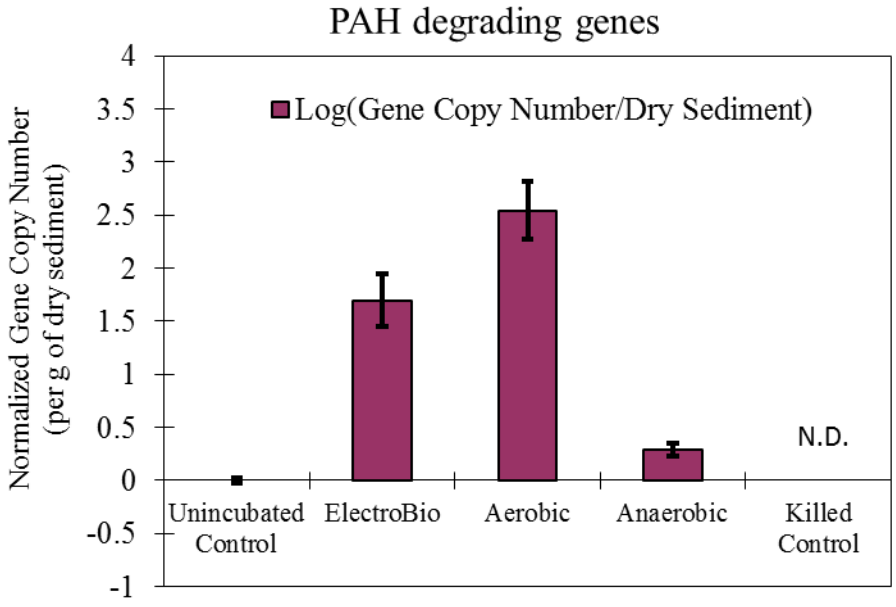

Figure 3.8 PAH degrading gene abundance by qPCR quantification. The PAH-RHD$_\alpha$ GN gene levels were normalized by the weight of dry sediment. All the values were reported as an increase from unincubated sediment control. The results are the means of triplicate, and error bars represent standard deviation. N.D. = Not Detectable.

3.4 CONCLUSIONS

Biodegradation of PAH under aerobic and nitrate reducing conditions shows the ability of native microorganism in Anacostia River sediment to degrade naphthalene and phenanthrene in several days or weeks. The degradation rate was slower under nitrate reducing conditions than that under aerobic conditions. qPCR was applied to detect the abundance of PAH degrading genes, and the results show increasing levels of PAH degrading genes under both conditions.

Feasibility of electrode enhanced capping for remediation of PAH contaminated sediment was implemented in the sediment slurry phase. An external potential of 3.5 V was applied to well mixed sediment slurry contaminated with two model compounds: naphthalene and phenanthrene. During a period of 4 days, naphthalene concentration

decreased from ~1000 μg/L to ~50 μg/L, and phenanthrene was degraded from ~150 μg/L to ~30 μg /L in ElectroBio reactor. These rates in ElectroBio reactor were about the same as observed under fully aerobic conditions, except a longer lag phase. By comparison to controls, the disappearance of naphthalene was a combined process of abiotic and biotic loss while the phenanthrene loss appeared to be solely controlled by biotic processes. Naphthalene concentration still remained 80% of initial concentration, and phenanthrene degradation was not observed under anaerobic condition.

The results of qPCR show significant increases of PAH degrading genes in ElectroBio reactor and aerobic conditions, but no increase in killed control and anaerobic conditions. qPCR analysis provided the evidence of PAH biodegradation in ElectroBio reactor and aerobic conditions.

Chapter 4: Electro-biodegradation of PAH and Redox Control in Sediment/Cap Microcosms

4.1 INTRODUCTION

Contaminated sediments cause adverse effects on aquatic life and pose a risk to ecology and human health. Although dredging and ex-situ disposal have been used as a remedial technology for contaminated sediment, the high cost and concern of recontamination after dredging have led to the use of an alternative technology – in-situ capping. In-situ capping has recently emerged as a remedial method for contaminated sediments, and it involves the placement of clean material (usually sand) on the sediment to isolate the contaminants into the overlying water. In-situ capping can be a relatively cost-effective and noninvasive approach compared to dredging. However, a potential consequence of placing a cap at the sediment-water interface is that it induces considerable changes of biogeochemical conditions within the underlying sediment. The anaerobic conditions induced by in-situ capping hinders PAH natural degradation, which might otherwise occur at the surface sediment. In addition, conventional capping usually doesn't promote contaminant degradation or removal, and the risk to ecological and human health may recur if the contaminant can migrate through the caps.

To overcome the limitation of conventional capping, electrode enhanced capping was proposed and investigated for the bioremediation of PAH contaminated sediment. In Chapter 3, the potential for this approach was assessed in completely mixed reactors to demonstrate the effectiveness of this approach under idealized conditions. In this Chapter, laboratory scale experiments were conducted in simulated sediments/caps to evaluate the effect of mass transfer limitations under a realistic but controlled laboratory environment. Phenanthrene concentration profiles in the sediments/caps were measured at different times to determine the biodegradation rates. Important parameters to

characterize redox conditions, such as pH, redox potential, and concentrations of redox-sensitive species, were determined to better understand the changes of biogeochemical condition with the application of electricity. PAH degrading genes were quantified in the vicinity of the anode to provide more insight on microbial biodegradation activity.

Three sets of experiments were conducted in this chapter. The experimental study was first conducted in PAH contaminated sediment with no capping layer to identify the key processes and parameters for further studies. The high pH buffer capacity in the sediment would be beneficial for biodegradation with less pH shift. Second, PAH degradation and redox control were studied in electrode enhanced caps, and upon the finish of this study, it was expected that some degree of PAH degradation would be observed. Third, PAH degradation and redox control were investigated in electrode enhanced caps with bicarbonate amendment. The purpose of the last study was to test whether PAH biodegradation could be further accelerated by providing an instant soluble pH buffer in the system.

The goal of all of these tests was to develop a thin aerobic zone in the vicinity of the anode. In this manner any contaminants that may migrate up out of the contaminated sediment into the overlying water or cap layer may experience degradation. That is, the anode is designed to serve as a biobarrier for migrating contaminants. The goal of the effort was not to change the redox conditions or encourage degradation over a large sediment zone. Non-migrating contaminants pose little risk to interfacial organisms or the water column and efforts to encourage degradation over a large volume of sediment would have substantially greater power requirements, limiting the feasibility of the approach.

4.2 PAH DEGRADATION AND REDOX CONTROL IN UNCAPPED SEDIMENT BY ELECTRODES

4.2.1 Materials and methods

4.2.1.1 Microcosm setup and operation

Three 400-mL beaker reactors were used to evaluate the ability of carbon electrodes to control the redox potential and encourage PAH degradation in simulated static contaminated sediment. One reactor served as a no-applied electricity control (Control) while electricity was applied to the other two (ElecR1 and ElecR2) through cloth electrodes. In Control and ElecR1 reactors, 0.05 g/mL of siderite (Prince Agri Products, Inc., Quincy, Illinois) was mixed with sediment to aid in buffering.

The reactors were filled with sieved (2 mm) sediment (mixture of contaminated Anacostia River sediment and clean University Lake sediment, ratio 1:5.6). The sediment was spiked with phenanthrene and naphthalene at a level of ~20 μg/g concentration for both compounds.

A 5cm×5cm woven carbon cloth (Graphite felt, Wale Apparatus Co, Hellertown, PA) was placed at 3 cm below the sediment water interface as the anode, and a second, identical, carbon cloth was placed at 0.5 cm below the sediment-water interface as the cathode. Deionized water was applied on top of the sediment as overlying water. Water lost due to evaporation was periodically replenished with deionized water to maintain the original salt composition.

The graphite electrodes were connected to copper wires by EPO-TEK® 377H (Epoxy Technology, Billerica, MA), which is a graphite filled epoxy designed for electronic industries. The graphite power component in the epoxy ensured its electrical conductivity. The connections between the graphite cloth and copper wires were sealed with Gardner Bender LTW-400 liquid electrical tape (Gardner Bender, Milwaukee, WI).

Powered reactors were connected to 2 V Extech 382202 DC power supply (Extech Instruments Corp., Waltham, MA), and external power was continuously applied for ~12 weeks except during microelectrode measurement.

4.2.1.2 pH and ORP measurement

pH was measured by MI-405 standard pH microelectrode (Microelectrodes Inc, Bedford, New Hampshire) and Oxidation Reduction Potential(ORP) was measured by Pt microelectrode against Ag/AgCl reference. Vertical profiles of pH and ORP from the sediment-water interface to a depth of 45 mm with 5 mm intervals were acquired. 2 minutes was allowed to reach equilibrium at each depth.

pH microelectrode was calibrated with pH 4, pH 7 and pH 10 standard buffer solution (Fisher Scientific, Fair Lawn, NJ) before and after each measurement.

Pt microelectrode for ORP measurement was calibrated in pH-buffered, saturated quinhydrone solution. Two standard solutions were prepared as follows: about 0.05 g quinhydrone was added to 30 mL of pH 4 and pH 7 buffer solution, respectively. The mixture was stirred and allowed at least 15 minutes to equilibrate, and then it was stirred again. Not all of the quinhydrone would dissolve so both solutions should be saturated by quinhydrone after equilibration. The readings of potential difference between Pt microelectrode and Ag/AgCl reference electrode in each buffer solution were compared to Table 4.1. If the reading was more than 10 mV from the proper value, Pt electrode was cleaned and tested again until it met the standards. The reading was converted and reported as versus standard hydrogen electrode (SHE).

Table 4.1 ORP of platinum and Ag/AgCl reference electrode pairs in quinhydrone dissolved in pH buffer (Sparks, 1996)

	pH 4		pH 7	
Temperature (K)	293	298	293	298
Reading (mV)	268	263	92	86

4.2.1.3 Voltammetric determination of redox-sensitive species

Redox-sensitive species (O_2, Fe^{2+}, Mn^{2+}, and S^{2-}) were analyzed electrochemically at discrete depths within the sediment by inserting voltammetric microelectrodes into sediment porewater. All voltammetric measurements were performed using an Au/Hg solid-state microelectrode, a platinum counter electrode, and an Ag/AgCl reference electrode. The Au/Hg microelectrodes consisted of a 100 μm diameter gold wire housed in glass tubing filled with nonconductive epoxy and connected via copper wire. They were fabricated according to methods developed by Brendel and Luther (1995) and Luther et al. (1999). The gold surface was first polished with diamond pastes of 15, 6, 1, and 0.25 μm (Buehler, Lake Bluff, IL), then plated with mercury at -0.1 V (vs Ag/AgCl reference electrode) in acidic $Hg(NO_3)_2$ solution for 120 s. The gold amalgam was stabilized by polarizing the microelectrodes at -9 V for 120 s.

Each Au/Hg microelectrode was calibrated for dissolved oxygen by linear sweep voltammetry, and then for manganese, ferrous iron, and sulfide by square wave voltammetry (SWV) in 2 mM acetate or HEPES buffers.

Voltammetric analyses for redox-sensitive species were performed by a DLK-100A potentiostat and a micromanipulator capable of vertical movements at the sub-

millimeter scale (Analytical Instrument Systems, Inc, Flemington, NJ). The small size of the working microelectrode, and the precise control of vertical movement, allowed repeated vertical profiling with high spatial resolution while minimizing bulk sediment disturbance. Scan parameters and detection limits were the same as those reported in Brendel and Luther (1995). Triplicate electrodes were used for the measurement and vertical profiles from the sediment-water interface to a depth of 45 mm with 5 mm intervals were obtained (the same location as pH and ORP profiles).

4.2.1.4 Phenanthrene porewater concentration measurement by PDMS-coated fiber

Phenanthrene profiles in the sediment interstitial water were measured by Polydimethylsiloxane (PDMS)-coated fibers manufactured by Fiberguide Industries (Stirling, NJ). Naphthalene could not be reliably measured by this technique due to its relatively modest sorption onto PDMS and high volatility. The PDMS-coated fibers (210/230) had a 210-μm core with a 10-μm PDMS coating or outer diameter of 230 μm. The ability of the PDMS-coated fibers to quantify sediment porewater concentrations has been tested in the laboratory (Lu et al., 2011; Mayer et al., 2000). The linear partitioning relationship of the phenanthrene concentration between the PDMS phase (C_{fiber}, ng/L PDMS) and the porewater (C_w, ng/L water) was assumed with a partition coefficient K_f of 8912.18 (Lu et al., 2011).

For all PDMS analyses, the method described by Lu et al. (2011) was used. The fiber was cleaned prior to deployment by sonication in hexane for a minimum of half an hour, followed by a rinse with acetone and then deionized water.

The equilibrium time varies considerably from one fiber type to another and also depends on the octanol-water partition coefficient (K_{ow}) of the hydrophobic organic compounds (Cornelissen et al., 2008; Lampert, 2010). Before using PDMS fiber for the

measurement of phenanthrene porewater concentration, the uptake kinetic of this type of fiber (210/230) for phenanthrene was tested and equilibrium time was determined. During the application of fiber for phenanthrene porewater measurement, fibers were inserted vertically in the sediment for a period long enough to reach equilibrium. Then fibers were pulled out from the sediment, rinsed clean (to remove any particles) with deionized water, cut into 1 cm pieces, and placed into 2 mL HPLC vials with 1 mL of HPLC-grade acetonitrile. Duplicate phenanthrene concentration profiles were measured every two weeks during the course of the experiment.

4.2.1.5 DNA extraction and qPCR analysis

At the end of the experiment, sediment cores were collected and dissected into 0.5 cm or 1 cm long subsamples and stored at -20 °C until further analysis. DNA was extracted and qPCR was performed as previously described.

4.2.2 Results and discussion

4.2.2.1 Redox control, pH changes and redox-sensitive species

When an external power of 2 V was applied to the electrodes in the sediment for ElecR1 and ElecR2, redox potentials in the sediment around the anode changed. A 2 V of potential was selected to ensure water electrolysis at the electrodes. A greater potential is not preferred for stimulating biodegradation since it causes a higher rate of water electrolysis, consequently results in severe pH changes at both the anode and the cathode. An increment of redox potential was observed in two powered reactors compared to control (Figure 4.1). The ORP around the anode (d = 3 cm) increased gradually from an initial value of ~100 mV, and finally reached ~200 mV after about one month of operation for both powered reactors. The ORP at the same depth in control reactor was about 80 – 160 mV during the course of the experiment. The changes in redox conditions

were not limited to the vicinity of the anode but also took place in the sediment below the anode. As shown in Figure 4.2, the ORP below the anode (d = 3 – 4.5 cm) was about 50 – 150 mV higher in powered reactors than that in the control. Although redox potential increased in the vicinity of the anode, the ORP at the cathode didn't decrease notably. Redox potentials around the cathode were maintained above 300 mv for all the three reactors though ORP in control was slightly higher than that in powered reactors. It implies that the oxidized condition at the surface of the sediment will not be altered by the electrodes, but the redox condition at the deeper sediment will become more oxidized in favor of PAH degradation.

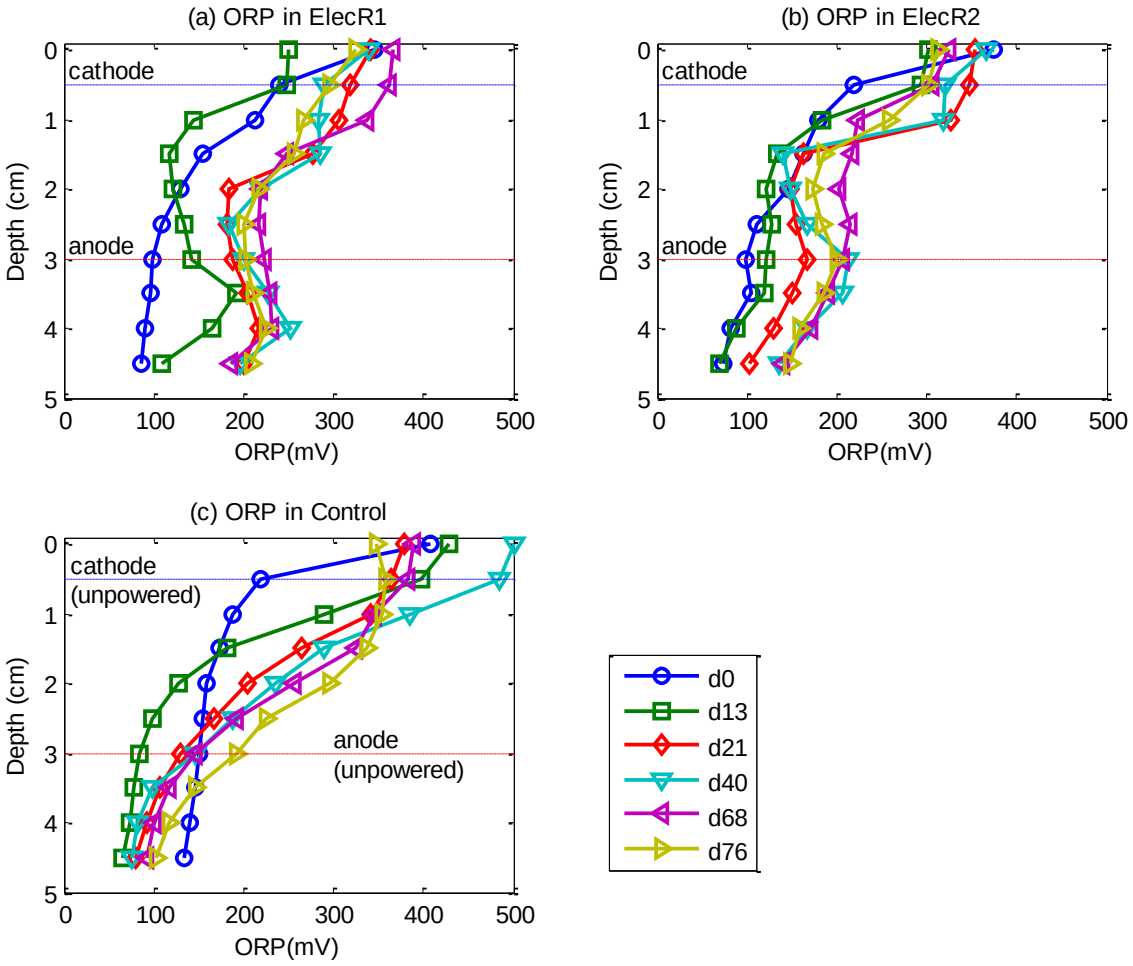

Figure 4.1 Vertical profiles of ORP in (a) ElecR1, (b) ElecR2 and (c) Control reactors on selected days. ORP values were versus standard hydrogen electrode (SHE). Depth zero was the water-sediment interface. Cathode was at d = 0.5 cm and anode was at d = 3 cm. All the measured profiles are in Appendix B.

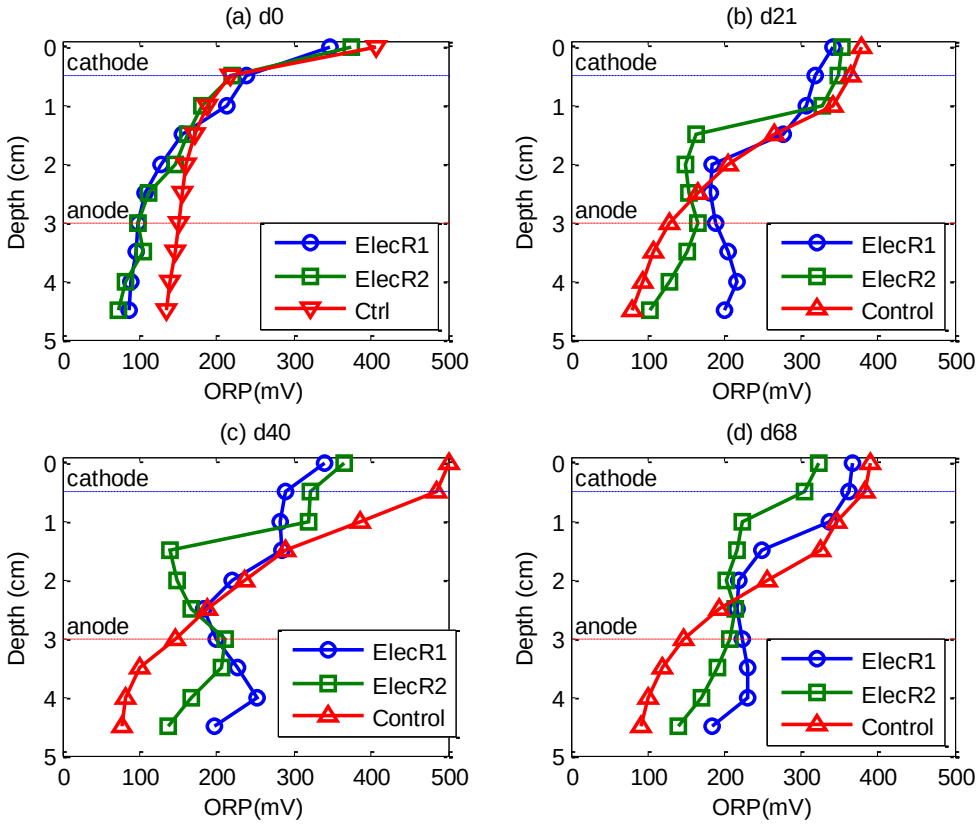

Figure 4.2 Vertical profiles of ORP at (a) Day 0, (b) Day 21, (c) Day 40 and (d) Day 68. ORP values were versus standard hydrogen electrode (SHE). Depth zero was the water-sediment interface. Cathode was at d = 0.5 cm and anode was at d = 3 cm.

With the application of potential, pH in the sediment for powered reactors changed with time. As shown in Figure 4.3, pH around the cathode (d = 0.5 cm) increased with time and reached the highest value after about 40 days. The peak pH of ElecR1 and ElecR2 was 9.7 and 8.9, respectively. pH around the cathode dropped to about 7.5 and kept at this level until the end of the experiment. pH around the anode decreased to ~6 from an initial value of 6.4 or 6.7 for powered reactors, and pH in this acidic zone remained relatively steady with time. Compared to the pH changes induced

by electrodes in powered reactors, the pH in the control reactor remained relatively steady with time and depth.

The acidic zone around the anode and the basic zone around cathode were the result of water electrolysis reactions at the electrodes as follows:

$$\text{Anode: } 2H_2O = O_2 + 4H^+ + 4e \qquad E^0 = 1.229V \qquad (4\text{-}1)$$

$$\text{Cathode: } 2H_2O + 2e = H_2 + 2OH^- \qquad E^0 = -0.827V \qquad (4\text{-}2)$$

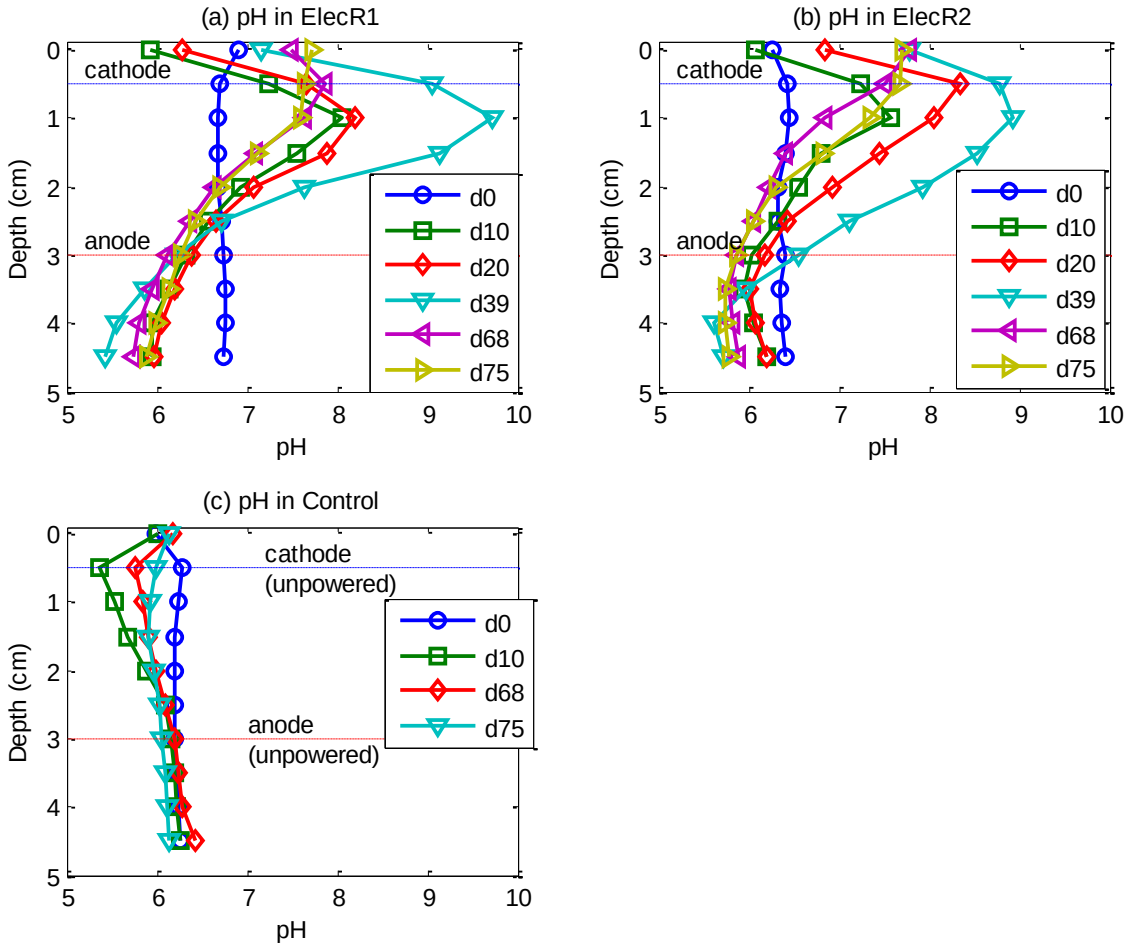

Figure 4.3 Vertical profiles of pH in (a) ElecR1, (b) ElecR2 and (c) Control reactors. Depth zero was the water-sediment interface. Cathode was at d = 0.5 cm and anode was at d = 3 cm. All the measured profiles are in Appendix B.

The profiles of redox-sensitive species were measured at day 79 when steady state was achieved (Figure 4.4). Oxygen concentrations at the sediment water interface for powered and control reactors were 53 - 80 % of saturation level and reached less than 5 % immediately at the depth of 1 cm. There was no observable difference between powered reactors and control in oxygen level in the superficial sediments. Beneath the oxic layer, concentrations of Mn^{2+} increased steadily with depth, while modest concentrations of Fe^{2+} concentrations were observed from d = 2 cm. The levels of ferrous iron in the deeper sediment in both powered reactors were considerably higher than that in control. The increased level of ferrous iron in powered reactors resulted from the metal released in the acidic conditions as follows:

$$Fe(OH)_3(s) + 3H^+ + e = Fe^{2+} + 3H_2O \qquad (4\text{-}3)$$

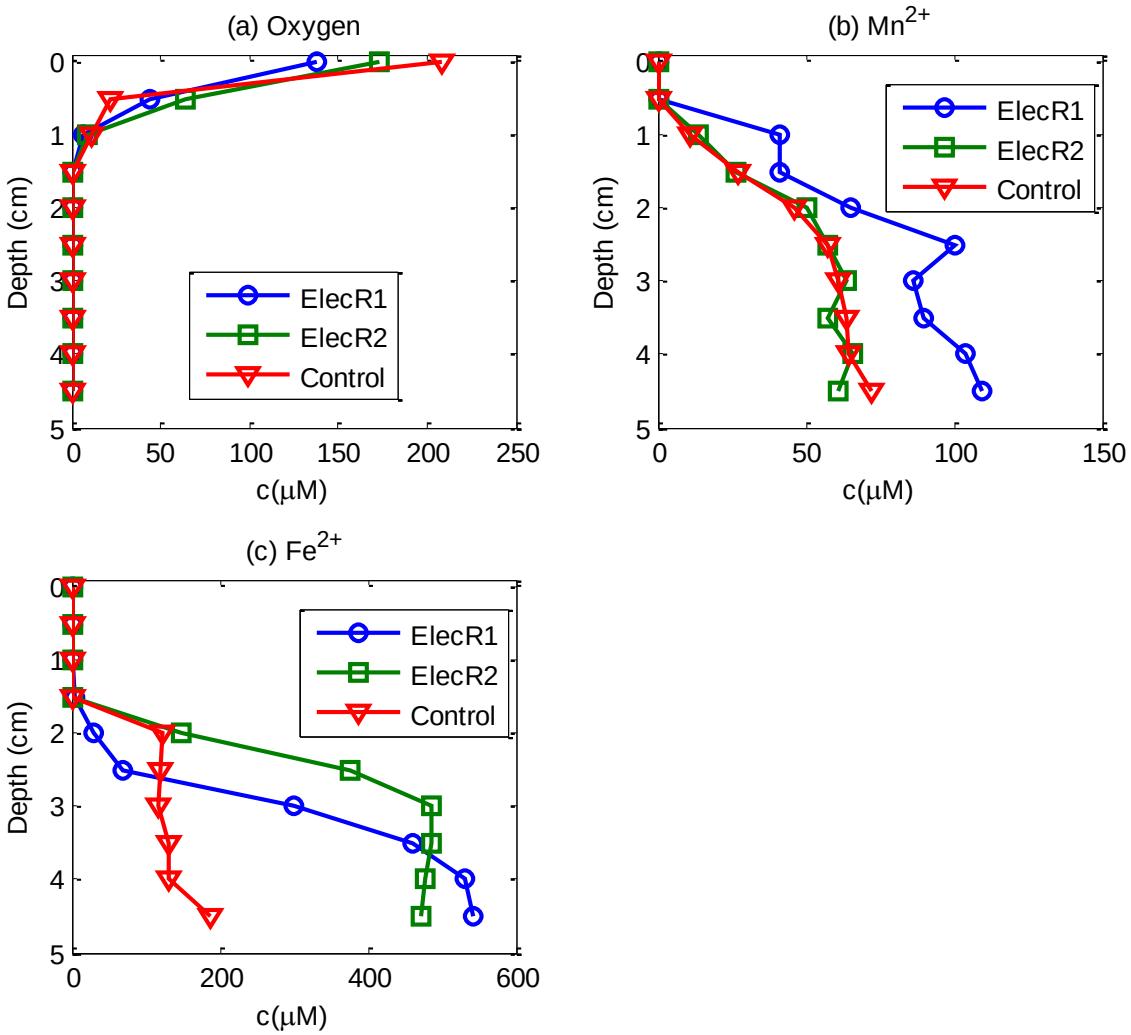

Figure 4.4 Vertical profiles of redox-sensitive species in ElecR1, ElecR2 and Control reactors: (a) Oxygen, (b) Mn^{2+} and (c) Fe^{2+}. Sulfide was not detected. Each point represents the mean of triplicate measurements from each electrode, and error bars are not shown for simplicity. Depth zero was the water-sediment interface. Cathode was at d = 0.5 cm and anode was at d = 3 cm. Figures with standard deviation are available in Appendix B.

4.2.2.2 Phenanthrene concentrations and PAH degrading genes

Study on uptake kinetics of phenanthrene by fiber (210/230) revealed that the concentration of phenanthrene in the PDMS coating reached equilibrium in about 10

hours (Appendix B). In this study, 24 hours of equilibration time were used during each measurement.

Porewater concentrations of phenanthrene were determined at different depths every two weeks during the experiment (Figure 4.5). In the superficial sediments (d = 0 and 1 cm), phenanthrene concentration decreased with time in both powered and control reactors due to biodegradation in oxic environment and volatilization loss. The phenanthrene levels in powered reactors were consistently higher than those in control in the superficial sediments because of the difference in initial conditions. Some operational inconsistence during the setup of the experiment might cause the difference in initial conditions.

In the control reactor, phenanthrene concentration in the anode zone (d = 3 cm) didn't change notably, whereas phenanthrene concentration decreased over time around the anode in both ElecR1 and ElecR2 (Figure 4.6). The phenanthrene concentrations were 60% and 71% of their initial concentrations at the end of the experiment for ElecR1 and ElecR2 respectively, but phenanthrene concentration still remained at 90% of initial concentration for control.

As shown in Figure 4.5, phenanthrene concentration at the anode (d = 3 cm) decreased with time, whereas phenanthrene concentration at 1 cm above the anode (d = 2 cm) remained almost unaffected throughout the study period in powered reactors. As a result, phenanthrene concentrations at the anode (d = 3 cm) were lower than those at 1 cm above the anode (d = 2 cm) after several weeks, showing a unique Z-shaped profile in the sediment (Figure 4.7). This phenomenon was not observed in the control reactor. The phenanthrene profile in the control reactor displayed a down gradient from the deeper sediment toward the sediment water interface. The decrease of phenanthrene at the anode and the unique Z-shaped profiles provided evidences that the anode placed in the

sediment could effectively decrease phenanthrene porewater concentration around the anode in the sediment.

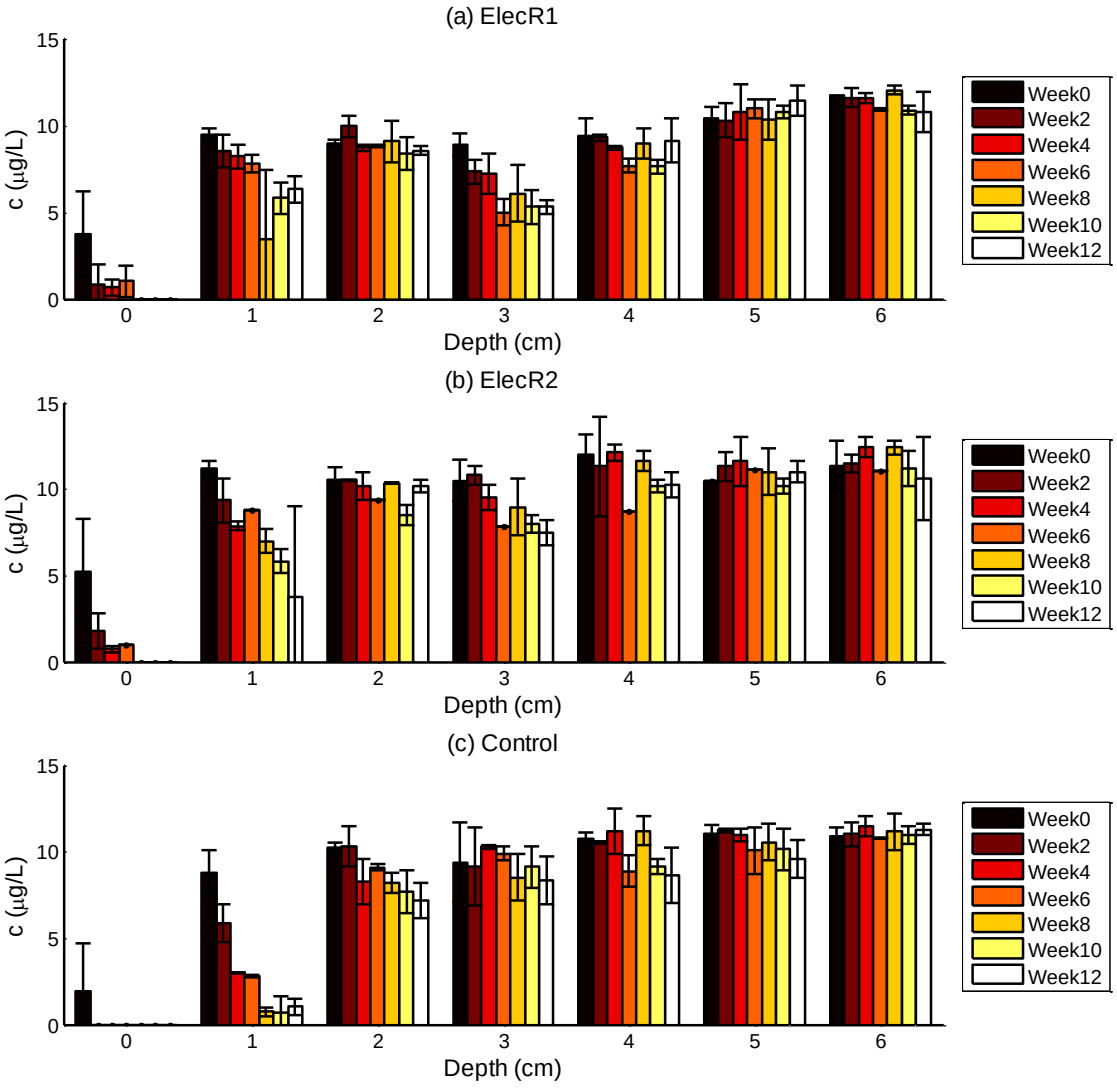

Figure 4.5 Phenanthrene porewater concentration at different depths for (a) ElecR1, (b) ElecR2 and (c) Control. The results are the means of duplicate samples, and error bars represent standard deviations.

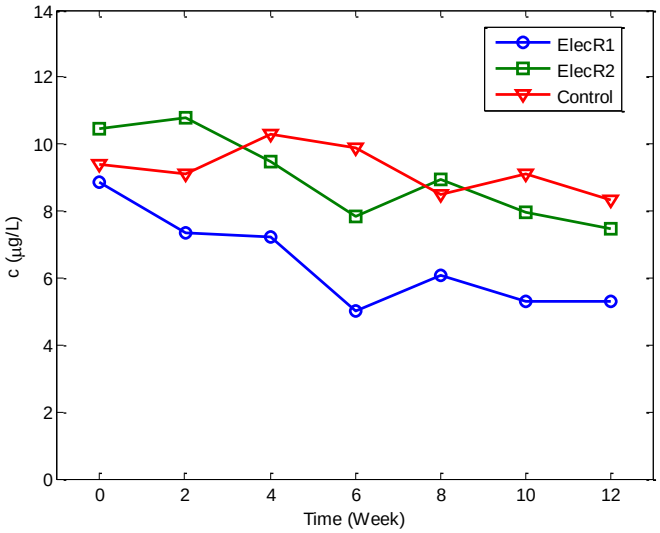

Figure 4.6 Phenanthrene porewater concentration around the anode (d = 3 cm). The results are the means of duplicate samples, and error bars are not shown for simplicity.

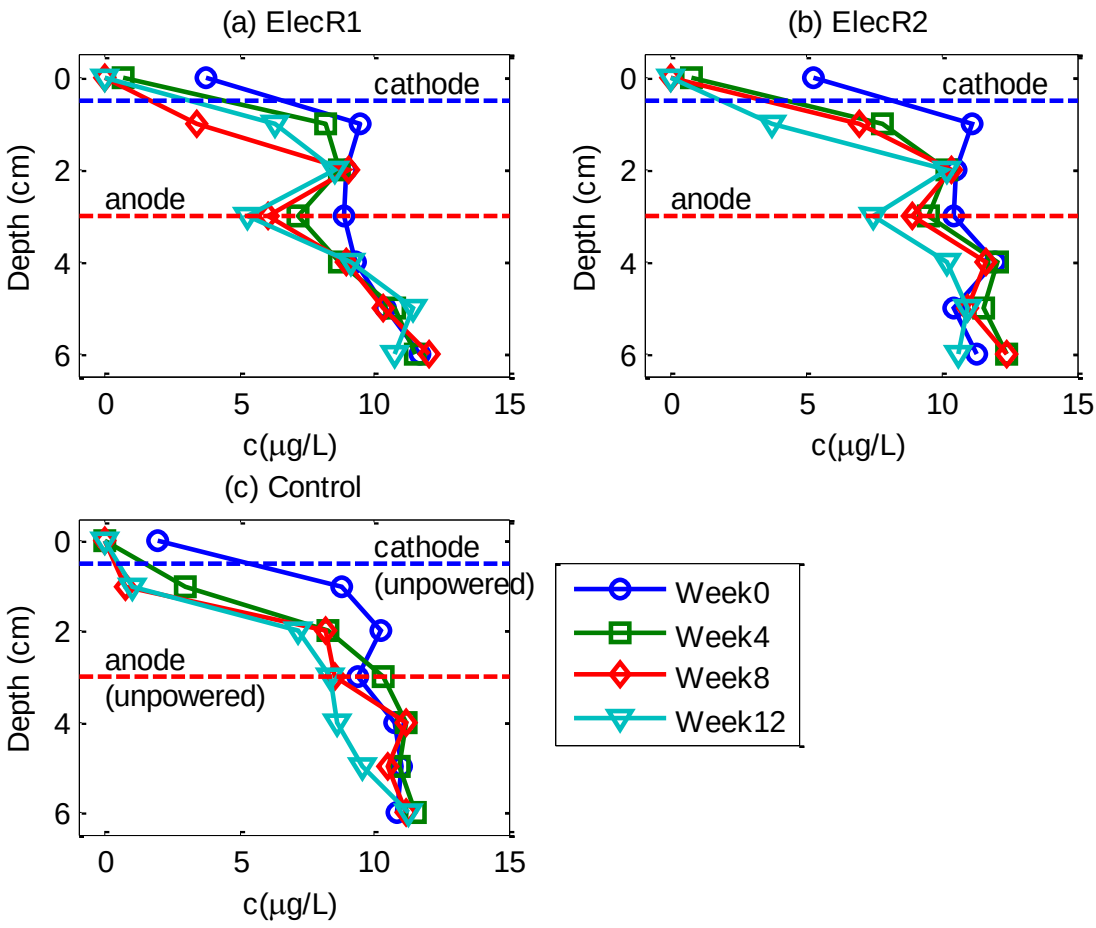

Figure 4.7 Vertical profiles of phenanthrene porewater concentration in (a) ElecR1, (b) ElecR2 and (c) Control reactors. Depth zero was the water-sediment interface. Cathode was at d = 0.5 cm and anode was at d = 3 cm. The results are the means of duplicate samples, and error bars are not shown for simplicity.

PAH degrading genes were quantified by qPCR for sediment at the depth of 0-0.5 cm above the anode, 0-0.5 cm below the anode and sediment at the bottom for each reactor (Figure 4.8). Because no apparent loss of phenanthrene was observed at the bottom sediment for all the reactors, the level of genes at this depth could be potentially used as the baseline for comparison. Specifically, all PAH degrading genes were reported

as an increase from the level of genes at the bottom sediment of ElecR1. The results show that the gene levels in the vicinity of the anode in ElecR1 increased by about 2 times, but there was no significant increase of genes in ElecR2 and control reactor. It is not clear why ElecR1 and ElecR2 behaved differently although it could be as simple as differences in current (but not measured). The lack of current measurements may have contributed to an inability to determine why ElecR1 performed better than ElecR2. A considerable increase of PAH degrading genes was not observed in this study despite the decrease of phenanthrene levels. It is possible that low PAH concentration may not provide enough selective pressure for PAH-degrading bacteria so the growth of these bacteria was slow. Although PAH was utilized as carbon sources, the growth of PAH-degrading bacteria didn't reach the exponential phase. Therefore an evident increase of gene levels was not detected in this study.

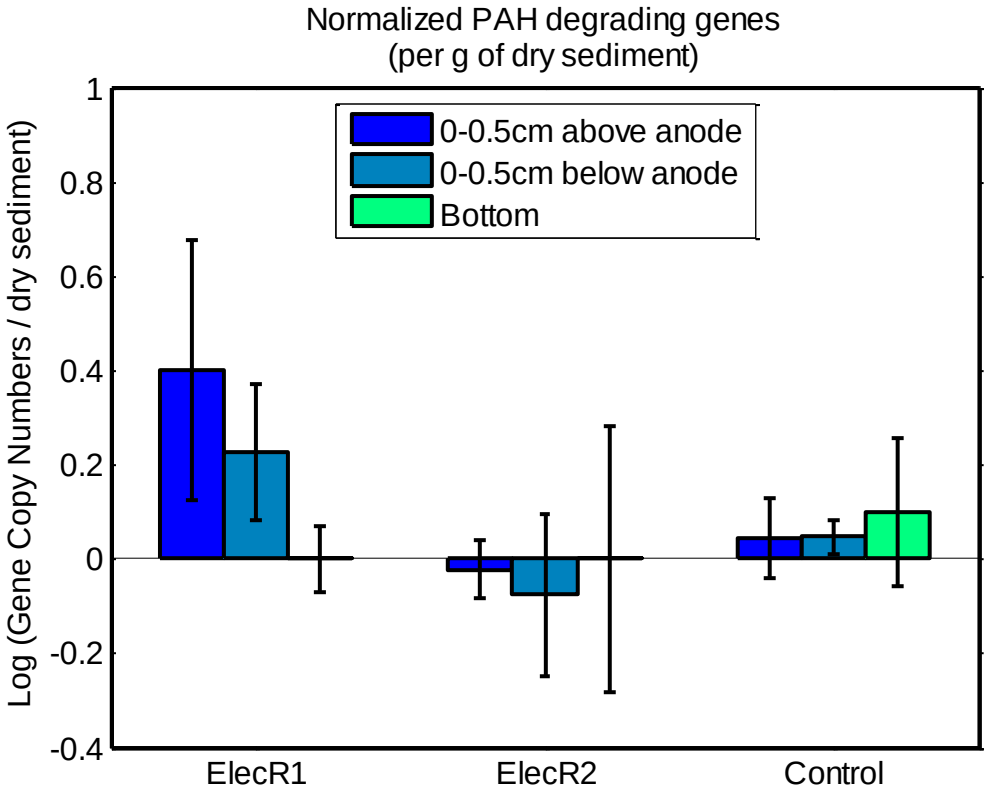

Figure 4.8 PAH degrading gene abundance by qPCR quantification at a depth of 0-0.5 cm below the anode, 0-0.5 cm above the anode, and in the bottom sediment in ElecR1, ElecR2, and Control. The PAH-RHD$_\alpha$ GN gene levels were normalized by the weight of dry sediment. All the values were reported as an increase from the level of genes at the bottom sediment of ElecR1. The results are the means of triplicate samples, and error bars represent standard deviations.

4.3 PAH DEGRADATION AND REDOX CONTROL IN ELECTRODE ENHANCED SAND CAPS

4.3.1 Materials and methods

Three 400-mL beaker reactors were used to evaluate the ability of carbon electrodes to control the redox potential and encourage PAH degradation in a simulated static sand cap placed over contaminated sediment. One reactor served as a no-applied electricity control (Control) while electricity was applied to the other two (ElecCap1 and

ElecCap2) through cloth electrodes in a layer composed of sand and a 10% mixture (mass basis) of siderite to serve as a buffer. In one of the two (ElecCap2), a 0.3-mm layer of siderite was also applied at the sediment and anode interface to aid in buffering.

The reactors were filled with sieved (2 mm) sediment (mixture of contaminated Anacostia River sediment and clean University Lake sediment, ratio 1:7). The sediment was spiked with phenanthrene and naphthalene at a level of ~70 μg/g concentration for both compounds. A 5cm×5cm woven carbon cloth (Graphite felt, Wale Apparatus Co, Hellertown, PA) was placed on top of the sediment as the anode. A 3.5-cm layer of sieved (0.425 mm) concrete sand (Riccelli Enterprises, Rush, NY) was placed over the anode and a second, identical, carbon cloth was placed on the sand layer as the cathode. A 0.5 cm sand layer was overlain on the cathode. The sand layers were saturated with electrolyte (2 mM NaCl and 2 mM Na_2SO_4 mixed electrolyte) initially. Water lost due to evaporation was periodically replenished with deionized water to maintain the original salt composition.

The graphite electrodes were connected to copper wires and sealed with liquid electrical tape as previously described. Powered reactors were connected to 2 V Extech 382202 DC power supply (Extech Instruments Corp., Waltham, MA), and external power was continuously applied for ~10 weeks except during microelectrode measurement. The anode and cathode of ElecCap2 were switched between day 56 to day 58 and day 66 to day 69 to test if alternating anode and cathode could reverse or reduce pH changes.

The current for ElecCap1 was initially ~200 μA and gradually dropped to ~100 μA possibly due to precipitation at the cathode (Franz et al., 2002). The current of ElecCap2 was about 200-250 μA through the entire course of the experiment.

pH was measured by MI-405 standard pH microelectrode and ORP was measured by Pt microelectrode as previously described. Vertical profiles of pH and ORP from the water-sand interface to a depth of 60 mm with 5 mm intervals were acquired.

Redox-sensitive species (O_2, Fe^{2+}, Mn^{2+}, and S^{2-}) were analyzed electrochemically as previously described.

Porewater concentration of phenanthrene was measured by PDMS-coated fiber as previously described.

At the end of the experiment, sediment cores were collected and dissected into 0.5 cm or 1 cm long subsamples and stored at -20 °C until further analysis.

Naphthalene and phenanthrene concentration of sediment samples was determined using a modified version of EPA Method 3550. Sediment samples were weighed, and mixed with sodium sulfate to disperse the particles and absorb excess water. 60 mL of hexane/acetone (volume ratio 1:1) were added to the jar and sonicated for 30 minutes to extract the PAHs. A 2-mL aliquot of hexane/acetone was added to a 5-mL blow down vial, and then evaporated with a Labconco (Kansas City, MO) Model 79100 RapidVap nitrogen Evaporation System to a volume of ~200 μL and reconstituted to a volume of 2 mL with acetonitrile. The vial was mixed thoroughly, blown down to the final volume, and analyzed.

DNA was extracted and qPCR was performed as previously described.

4.3.2 Results and discussion

4.3.2.1 Redox control, pH changes and redox-sensitive species

Figure 4.9 shows the observed changes in redox conditions after application of power. The average ORP in the sediment layer near the unpowered anode (d = 4-6 cm) in control reactor was ~90 mv, while those in the powered microcosms, ElecCap1 and

ElecCap2, were ~150 mv and ~190 mv, respectively. The increase of ORP in ElecCap1 was less than that of ElecCap2 because of the smaller current in ElecCap1 and consequently smaller proton and oxygen production rate at the anode. Although redox potential increased in the vicinity of the anode, the ORP at the cathode didn't decrease dramatically. Redox potentials around the cathode were maintained above 300 mv for all the three reactors. The cathode placement near the interface with the overlying water was sufficient maintain oxidizing conditions near the cathode.

The pH profile in the sand cap demonstrated a similar change in ElecCap reactors (Figure 4.10). On day 0, the pH between the anode and cathode in all reactors varied from around 7 in the deeper sand/sediment to 9 at the surface. After 2 V potential was applied, the pH gradient through the cap was established: pH in the vicinity of the anode dropped while pH near the cathode increased slightly. pH in the sediment layer of ElecCap1 and ElecCap2 dropped to 6 and 5.7, respectively. The additional buffer in ElecCap2 likely aided in minimizing the pH change in ElecCap2, despite a higher current flow. The pH in the control reactor remained relatively steady with time and depth.

The relatively poor level of pH control using the siderite buffer led to investigation of an alternative means of pH control, switching the anode and cathode of ElecCap2 for a short period (2-3 days) to test the ability to recover pH. Although a pH of 5.7 should not lead to total inhibition of bacterial activity (Kastner et al., 1998), neutralization of soil and sediment is generally considered to be favorable for the degradation of mineral oil components by bacteria. pH at day 69 was measured after the anode and cathode were switched (anode at d = 0.5 cm and cathode at d = 4 cm) for 3 days. pH profile at day 69 shows that pH recovery was achieved by this method. pH around the anode was neutralized to ~6.6 from ~5.7, and pH around the cathode dropped to ~7.2 from ~9. In general, pH was maintained between 6.3 to 7.2 along the vertical

profile. Although the goal of pH neutralization was achieved by this method, oxidized redox conditions developed around the anode diminished somewhat. ORP around the anode at day 70 decreased to ~110 mv from ~150 mv, only slightly higher than that in the control.

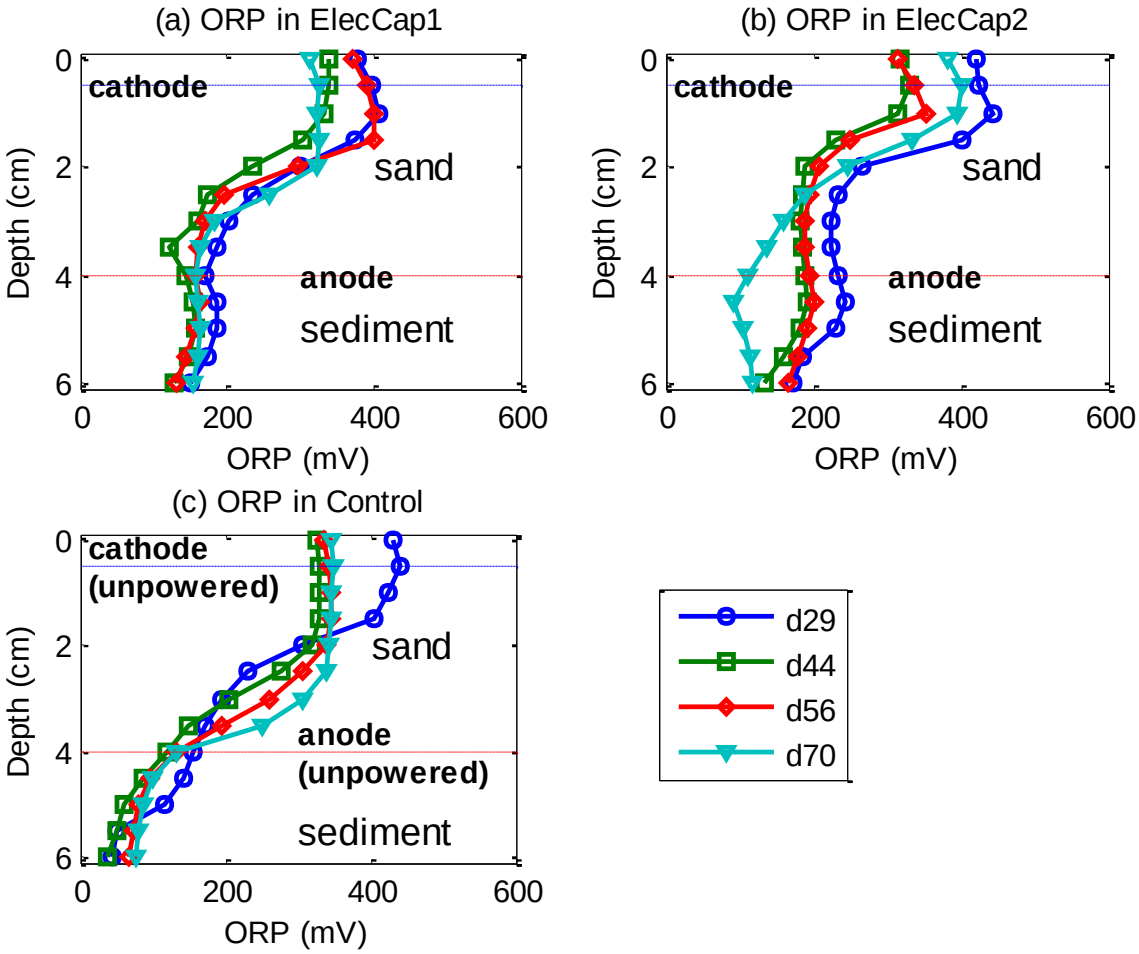

Figure 4.9 Vertical profiles of ORP in (a) ElecCap1, (b) ElecCap2 and (c) Control reactors. Depth zero was the water-cap interface. Cathode was at d = 0.5 cm and anode was at d = 4 cm. All the measured profiles are in Appendix B.

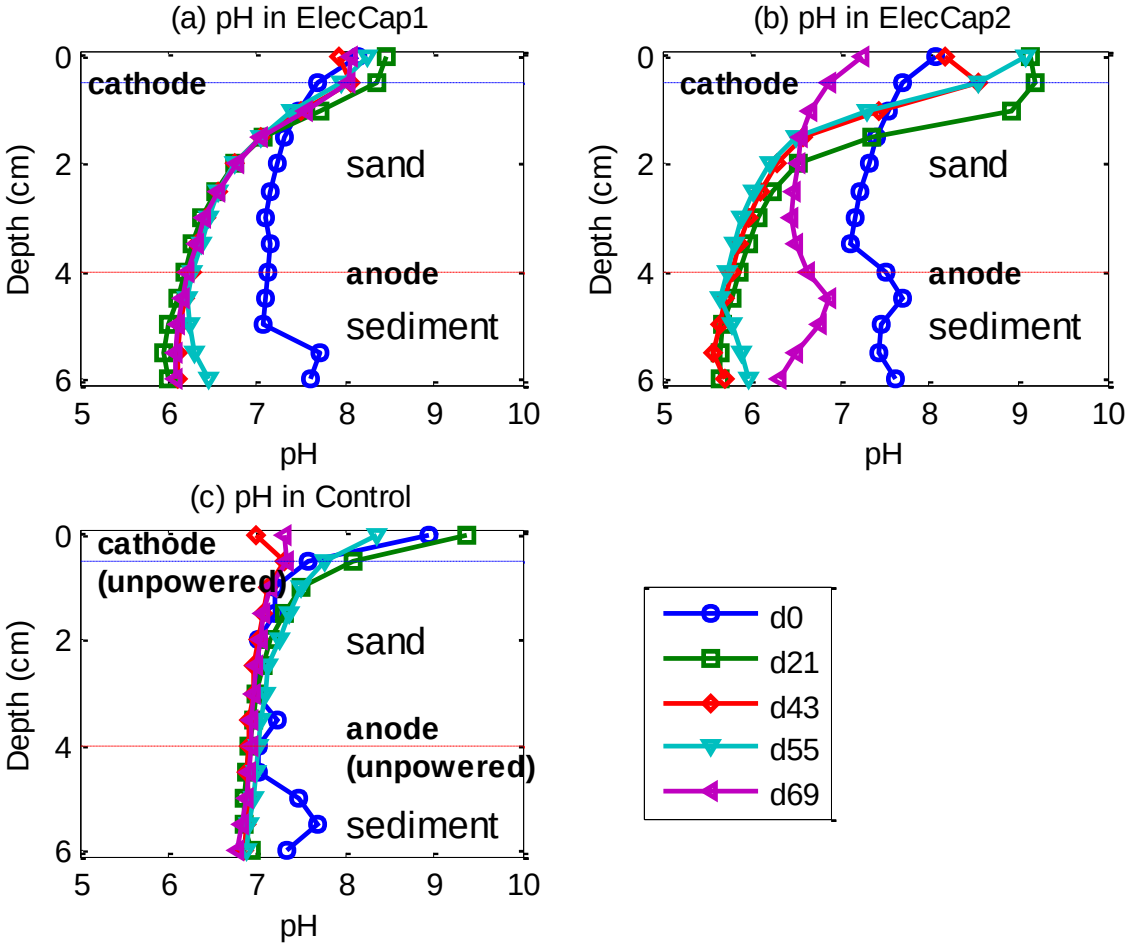

Figure 4.10 Vertical profiles of pH in (a) ElecCap1, (b) ElecCap2 and (c) Control reactors. Depth zero was the water-cap interface. Cathode was at d = 0.5 cm and anode was at d = 4 cm. All the measured profiles are in Appendix B.

The concentrations of redox-sensitive species were measured at day 50 when steady state was achieved. As shown in Figure 4.11, there was almost no difference for oxygen and Mn^{2+} profiles between powered reactors and control. Compared with oxygen profiles in the sediments (Figure 4.4), oxygen penetrated deeper beneath the water-cap interface in the capping layer. In the sediment, oxygen levels were almost zero at 1 cm beneath the water-sediment interface, whereas oxygen levels were still 6 – 16 % at the

same depth in the capping layer. Dissolved oxygen penetration depth in sediments is controlled by aerobic heterotrophic activity, reoxidation of reduced compounds produced by anaerobic mineralization, and transport by diffusion, advection and bioturbation (Burdige, 2007). The deeper penetration depth in sand capping was mainly due to lower organic carbon content of sand cap, and thus less microbial activities.

Similarly to the observations in the experiment of sediments with electrodes, the concentrations of ferrous iron in the sand/sediment in both electrode enhanced capping reactors were higher than that in control, especially in ElecCap2. Since pH of ElecCap2 was only ~5.7 compared with circumneutral pH in control, this observation confirmed that ferrous iron was release from solid phase under acidic conditions in electrode enhanced capping reactors.

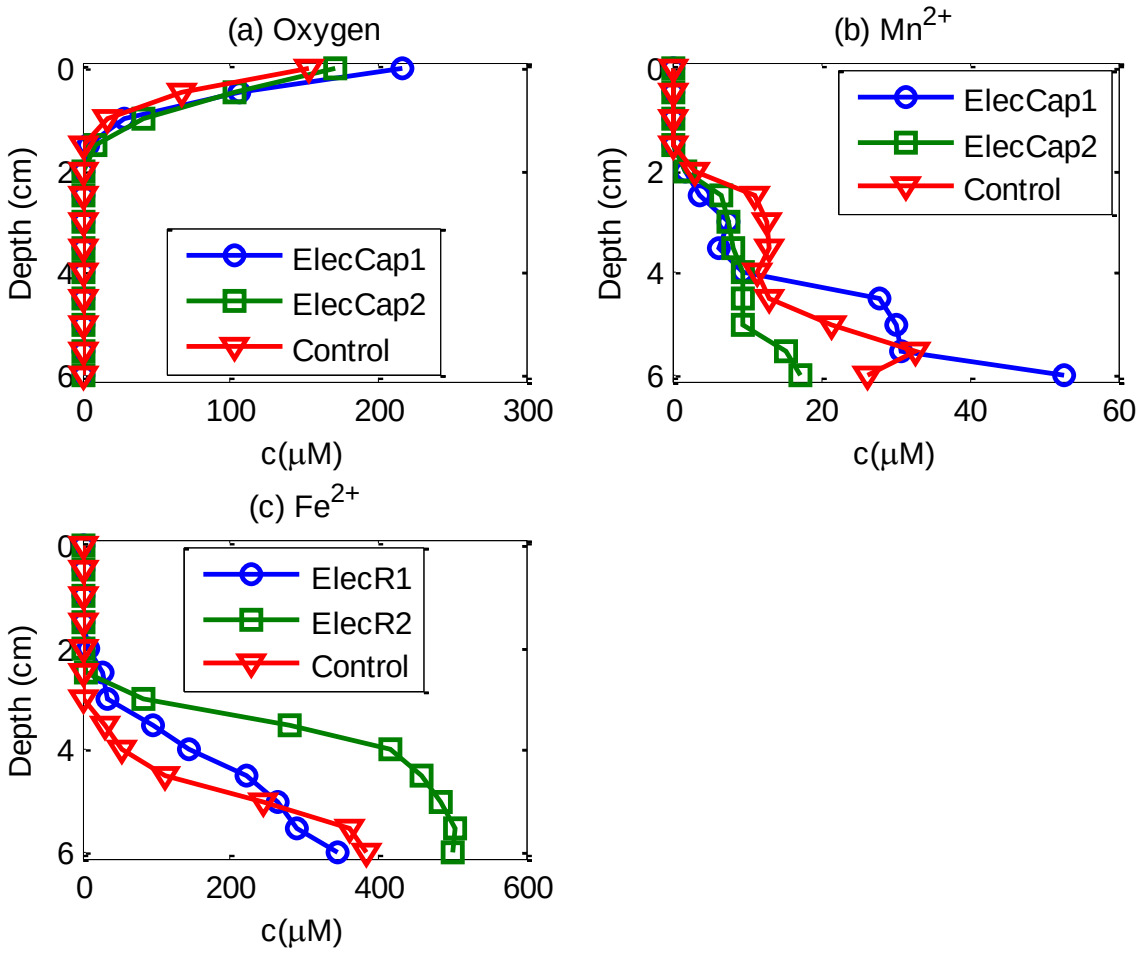

Figure 4.11 Vertical profiles of redox-sensitive species in ElecCap1, ElecCap2 and Control reactors: (a) Oxygen, (b) Mn^{2+} and (c) Fe^{2+}. Sulfide was not detected. Each point represents the mean of triplicate measurements from each electrode, and error bars are not shown for simplicity. Depth zero was the water-cap interface. Cathode was at d = 0.5 cm and anode was at d = 4 cm. Figures with standard deviation are listed in Appendix B.

4.3.2.2 PAH concentrations and PAH degrading genes

PAH degradation experiments in electrode enhanced cap simulators were conducted for about 10 weeks. From week 0 to week 6, the PDMS fibers were cut into 1 cm pieces, so the spatial resolution of phenanthrene profile was 1 cm. The average

porewater concentration of phenanthrene at the following four depths were obtained during this period: 1) in the sand at 0-1 cm above the anode; 2) in the sediment at 0-1 cm below the anode; 3) in the sediment at 1-2 cm below the anode; 4) in the sediment at 2-3 cm below the anode. From week 8 to week 10, spatial resolution was changed to 0.5 cm in the vicinity of the anode. For ease of comparison, average concentrations at a spatial resolution of 1 cm were still used in Figure 4.12. With the assumption of local equilibrium, the porewater concentration of phenanthrene can be used as an indicator for the total concentration of phenanthrene in the sediment/sand. At deeper sediment (1-3 cm below the anode), porewater concentration of phenanthrene remained unchanged in the control reactor and two ElecCap reactors. However, in the vicinity of the anode, phenanthrene concentration decreased over time in both sediment and sand for two ElecCap reactors, and its concentrations remained constant in the control reactor (Figure 4.13). It was also observed that phenanthrene concentration decreased from an initial value of ~35 μg/L to ~20 μg/L after about 1 month and then increased to ~25 μg/L at the end of the experiment for both ElecCap reactors. The heterogeneous nature of the biodegradation gave rise to uncertainty in the measurement as shown in Figure 4.12. Phenanthrene concentration was averaged in 1 cm section in Figure 4.13; however, there was a steep concentration gradient within this 1 cm segment as revealed by the profiles with 0.5 cm resolutions at week 8 and week 10 (Figure 4.14). At d = 0.75 cm in ElecCap1 and ElecCap2 reactors, phenanthrene concentrations were still about the same as their initial concentration (~35 μg/L), but at d = 0.25 cm, the concentrations decreased to about 20 μg/L. This implied that biodegradation was limited within sediment immediately adjacent to the anode (< 1cm separation). Although the increase of redox potential was observed in a broader area, biodegradation was not significantly accelerated beyond the most adjacent sediment layer.

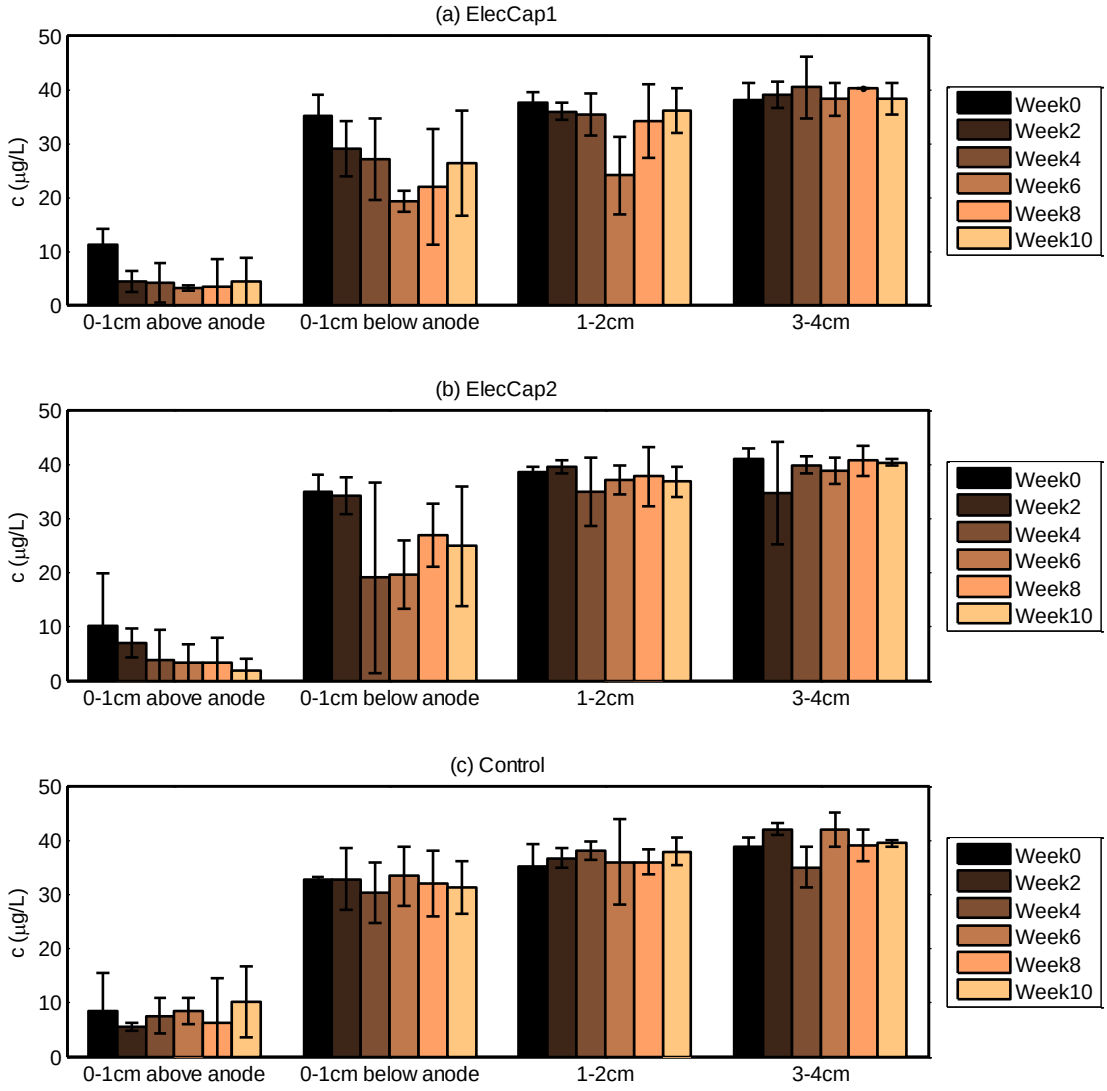

Figure 4.12 Phenanthrene porewater concentration at different depths for (a) ElecCap1, (b) ElecCap2 and (c) Control. The results are the means of duplicate samples or four samples, and error bars represent standard deviations.

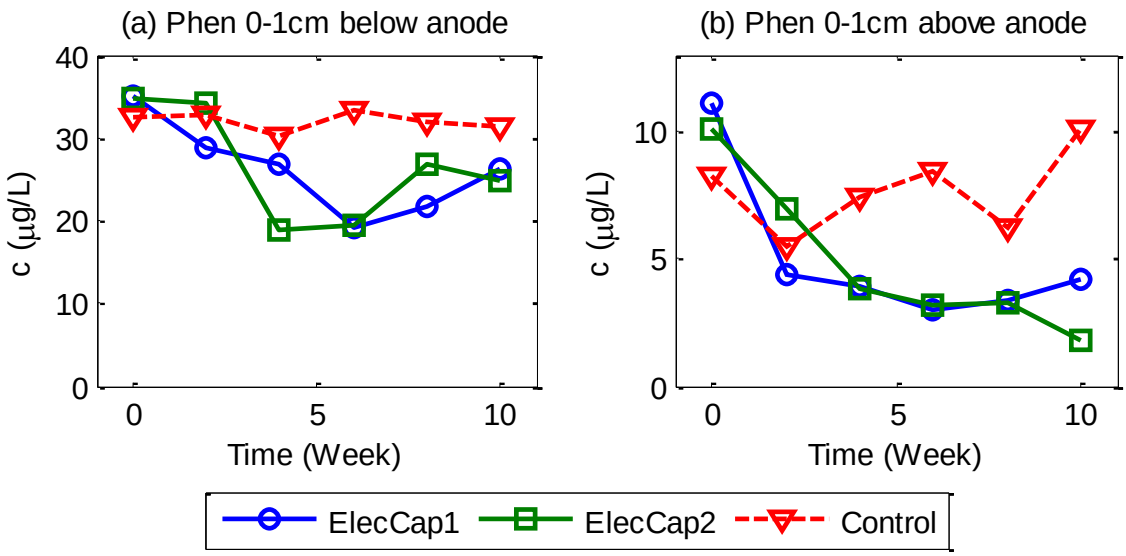

Figure 4.13 Phenanthrene porewater concentration around the anode: (a) 0-1 cm below the anode; (b) 0-1 cm above the anode. The results are the means of duplicate samples, and error bars are not shown for simplicity.

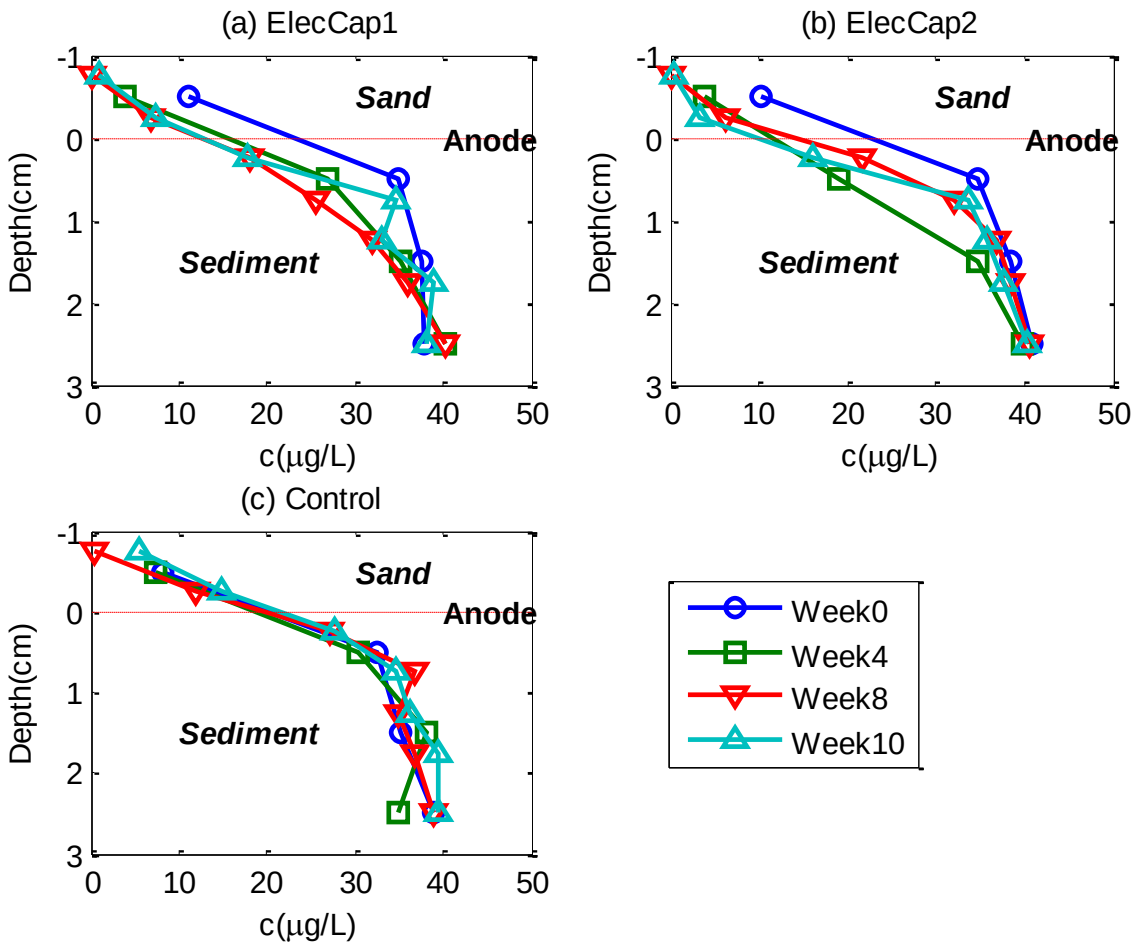

Figure 4.14 Vertical profiles of phenanthrene porewater concentration in (a) ElecCap1, (b) ElecCap2 and (c) Control reactors. Depth zero was the cap-sediment interface. Anode was at the interface. The results are the means of duplicate samples, and error bars are not shown for simplicity.

Phenanthrene and naphthalene sediment concentrations in the sediment were quantified at the end of the experiment. Table 4.2 shows that phenanthrene levels at a depth of 0-0.5 cm below the anode were 77% and 72% of that in the deeper sediment for ElecCap1 and ElecCap2, respectively. This was consistent with the porewater measurement by PDMS fiber. The naphthalene concentrations at a depth of 0-0.5 cm

below the anode to that in the deeper sediment were 69% and 46% for ElecCap1 and ElecCap2, respectively.

Table 4.2 Phenanthrene and naphthalene concentration in solid phase

Phenanthrene (μg/g dry sediment)	**Control**	**ElecCap1**	**ElecCap2**
C_0: 0.5-3cm below anode	69.87 ± 4.98	78.47 ± 8.29	66.53 ± 4.80
C_1: 0-0.5cm below anode	61.23 ± 3.34	60.57 ± 2.37	47.68 ± 4.15
C_1/C_0	88%	77%	72%
Naphthalene (μg/g dry sediment)	**Control**	**ElecCap1**	**ElecCap2**
C_0: 0.5-3cm below anode	69.65 ± 13.14	77.39 ± 8.13	70.09 ± 18.35
C_1: 0-0.5cm below anode	45.75 ± 8.20	53.56 ± 3.43	32.58 ± 0.71
C_1/C_0	66%	69%	46%

Results are average values from triplicate samples, and values after ± denote standard deviation.

PAH degrading genes were quantified by qPCR for sediment at the depth of 0-0.5 cm below the anode (Figure 4.15). An increase of PAH degrading genes was observed in two ElecCap reactors compared to the control reactor. The normalized gene copy numbers in ElecCap1 and ElecCap 2 reactors were 7 and 3 times greater than that in the control reactor.

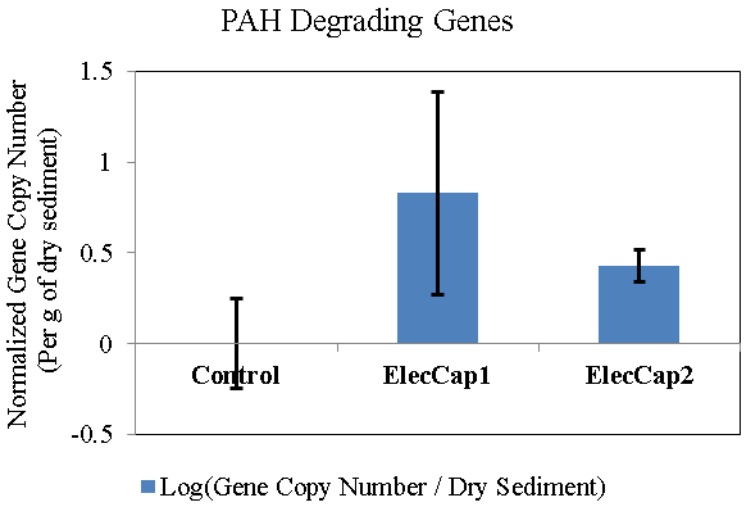

Figure 4.15 PAH degrading gene abundance by qPCR quantification at a depth of 0-0.5 cm below the anode in control, ElecCap1 and ElecCap2 reactors. The PAH-RHD$_\alpha$ GN gene levels were normalized by the weight of dry sediment. All the values were reported as an increase from control reactor. The results are the means of triplicate, and error bars represent standard deviation.

4.4 PAH DEGRADATION AND REDOX CONTROL IN ELECTRODE ENHANCED CAPS WITH BICARBONATE AMENDMENT AS A pH BUFFER

4.4.1 Materials and methods

Four microcosm reactors were used in this study to further investigate PAH degradation and redox control in electrode enhanced caps with the amendment of bicarbonate buffers. The control reactor had no power applied, and the sand caps of control was 1 mm-sieved concrete sand (Riccelli Enterprises, Rush, NY) without any amendment. The external power was applied to the other three reactors through graphite cloth electrodes in the amended sand capping layer. The composition of the amended sand caps was 80 g of siderite, 80 g of calcite, 3.6 g of $NaHCO_3$ and 1 L of 1 mm-sieved concrete sand. It was expected that siderite and calcite would provide long term pH buffering capacity while bicarbonate would provide short term pH buffering capacity.

The reactors were filled with sieved (2 mm) sediment (mixture of contaminated Anacostia River sediment and clean University Lake sediment, ratio 1:6). The sediment was spiked with phenanthrene and naphthalene at a level of ~60 μg/g concentration for both compounds. A 13cm×6cm carbon cloth (Carbon Cloth CC6 Plain, Fuel Cell Earth LLC, Wakefield, MA) was placed on top of the sediment as the anode. A 3.5-cm layer of amended sand was placed over the anode and a second, identical, carbon cloth was placed on the amended sand layer as the cathode. A 0.5 cm amended sand layer was overlain on the cathode. The sand layers of powered and control reactors were saturated with freshwater. Freshwater was made by diluting saltwater by a factor of 150. The saltwater was made by dissolving 35 g of Instant Ocean® sea salts in 1 L of DI water (Stumm and Morgan, 1996). A multi-channel peristaltic pump (Watson Marlow 205s) was used to flow the freshwater into the microcosms.

The graphite electrodes were connected to copper wires and sealed with WEST SYSTEM 105 epoxy resin and 206 slow hardener (WEST SYSTEM, Bay City, MI). Powered reactors were connected to Extech 382202 DC power supply (Extech Instruments Corp., Waltham, MA). Among all the three powered reactors, two of them (CtnCap1 and CtnCap2) were operated in a continuous power mode: an external voltage of ~2 V was applied continuously except during microelectrode measurement; the third powered reactor (IntmtCap) was operated in an intermittent power mode: an external voltage of ~2 V was applied 16 hours continuously over a 24-hour period. The applied voltage and current for all the three reactors are available in Appendix B.

pH was measured by MI-405 standard pH microelectrode and ORP was measured by Pt microelectrode. Vertical profiles of pH and ORP from the water-sand interface to a depth of 55 mm with 5 mm intervals were acquired. Redox-sensitive species (O_2, Fe^{2+}, Mn^{2+}, and S^{2-}) were analyzed electrochemically. Porewater concentration of

phenanthrene was measured by PDMS-coated fiber with 5 mm spatial resolution. At the end of the experiment, sediment cores were collected and dissected into 0.5 cm long subsamples and stored at -20 °C until further analysis. DNA was extracted and qPCR was performed at the end of the experiment. The detailed experimental procedures were described in previous sections in this dissertation.

4.4.2 Results and discussion

4.4.2.1 Redox control, pH changes and redox-sensitive species

With the aid of sodium bicarbonate buffer, pH around the anode was buffered above 6 in all the three powered reactors (Figure 4.16). Compared with control reactor, only a small drop of pH from 6.4 to 6 was observed in the powered reactors. With pH maintained at circumneutral pH, PAH biodegradation rates were expected to be accelerated by the oxygen produced at the anode with less influence of pH shift. While the pH changes were minimized by bicarbonate buffers, the increase of ORP were not as obvious as observed in previous experiments. As shown in Figure 4.17, only ORP in CtnCap1 reactor was over 50 mV higher than that in control. The difference of ORP between the other two powered reactors (CtnCap2 and IntmtCap) and the control was only 10 – 40 mV.

This phenomenon implies that pH and ORP are strongly coupled in the sediments under electrode enhanced capping. The coupled pH and redox changes are governed by a complex array of biogeochemical processes.

First, proton produced at the anode not only resulted in pH drop in sediments but also increased redox potential. This could be explained by Nernst equation of the dominant redox couple in the sediment. Assumed the dominant redox couple was $Fe(OH)_3/Fe^{2+}$ in the sediment, the redox reaction being (4-3).

Thus

$$E_h = E_0 - 3pH + pFe^{2+} \quad (4\text{-}4)$$

Where E_h is the potential of the redox reaction (ORP) and E_0 is the standard redox potential (Stumm and Morgan, 1996).

At the anode, pH drop caused by the production of proton gave rise to ORP according to Equation (4-4). The contribution of pH on redox change might diminish if pH changes disappear.

Second, biogeochemical reactions that involve oxygen produced at the anode also result in the increase of redox potential and the decrease of pH. Take the dominant redox couple $Fe(OH)_3/Fe^{2+}$ as an example, Fe(II) oxidization by oxygen reduced the level of Fe(II), consequently increasing ORP according to Equation (4-4). For pH changes, many oxidation reactions by oxygen in the sediment lead to the release of proton, such as the organic matter oxidation process as follows (Bender and Heggie, 1984):

$$(CH_2O)_{106}(NH_3)_{16}(H_3PO_4) + 138\,O_2 = 106\,CO_2 + 16\,HNO_3 + H_3PO_4 + 122\,H_2O \quad (4\text{-}5)$$

In this study, oxygen and proton were always produced at the same time at the anode, and it was difficult to accurately distinguish the net effect of each species and every process involved. Nevertheless, all the observations consistently display an increase of ORP around the anode, indicating a possible shift in favor of PAH biodegradation.

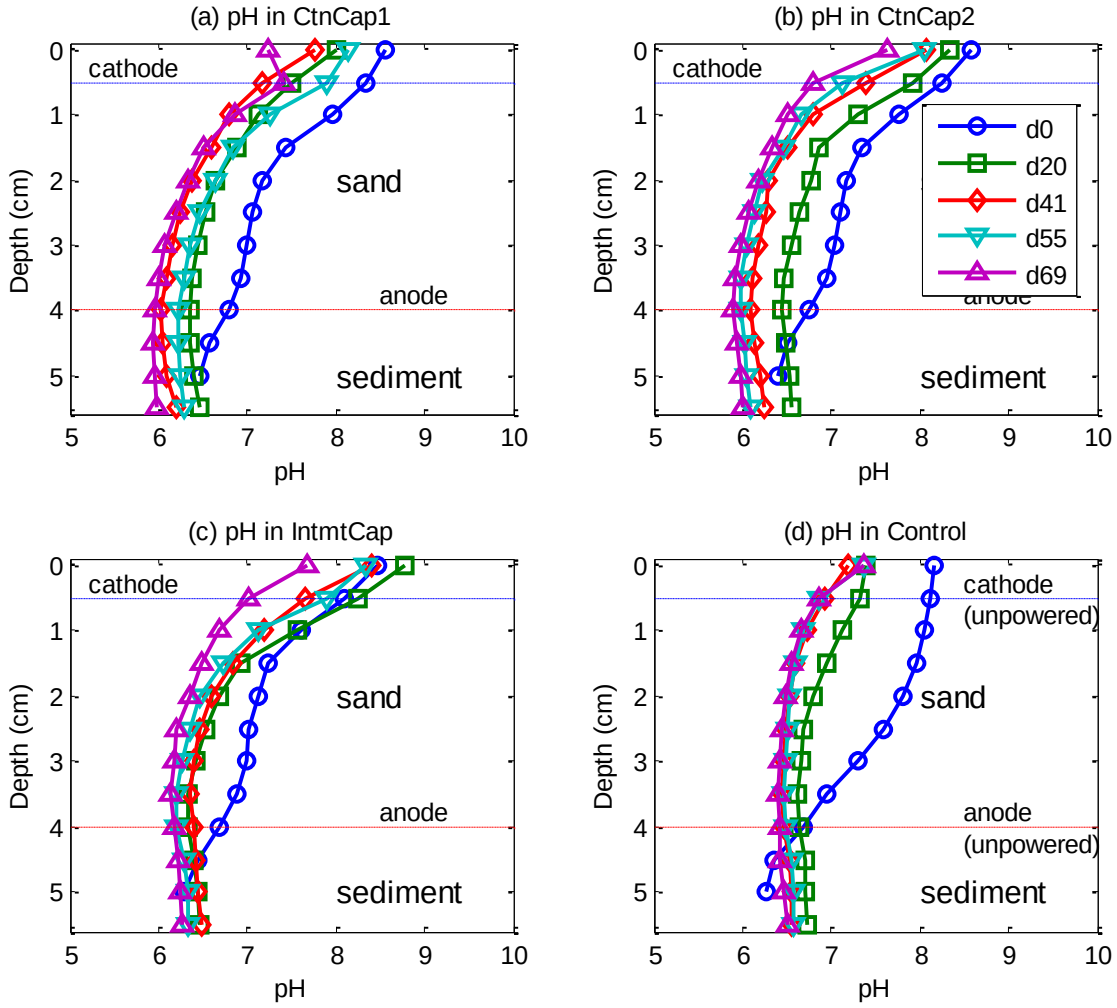

Figure 4.16 Vertical profiles of pH in (a) CtnCap1, (b) CtnCap2, (c) IntmtCap and (d) Control reactors. Depth zero was the water-cap interface. Cathode was at d = 0.5 cm and anode was at d = 4 cm. All the measured profiles are in Appendix B.

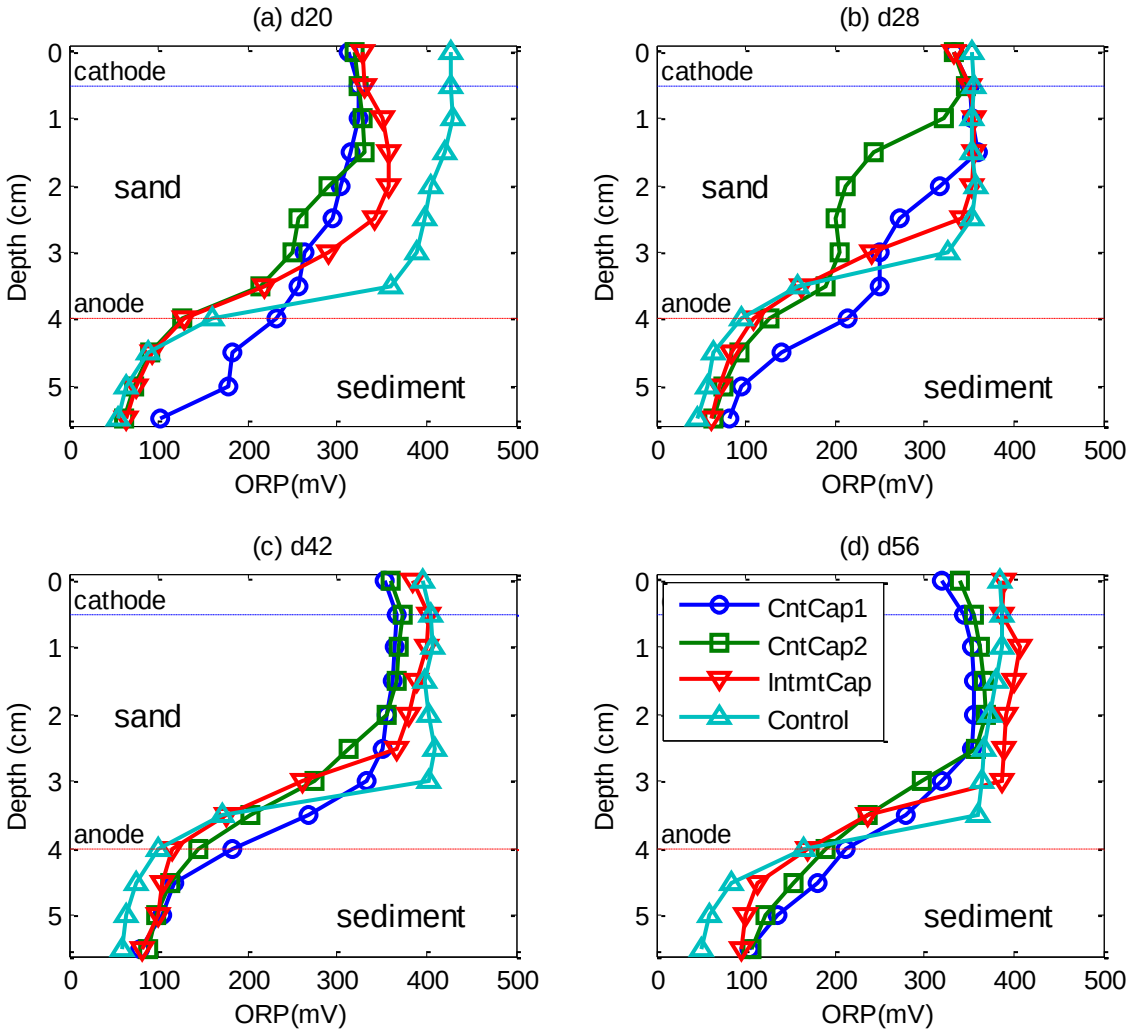

Figure 4.17 Vertical profiles of ORP at (a) Day 20, (b) Day 28, (c) Day 40 and (d) Day 68. ORP values were versus standard hydrogen electrode (SHE). Depth zero was the water-sand interface. Cathode was at d = 0.5 cm and anode was at d = 4 cm. All the measured profiles are in Appendix B.

Profiles of redox-sensitive species at day 37 (Figure 4.18) show that the concentrations of ferrous iron in the powered reactors increased slightly compared with the control reactor, a similar trend as observed in Figure 4.11. The elevated ferrous iron level was considered to be associated with decrease of pH in the powered reactors.

Because of the prevalence of ferrous iron and the absence of sulfide in the sediment beneath the capping layer, it was determined that the predominant terminal electron accepting process (TEAP) was ferric iron reduction for all the powered reactors and control. Although increase of redox potentials was observed in all the powered reactors, the predominant TEAP in the sediments didn't change with electrode enhanced caps.

The voltammetric techniques are able to detect dissolved oxygen with a detection limit of 5 – 25 μM (Brendel and Luther, 1995). But in this study, the voltammetric techniques failed to detect any dissolved oxygen around the anode though oxygen was produced at the anode by water electrolysis reaction. Due to the high sediment oxygen demand, it is unambiguous that only a very thin layer of sediment beneath the anode had detectable levels of oxygen. The thickness of this thin layer with oxygen present remained unknown in this study but it should be in the order of millimeters or less. During the microelectrode measurement, all the microelectrodes were inserted through l-cm-diameter precut openings in the graphite cloth. So it is very possible that the microelectrodes didn't reach the sediment with detectable levels of oxygen. These practical or operational limitations of instruments make it very difficult for in-situ monitoring of oxygen concentration.

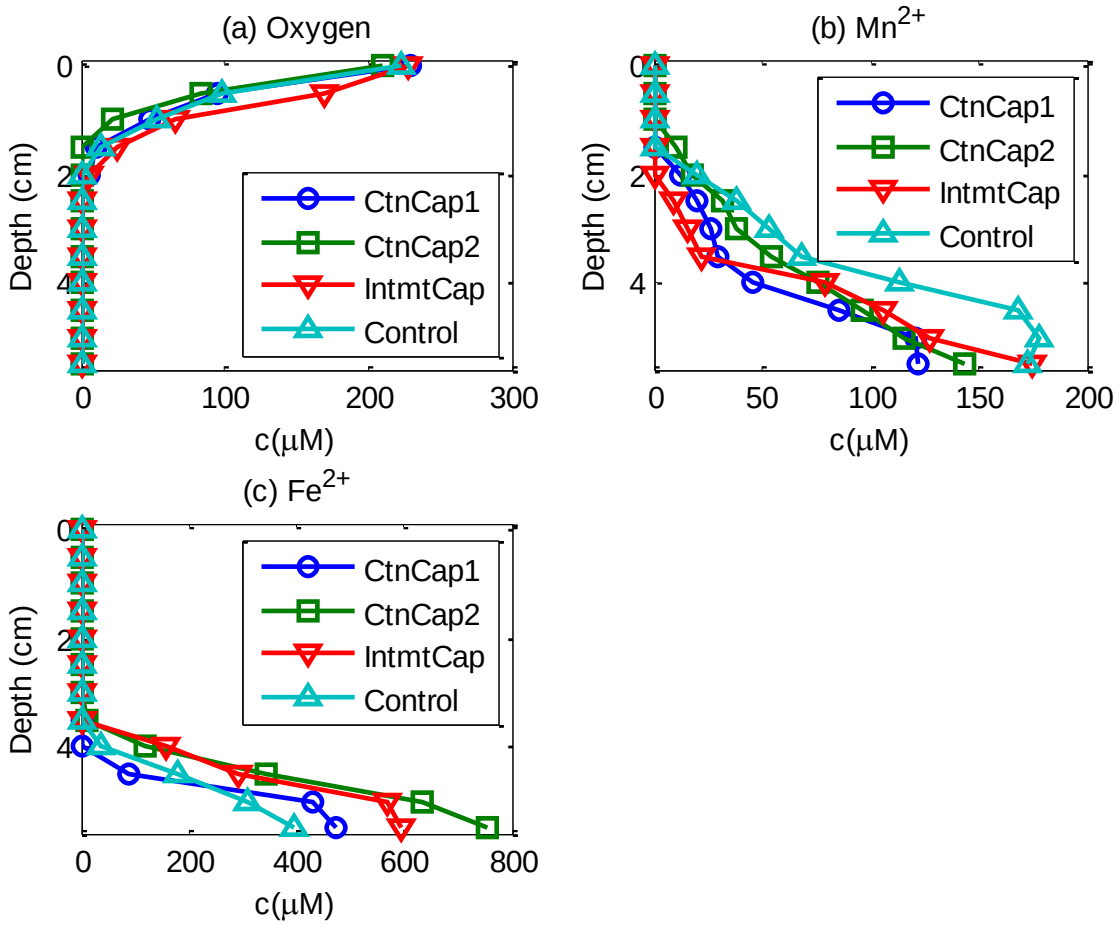

Figure 4.18 Vertical profiles of redox-sensitive species in CtnCap1, CtnCap2, IntmtCap and Control reactors: (a) Oxygen, (b) Mn^{2+} and (c) Fe^{2+}. Sulfide was not detected. Each point represents the mean of triplicate measurements from each electrode, and error bars are not shown for simplicity. Depth zero was the water-cap interface. Cathode was at d = 0.5 cm and anode was at d = 4 cm. Figures with standard deviation are listed in Appendix B.

4.4.2.2 Phenanthrene concentrations and PAH degrading genes

Phenanthrene porewater concentrations were measured with a vertical resolution of 0.5 cm during a period of 70 days. As presented in Figure 4.19, phenanthrene porewater concentration remained fairly constant in the deeper sediments (1 – 3 cm below the anode) in all the powered reactors and control. However, phenanthrene

concentration in the 1 cm vicinity of the anode displays different trends over time between powered reactors and control (Figure 4.20). In the powered reactors, the phenanthrene concentrations at 0.5-1 cm sand above the anode were initially at very low concentration (< 1 μg/L) and almost non-detectable during the rest of the time; the concentrations at 0-0.5 cm sand above the anode were initially ~ 2 μg/L and decreased to less than 0.2 μg/L at the end. On the contrary, in the control reactor phenanthrene concentrations increased over time in the sand above the anode (at both 0-0.5 cm and 0.5-1 cm) due to the diffusion of phenanthrene from the underlying sediment. In the sediments beneath the anode, phenanthrene concentrations decreased over time in powered reactors, whereas phenanthrene concentrations increased slightly (at 0-0.5 cm below the anode) or kept constant (at 0.5-1 cm below the anode) in the control. Not considering the mass in the sand layer, the reduction of phenanthrene mass in the 1 cm vicinity of sediment were 51%, 44% and 47% compared to initial mass for CtnCap1, CtnCap2, and IntmtCap, respectively. In the experiment with no bicarbonate amendment, a lower removal efficiency of phenanthrene (~30%) was observed during a time period of about the same length. This difference of removal efficiency indicated that maintaining pH at the normal range (6-8) may be a critical success factor for effective biodegradation of PAH in electrode enhanced capping.

The low levels of phenanthrene present in the sand layer demonstrated the effectiveness of the electrode enhanced capping as a biobarrier for remediation of contaminated sediment. By placing the anode at the sand-sediment interface, migration of phenanthrene from the underlying sediment was prevented or inhibited considerably. While contaminant may breakthrough conventional sand capping over time, electrode enhanced capping could overcome this limitation by creating a biobarrier at the cap-sediment interface.

qPCR analysis confirmed increased PAH degrading genes in all the three reactors (Figure 4.21), indicating that electrode enhanced capping stimulated microbial PAH biodegradation. The normalized gene copy numbers increased about 2 - 6 fold in powered reactors compared to those in control, which were comparable to the observations in the experiments described in 4.3. Compared with the gene increase observed in the slurry experiment, i.e., nearly 2 orders of magnitude increase, the gene increases in the sediments under electrode enhanced capping were much less. In the slurry experiment, the concentrations of phenanthrene and naphthalene decreased rapidly and thus populations of PAH-degrading bacteria increased significantly. However, in the sediment under the anode, biodegradation occurred slowly. After about 10 weeks, only approximate 30% (no bicarbonate amendment) or 50% (with bicarbonate amendment) of phenanthrene was degraded. It is coherent that the growth of PAH degrading bacteria in the sediment was much slower than that in well mixed slurry systems.

The IntmtCap reactor was running in an intermittent mode: two third of the time with power and one third of the time with no power. The results from phenanthrene concentration show that the biodegradation rates of IntmtCap were almost the same as those of continuous reactors. In addition, IntmtCap even shows a slightly higher level of PAH degrading genes, though it is not conclusive to state that IntmtCap is better than continuous reactors for PAH biodegradation. The success of IntmtCap indicates the flexibility of electrode enhanced capping for remediation of PAH contaminated sediment. For instance, the power can be turned off for a short period to diminish pH changes at the anode. In the field application, if the power is accidently shut down temporally, it is very possible that the effect is not detrimental but can be recovered when the power resumes.

The noticeable increase in PAH degrading genes between powered reactors and control indicated that electrodes placed between sand and sediments worked by

increasing the population of PAH degrading bacteria. This in turn would have led to the accelerated phenanthrene degradation rates discussed previously. This correlation between PAH decrease and gene increase supported microbial biodegradation as a mechanism of decay in electrode enhanced capping. However, a quantitative relationship between PAH removal efficiency and gene increase can't be established with limited data in this study. For instance, the fold changes of genes were between 2 to 6 despite about the same biodegradation rates among all the three powered reactors with bicarbonate amendment; in addition, the results from bicarbonate amendment experiments show relatively higher removal efficiency in the vicinity of the anode, but didn't show significant difference in gene increase compared with the no bicarbonate amendment experiments. Given the uncertainty in biodegradation and the heterogamous nature of the sediments, a correlation between biodegradation rates and gene copy numbers would prove difficult (Baldwin et al., 2008). Nevertheless, the consistent detection of PAH degrading gene increment was seen while PAH biodegradation occurred.

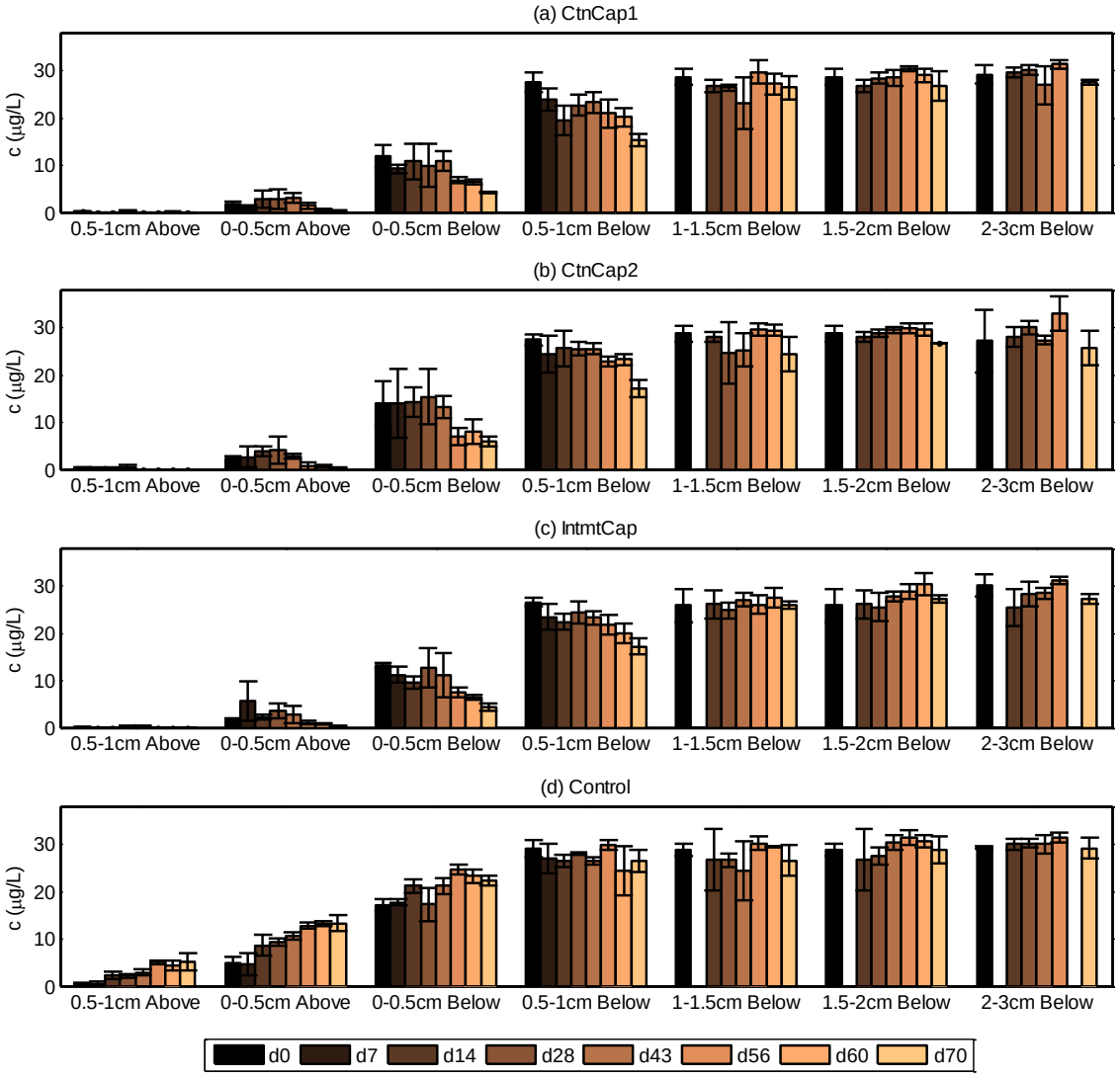

Figure 4.19 Phenanthrene porewater concentration at different depths for (a) CtnCap1, (b) CtnCap2, (c) IntmtCap and (d) Control. The results are the means of triplicate samples, and error bars represent standard deviations.

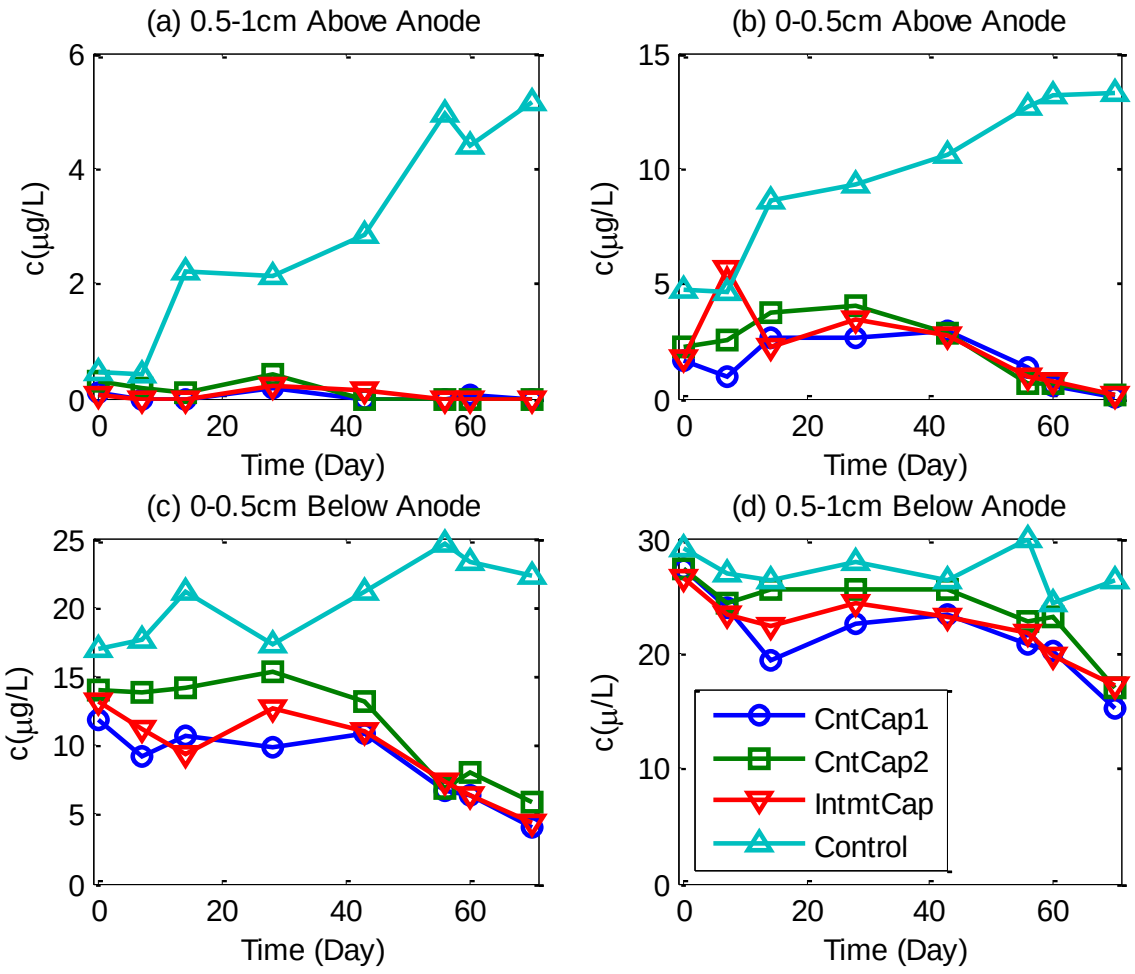

Figure 4.20 Phenanthrene porewater concentration at (a) 0.5–1 cm above the anode, (b) 0-0.5 cm above the anode, (c) 0-0.5 cm below the anode and (d) 0.5-1cm below the anode. The results are the means of triplicate samples, and error bars are not shown for simplicity.

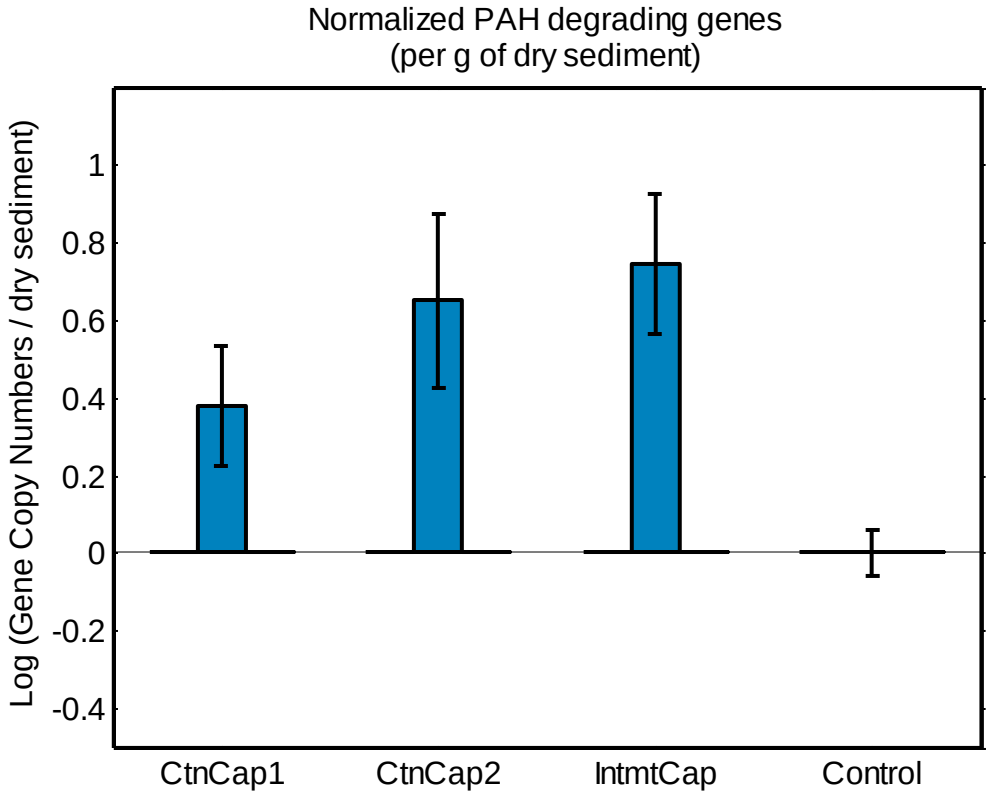

Figure 4.21 PAH degrading gene abundance by qPCR quantification at a depth of 0-0.5 cm below the anode in CtnCap1, CtnCap2, IntmtCap and control reactors. The PAH-RHD$_\alpha$ GN gene levels were normalized by the weight of dry sediment. All the values were reported as an increase from control reactor. The results are the means of triplicate, and error bars represent standard deviation.

4.4.2.3 Cost analysis

It is too early to develop verifiable cost scenarios for electrode enhanced capping at this initial stage in the development of the technology. However, certain preliminary estimates have been attempted to assess the potential cost-effectiveness of this technology. The additional capital costs (compared to conventional capping) mainly include the energy cost and the material cost of electrode materials. In the experiment of electrode enhanced capping with bicarbonate amendment, the energy costs for three

powered reactors ranged from 0.35 to 0.5 mW. Considering an electrode area of ~78 cm^2, the energy cost per unit area was only 45-64 mW/m^2, i.e. 0.39-0.56 kWh/m^2. The average retail price of electricity to ultimate customers of US in 2011 was 9.99 cents per kWh (US EIA, 2012). So the additional cost for energy of electrode enhanced capping is about 3.9-5.6 c/m^2, i.e. $158-$227 per acre, only a very insignificant portion of the total cost of in-situ capping. Typical costs of large-scale cap applications are approximately $17–$21/m^2 plus the cost of materials (Reible, 2004). In total, the overall placement cost of electrode enhanced capping is about $30/$m^2$, which is similar to the use of a reactive core mat (McDonough et al., 2007).

The use of solar panels (photovoltaic modules) as a power supply for chemical /electrochemical systems and remote sensors has previously been reported (Hart and Martinez, 2006; Schafer et al., 2007; Park et al., 2008). Solar panels as a power supply has almost zero pollution, low maintenance cost and a long life, and can be used as a power source for electrode enhanced capping. To avoid energy fluctuations and for working during night hours, solar panels need to be connected to a storage battery. The output of a single solar panel with 40 solar cells ranges from 10 to 300 watts (US DOE, 2011). Because of its low power requirement, a single solar panel can power a large area of electrode enhanced capping. If the power requirement is 45-64 mW/m^2 as previously discussed, a solar panel with a capacity of 100 W can power an area of 1560-2229 m^2. So a one-acre area needs only 2-3 solar panels of 100 W for the application of electrode enhanced capping.

These analyses shows that electrode enhanced capping can be a cost-effective and sustainable remediation technology for the management of contaminated sediment. Of course, for successful application to a specific site, feasibility studies to characterize the site hydraulics and geochemical parameters need to be performed, and operating

parameters will likely need to be optimized before scaling up from bench scale to field scale.

4.5 CONCLUSIONS

The results in this study show that electrode enhanced capping can be used to control redox potential in a sediment cap, provide microbial electron acceptor, and stimulate PAH degradation.

Microcosm study was first implemented in the sediments with electrodes placed horizontally at different depths. The ORP around the anode in powered reactors increased gradually, and was 50 – 150 mV higher than that in the control. pH around the anode decreased to ~6 from an initial value of 6.4 or 6.7 in powered reactors. Phenanthrene concentration at the anode decreased with time, showing a unique Z-shaped profile in the sediment in powered reactors. These observations provided evidences that the anode placed in the sediment could effectively decrease phenanthrene porewater concentration around the anode.

PAH biodegradation and redox control by electrode enhanced capping were further studied in simulated microcosm reactors. Two carbon cloth electrodes were emplaced within a sediment cap with an applied potential of 2 V. In the experiment with no bicarbonate buffer, ORP in the vicinity of the anode increased 60 - 100 mV compared to the control reactor, and pH dropped to 5.7 and 6 from circumneutral pH. Average phenanthrene concentrations decreased to ~ 70% of initial concentration in the 1 cm vicinity of the anode in 10 weeks. In the experiment with bicarbonate buffer, ORP in one powered reactor was over 50 mV higher than that control and the other two displayed less ORP changes. With the aid of bicarbonate buffer, only a small drop of pH from 6.4 to 6 was observed in the powered reactors. The results imply that pH and ORP are strongly

coupled in the sediments under electrode enhanced capping. With pH maintained at circumneutral pH, PAH biodegradation rates were accelerated by the oxygen produced at the anode with less influence of pH shift. The reduction of phenanthrene mass in the 1 cm vicinity of sediment was ~ 50 % compared to initial mass in powered reactors in 10 weeks. qPCR results also show an increase of PAH degrading genes at the depth of 0 - 0.5 cm below the anode. Although these changes are confined to a small layer (< 1 cm), the encouragement of PAH degradation in this layer could reduce PAH migration toward the surface and biota in the sediment and overlying water. These findings demonstrated the capability of this novel technology for the remediation of contaminated sediment.

Chapter 5: Model of Electrode Enhanced Capping

5.1 INTRODUCTION

A model of the electrode enhanced capping was developed to enable prediction of performance to a broader range of conditions than were evaluated experimentally and to make preliminary predictions of long-term performance of an electrode enhanced cap under field conditions. Key goals of the model were to predict performance and behavior as well as power requirements. The application of an external potential across a capping layer causes a very complex set of reaction and transport processes to occur within the system. Numerical simulation of the technology requires a grasp of the physical and chemical phenomena and mathematical formulation of these processes. These processes include electrolysis reactions at the electrodes, geochemical reactions in aquatic sediments and capping layer, electrokinetic processes, and contaminant transport, etc.

Water electrolysis is a major reaction with the application of an external voltage. The production of oxygen at the anode and the generation of pH gradient in the system are all driven by water electrolysis reaction. Their reaction rates are proportional to current as follows (Bard and Faulkner, 2001):

$$\mathrm{Rate(mol/s)} = \mathrm{I/nF} \tag{5-1}$$

Where I is the current, n is the stoichiometric number of electrons consumed in the electrode reaction, and F is Faraday constant.

As shown in (5-1), current is an important parameter in determining the chemical reaction rates at the electrodes. However, controlled-voltage instead of controlled-current technique is generally employed in the application of electrode enhanced capping. So the first step in model develop of electrode enhanced capping is to predict the current based

on applied voltage and other parameters, such as thickness of the capping layer and area of the electrodes.

Once the current is determined, electrode reaction rates can be calculated and they can serve as inputs for the model of transport and reaction processes. Coupled reactive transport modeling simulates the distribution of all important species with time, e.g. pH gradient.

Several mathematical models have been developed to predict transport and reaction processes during electrokinetic remediation (Alshawabkeh and Acar, 1992; Alshawabkeh and Acar, 1996; Shapiro et al., 1989; Shapiro and Probstein, 1993; Haran et al., 1997; Yu and Neretnieks, 1996; Choi and Lui, 1995; Yeung and Datta, 1995; Al-Hamdan and Reddy, 2008). However, many of these models focus on heavy metals extraction by electrokinetic process, and do not accurately account for the geochemistry in the sediment and/or soil. In most of these studies, pH buffering of soil/sand was not considered, and these models are not suitable for electrode enhanced capping due to the high pH buffer capacity of sediment. pH is one of the limiting factors have been recognized to affect the biodegradation of PAH (Das and Chandran, 2011). Therefore it is necessary to build a model that can accurately describe the pH of sediment/sand with the application of an external potential across a capping layer.

In this chapter, a voltage-current relationship is developed first and then a coupled reactive transport model is presented to describe the processes involved and this model can serve as a design tool for electrode enhanced capping.

5.2 VOLTAGE-CURRENT RELATIONSHIP

5.2.1 Model development

Water electrolysis is the primary electrochemical reaction at the electrodes during the application of external power as follows:

$$\text{Anode: } 2H_2O = O_2 + 4H^+ + 4e \qquad E^0 = 1.229V \tag{5-2}$$

$$\text{Cathode: } 2H_2O + 2e = H_2 + 2OH^- \qquad E^0 = -0.827V \tag{5-3}$$

The half-cell potential of the anode reaction (5-2) can be expressed by Nernst equation as follows:

$$E_{anode} = E^0_{anode} + \frac{RT}{4F} * \ln\{p(O_2)[H^+]^4\} \tag{5-4}$$

Where E_{anode} is the half-cell potential of the anode reaction, E^0_{anode} is the standard electrode potential, R is ideal gas constant, T is absolute temperature, $p(O_2)$ is oxygen partial pressure at the anode, and $[H^+]$ is the H^+ concentration at the anode. At pH = 7 and $p(O_2)$ = 1 atm, E_{anode} = 0.816 V.

The half-cell potential of the cathode reaction (5-3) can be expressed by Nernst equation as follows:

$$E_{cathode} = E^0_{cathode} - \frac{RT}{2F} * \ln\{p(H_2)[OH^-]^2\} \tag{5-5}$$

Where $E_{cathodee}$ is the half-cell potential of the cathode reaction, $E^0_{cathode}$ is the standard electrode potential, R is ideal gas constant, T is absolute temperature, $p(H_2)$ is hydrogen partial pressure at the cathode, and $[OH^-]$ is the OH^- concentration at the cathode. At pH = 7 and $p(H_2)$ = 1 atm, $E_{cathode}$ = -0.414 V.

The overall cell potential is written as

$$E_0 = E_{anode} - E_{cathode} \quad (5\text{-}6)$$

That is

$$E_0 = E^0_{anode} - E^0_{cathode} + \frac{RT}{F} * \ln\{[H^+][OH^-]\} + \frac{RT}{4F} * \ln[p(O_2)] + \frac{RT}{2F} * \ln[p(H_2)] \quad (5\text{-}7)$$

Although other electrochemical reactions may occur depending on the concentration of species, their electrochemical potential, and the reaction kinetics, water electrolysis reaction is considered the dominant reaction and thus only this reaction is considered during the model development. This likely limits the model to the prediction of an electrode enhanced cap to freshwater systems.

The overall applied cell voltage is composed of a number of terms, i.e.

$$V = E_O + |\eta_A| + |\eta_C| + \eta_{ohmic} \quad (5\text{-}8)$$

Where V is the applied voltage, η_A and η_C are the overpotentials at the anode and cathode, respectively, η_{ohmic} is the ohmic loss of the system, and E_0 is the thermodynamic potential of water electrolysis. Equation (5-7) shows that E_0 depends on $[H^+]$ and $p(O_2)$ at the anode, and $[OH^-]$ and $p(H_2)$ at the cathode. Although pH may change at both cathode and anode during the application of an extern power, it is assumed that E_0 has a constant value of 1.23 V, i.e. thermodynamic potential of water electrolysis at 25 °C at pH = 7.

Theoretically, the relationship between the current at the electrode and the overpotential follows Butler-Volmer expressions as follows (Newman and Thomas-Alyea, 2004):

$$I = Ai_0 \left[\exp\left(\alpha_a \frac{F}{RT}\eta\right) - \exp\left(-\alpha_c \frac{F}{RT}\eta\right)\right] \quad (5\text{-}9)$$

Where I is current, A is electrode active surface area, i_0 is exchange current density, F is Faraday constant, R is ideal gas constant, T is absolute temperature, η is overpotential, α_a and α_c are apparent transfer coefficients, which gives the magnitude of the potential dependence of the electrochemical reaction rates.

In most systems, α_a and α_c turn out to lie between 0.3 and 0.7, and they can usually be approximated by 0.5 in the absence of actual measurement (Bard and Faulkner, 2001).

In practice, Tafel equation is generally used to simplify the reaction kinetics as follows (Bard and Faulkner, 2001; Pletcher and Walsh, 1990):

$$\eta = a' + b' * \log_{10} I \tag{5-10}$$

Or

$$\eta = a' + b' * \log_{10}(iA) = a' + b' * \log_{10} A + b' * \log_{10} i \tag{5-11}$$

Where a' and b' are empirical parameters, and i is current density (current per unit area).

Assuming both oxygen and hydrogen generation reactions have apparent transfer coefficients of 0.5 for α_a and α_c, then parameter b' in Tafel equation will have the same value for these two reactions (Appendix C). $|\eta_A| + |\eta_C|$ term in Equation (5-8) can be combined into one expression with only two empirical parameters as follows:

$$|\eta_A| + |\eta_C| = a + b * \log_{10}(I) \tag{5-12}$$

The ohmic loss η_{ohmic} can be expressed as

$$\eta_{ohmic} = \frac{iAL}{\kappa_a} = \frac{IL}{\kappa_a} \tag{5-13}$$

Where L is the distance between the anode and the cathode, κ_a is the effective electrical conductivity of porous media.

Effective electrical conductivity of water-saturated soil κ_a can be estimated by Archie's empirical law (Archie, 1942; Friedman, 2005):

$$\kappa_a = \kappa\theta^m \tag{5-14}$$

Where κ is the electrical conductivity of electrolyte, θ is the porosity of the sand and m is a material-dependent empirical exponent.

The conductivity of electrolyte κ can be estimated by values of equivalent conductances of ionic species (Bard and Faulkner, 2001)

$$\kappa = F \Sigma (|z_i| u_i c_i) \tag{5-15}$$

Where z_i is charge number, u_i is mobility and c_i is concentration of the *i*th specie.

Therefore, the overall cell voltage-current relationship can be obtained by combing Equation (5-8), (5-12), and (5-13):

$$V = E_0 + a + b * \log_{10} I + \frac{LI}{\kappa_a} \tag{5-16}$$

It can also be written in terms of current density i instead of current I as follows:

$$V = E_0 + a + b * \log_{10} A + b * \log_{10} i + \frac{LiA}{\kappa_a} \tag{5-17}$$

Once all the parameters in Equation (5-16) or (5-17) are given, cell voltage-current (or current density) equation is deterministic though the function to determine current I by voltage V: I = f(V) is implicit. However, a plot of voltage V verses current I

can be constructed and the current I under a given value of V can be easily read from the graph.

5.2.2 Model calibration

The input voltage by an external power and current were measured in three beakers as described in section 4.2. The sand layers were saturated with electrolyte (2 mM NaCl and 2 mM Na_2SO_4 mixed electrolyte) initially though the porewater composition would be different due to dissolution and ionic species transport. Due to uncertainty in ionic species composition, porosity of sand θ, and empirical exponent m, a lumped parameter R_{rstc} is used and Equation (5-16) is written as :

$$V = E_0 + a + b * \log_{10}(I) + R_{rstc}I \tag{5-18}$$

Where R_{rstc} represents the total resistance between the electrodes.

Parameter a, b and R_{rstc} can be obtained by fitting the model to experimental results. The model was calibrated using three data sets, and Table 5.1 shows the calibrated value of parameter a, b and R_{rstc}. Although these three beaker experiments were conducted as replicates, measured current value at the same input voltage was slightly different between replicates. Consequently, fitted parameters show some variation for the different data sets. As shown in Figure 5.1, the model presented above can be used to describe voltage-current relationship, no matter which set of calibrated parameters is used. All the three sets of parameters gave very similar results although each parameter may have some variation between data sets (Figure 5.1 (d)).

Table 5.1 Fitted parameters a, b and R_{rstc}, coefficient determination R^2 and root-mean-square-error (RMSE)

	a	b	R_{rstc}	coefficient of determination R^2	root-mean-square error (RMSE)
Exp1	726.6 (406.2, 1047)	438.7 (78.62, 798.8)	665.5 (417.8, 913.2)	0.9861	93.33
Exp2	829.2 (559.2, 1099)	451.7 (176.6, 726.9)	609.8 (403.4, 816.2)	0.9871	90.14
Exp3	1109 (692.5, 1525)	684.2 (238.4, 1130)	373.8 (76.95, 670.7)	0.9738	128.3
All	894.7 (715.1, 1074)	524.6 (332.4, 716.8)	540 (405.4, 674.6)	0.9764	110

Values in parentheses denote lower and higher bound of 95% confidence intervals.

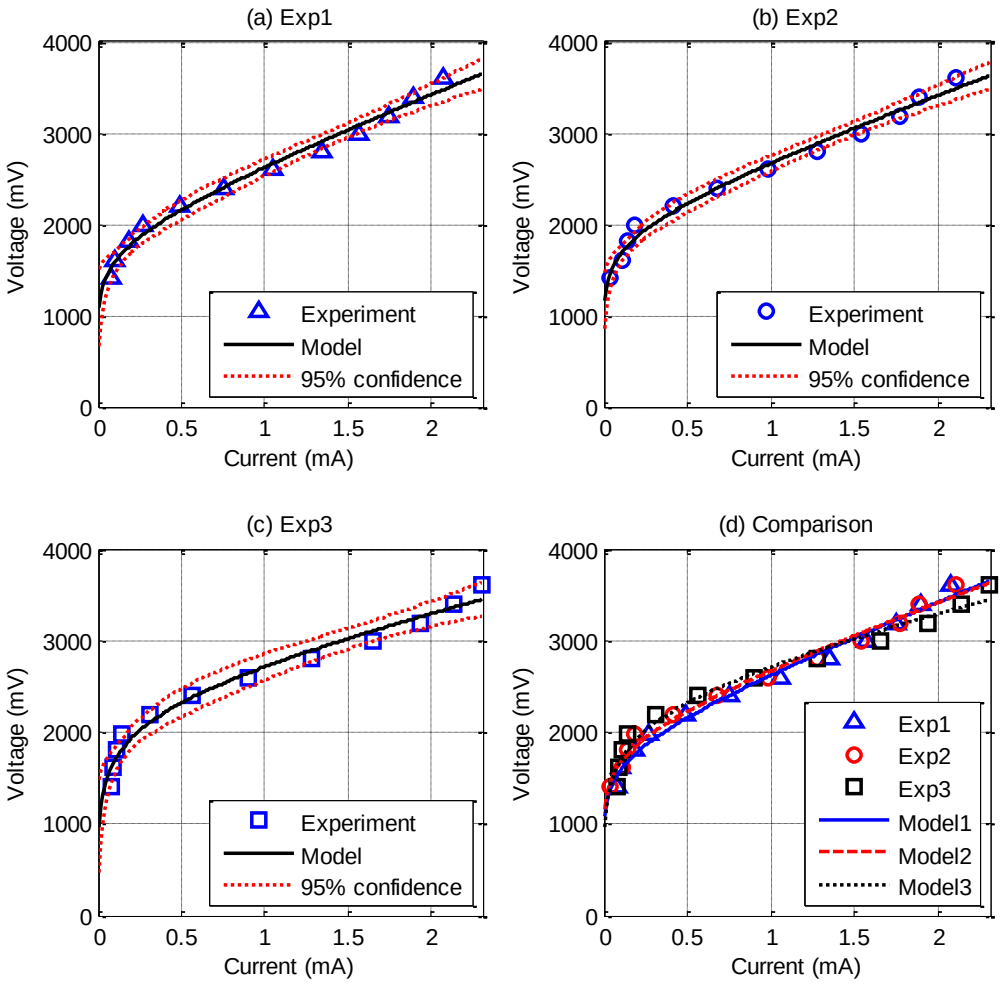

Figure 5.1 Comparison of the model with experiments: (a) Exp1, (b) Exp2, (c) Exp3, (d) All the three experiments. Dotted lines represent 95% confidence intervals.

The currents predicted by Equation (5-16) are higher than experimental data when the currents exceed ~1.8 mA for all the three datasets. Figure 5.2 illustrates the effect of limiting current for Exp2. It is observed that when the current is greater than ~1.8 mA or the voltage is greater than ~3.2 V, the model's predicted currents are higher than measured currents. This inconsistency is due to the effect of ion migration on limiting

currents. The electric current is carried by salt ions migrating between the electrodes, and slow ion migration will limit the current driven by the electrode reactions. Therefore the model developed here is only suitable for low current situation. However, in the application of electrode enhanced capping, the observed current is only about 0.2 mA, so the model is still valid under this low current application.

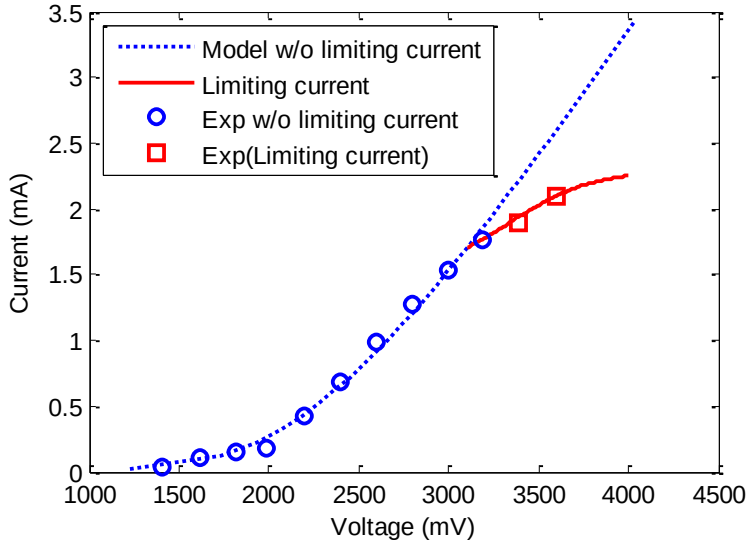

Figure 5.2 The effect of limiting current in Exp2. Dotted line is the fitted model excluding the last two experimental data.

5.2.3 Voltage components analysis

The overall input voltage is composed of three components:

1) A constant thermodynamic potential of water electrolysis E_0;

2) The sum of overpotential η at both electrodes, $\eta = a + b*\log_{10}(I)$;

3) Ohmic loss between the anode and cathode, $\eta_{ohmic} = R_{rstc}*I$.

In this study, when applied voltage is greater than about 1.6 V, significant water electrolysis reactions occur at electrodes. Both overpotential and ohmic loss increase with input voltage, but E_0 remains a constant. In Exp2 (Figure 5.3), overpotential increases

significantly initially from ~1.6 V but the increase rates declined with input voltage. However, ohmic loss increases slowly from ~1.6V to ~2.0 V, and then it increases almost linearly with input voltage. Although the above voltage component analysis was only performed for Exp2 as an example, the results for other systems should be similar. In practice, both ohmic loss and overpotential should be kept low so as to maximize the voltage efficiency provided water electrolysis is driven by an external potential. To perform voltage component analysis will help determine the energy distribution in electrode enhanced capping and simplify the voltage-current relationship. For example, when overpotential term is negligible compared to the sum of ohmic loss term and E_0 ($\eta_{overpotential} << \eta_{ohmic} + E_0$), V-I relationship can be approximated by a linear equation .

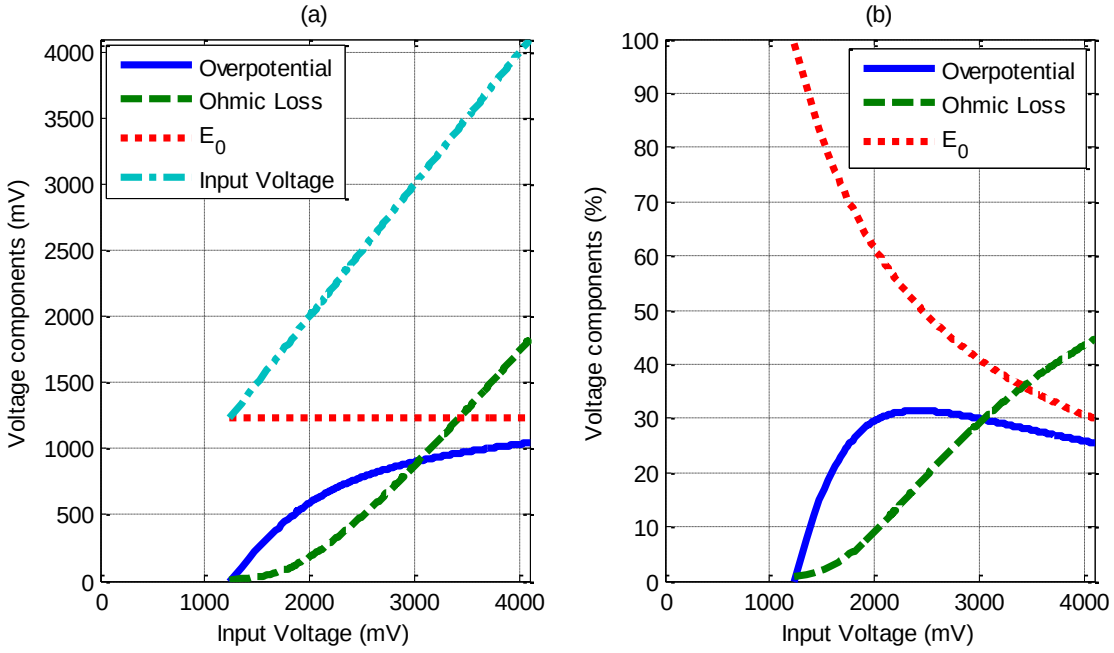

Figure 5.3 Voltage components in electrode enhanced capping in Exp2. (a) voltage components and (b) percentage of voltage components at different input voltage.

5.2.4 Application of model in capping design

The model can be used to predict the current and current density of electrode enhanced capping. In the following analysis, all the results are based on ideal model and the effect of limiting current is not considered.

Parameter a and b are always associated with electrode materials and need to be calibrated in laboratory scale experiment. Voltage-current density model is preferred instead of voltage-current model if the electrode areas will be changed in capping design.

Another important parameter in capping design is the thickness of electrode enhanced capping, i.e. the distance between the electrodes. According to Equation (5-16), ohmic loss is proportional to thickness L or resistance R_{rstc}. Figure 5.4 shows the voltage-current density relationship with different cap thickness. For the cases of r_t=1, 2, 5 and 10, when input voltage V is large, the relationship between V and current density i is almost linear. The linear range of this relationship is extended with an increase of resistance R_{rstc}. This can be explained by voltage component analysis. As shown in Figure 5.3, although overpotential increases with input voltage, the percentage of overpotential decreases when V increases beyond ~2.4 V. When overpotential term is negligible compared to the sum of ohmic loss term and E_0, voltage-current density relationship will be approximated by a linear expression.

Figure 5.5 shows the input voltage required to achieve the same magnitude of current density when cap thickness changes. For example, to generate a current density of 12 $\mu A/cm^2$, 2 V is required in Exp2, but 2.74 V and 3.65 V are required if the cap is 5 and 10 times thicker, respectively. Unlike ohm's law, the voltage requirement to obtain the same current density is not proportional to resistance, but much less, in electrode enhanced capping.

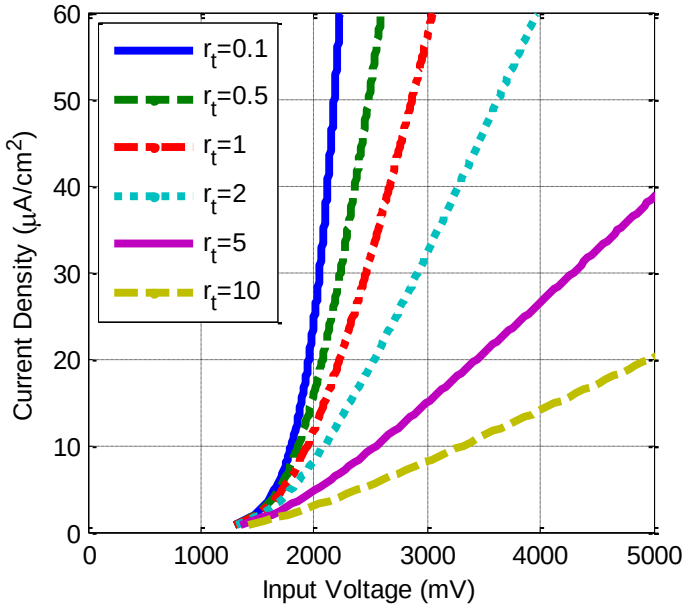

Figure 5.4 Voltage-current density relationship for different cap thickness. r_t is the ratio of the cap thickness to that of Exp2.

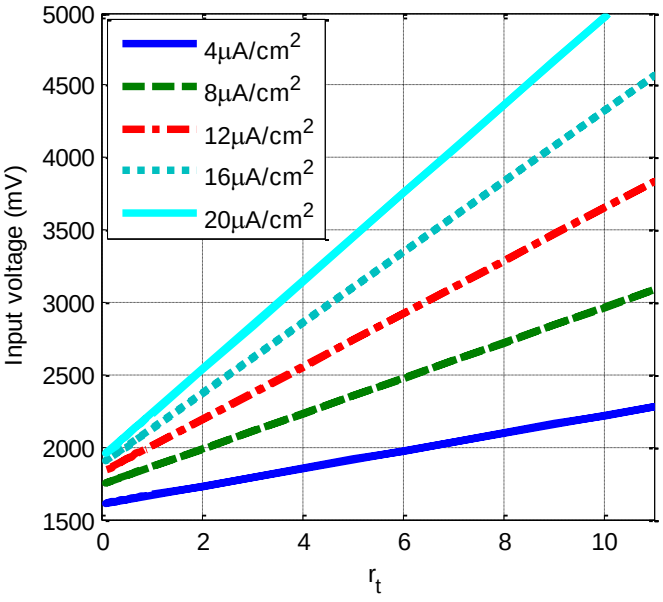

Figure 5.5 Input voltage required to achieve the same current density with different cap thickness. r_t is the ratio of the cap thickness to that of Exp2.

Figure 5.6 shows the sensitivity of current density with respect to voltage change. It is noticed that current density is less sensitive to voltage change with a larger cap thickness (a larger r_t). In general, current density is more sensitive to voltage change when voltage increase (Figure 5.6 a). For the cases of r_t = 1, 2, 5 and 10, di/dV increases first, and then reach a plateau when V increases. For r_t = 0.1 and 0.5, current density increases significantly with voltage, and this increase will finally reach the limiting current phase (not shown in Figure 5.6), which means the model can't predict the current and current density correctly.

Though current density is less sensitive at lower voltage, relative current density change (di/i) is more sensitive to relative voltage change (dV/V) at lower voltage (under 2 V) compared to that at higher voltage. For the application of electrode enhanced capping in Exp2 (r_t = 1), it is calculated that under 2 V condition, relative current density change (di/i) is five times larger than relative voltage change (Figure 5.6 b). So a small change of input voltage will result in more significantly change in current density.

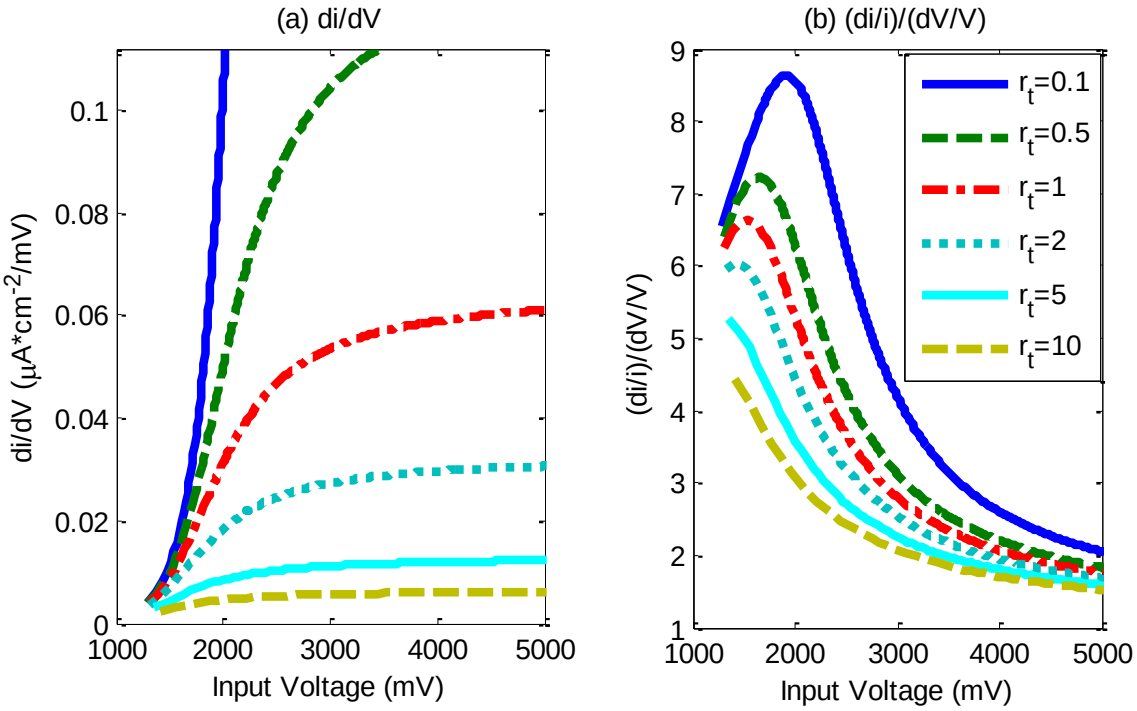

Figure 5.6 Sensitivity analysis of current density with respect to voltage changes for different cap thickness: (a) current density change with respect to voltage change (di/dV); (b) relative current density change with respect to relative voltage change [(di/i)/(dV/V)].

5.3 MODELING OF TRANSPORT AND REACTION PROCESSES

5.3.1 Modeling of transport processes

The model takes into consideration the following four transport mechanisms of aqueous species in capping sand and sediment under the influence of DC electrical field:

(1) Advection due to the movement of groundwater under hydraulic gradient.

$$J_{adv} = cq \tag{5-19}$$

Where J_{adv} is the advective flux, c is the concentration of species in porewater, and q is Darcy velocity.

(2) Advection due to electroosmosis.

$$J_{eo} = -\theta c k_{eo} \nabla V_{ep} \quad (5\text{-}20)$$

Where J_{eo} is the advective flux due to electroosmosis, θ is porosity, V_{ep} is electrical potential, and k_{eo} is the electroosmotic permeability which depends on the ionic strength, viscosity and permittivity of the fluid and the properties of the porous medium (Alshawabkeh and Acar, 1992). A simplified expression for k_{eo} is known as Helmboltz-Smoluchowski equation (Probstein, 1989):

$$k_{eo} = \frac{\varepsilon_p \zeta}{\mu} \quad (5\text{-}21)$$

Where ε_p is permittivity of the medium, ζ is zeta potential of the porous medium, and μ is viscosity of water.

(3) Diffusion due to concentration gradient.

$$J_{dif} = -\theta D_{ef} \nabla c \quad (5\text{-}22)$$

Where J_{dif} is the diffusive flux due to concentration gradient, and D_{ef} is effective diffusion coefficient.

(4) Ion migration due to ionic movement of charged ions in response to an electric field.

$$J_{mgt} = -\theta z u_{ef} F c \nabla V_{ep} \quad (5\text{-}23)$$

Where J_{mgt} is the ion migrational flux, z is the charge of the ion, u_{ef} is the effective ionic mobility of the ion, and F is Faraday constant (96485 C/mol). The relationship of the ionic mobility u_{ef} and diffusion coefficient D_{ef} is provided by Nernst-Einstein equation:

$$u_{ef} = \frac{D_{ef}}{RT} \quad (5\text{-}24)$$

Where R is ideal gas constant and T is absolute temperature.

So the total flux J is expressed as

$$J = cq - \theta c k_{eo} \nabla V_{ep} - \theta D_{ef} \nabla c - \theta z u_{ef} F c \nabla V_{ep} \quad (5\text{-}25)$$

The equation for the transport of solute based on continuity equation is

$$\frac{\partial \theta c}{\partial t} + \nabla J = \theta R_L \quad (5\text{-}26)$$

Where J is the total flux, and R_L is the reaction rate of species per fluid volume due to chemical reaction.

In this study, the following simplifying assumptions were assumed in the transport model:

(1) The transport processes can be described by a one-dimensional model;

(2) The porosity θ is constant with time and space.

The one-dimensional equation for the solute transport and reaction is simplified as

$$\frac{\partial c}{\partial t} + \frac{\partial}{\partial x}\left(-D_{ef}\frac{\partial c}{\partial x} - z u_{ef} F c \frac{\partial V_{ep}}{\partial x} + \frac{q}{\theta} c - k_{eo} c \frac{\partial V_{ep}}{\partial x}\right) = R_L \quad (5\text{-}27)$$

Similarly, the governing equation for solid species (e.g. calcite) is

$$\frac{\partial c_s}{\partial t} + \frac{\partial}{\partial x}\left(-D_{ef}\frac{\partial c_s}{\partial x}\right) = R_S \quad (5\text{-}28)$$

Where c_s is the concentration of solid species (mole per weight of dry sediment/sand), and R_S is the reaction rate of solid species per weight of dry sediment/sand due to chemical reaction.

In the case of compacted sediment and sand, particle movement such as advection and electrophoresis is insignificant compared to solute transport processes. So it is

assumed that advection and electrophoresis processes are negligible in the system (Alshawabkeh, 1994).

5.3.2 Modeling of chemical reactions

The chemical reactions occur in in electrode enhanced capping system are very complicated due to the complex nature of sediment/sand. The major purpose of this model is to model pH changes with time in both sediment and sand, so the model only considers those important reactions that are related to pH changes. These reactions include:

(1) Water electrolysis at the electrodes during the application of external power as shown in reactions (5-2) and (5-3).

The water oxidation at the anode is the major proton source in the system, and the water reduction at the cathode is the major hydroxyl source in the system. The reaction rate of both reactions can be estimated by the current as in equation (5-1).

(2) Self-ionization of water

$$H_2O = H^+ + OH^- \tag{5-29}$$

The equilibrium constant K_w for equation (5-29) is

$$K_w = [H^+][OH^-] \tag{5-30}$$

(3) Equilibrium reactions of carbonate species

$$H_2CO_3 = H^+ + HCO_3^- \tag{5-31}$$

$$HCO_3^- = H^+ + CO_3^{2-} \tag{5-32}$$

The first and second proton dissociation constants for carbonic acid are expressed as:

$$K_{a1} = \frac{[H^+][HCO_3^-]}{[H_2CO_3]} \tag{5-33}$$

$$K_{a2} = \frac{[H^+][CO_3^{2-}]}{[HCO_3^-]} \tag{5-34}$$

The relative distribution of acid and different conjugate bases is calculated as a function of pH:

$$\alpha_0 = \frac{[H_2CO_3]}{c(TC)} = \frac{[H^+]^2}{[H^+]^2 + K_{a1}[H^+] + K_{a1}K_{a2}} \tag{5-35}$$

$$\alpha_1 = \frac{[HCO_3^-]}{c(TC)} = \frac{K_{a1}[H^+]}{[H^+]^2 + K_{a1}[H^+] + K_{a1}K_{a2}} \tag{5-36}$$

$$\alpha_2 = \frac{[CO_3^{2-}]}{c(TC)} = \frac{K_{a1}K_{a2}}{[H^+]^2 + K_{a1}[H^+] + K_{a1}K_{a2}} \tag{5-37}$$

Where c(TC) is the concentration of total carbonate species:

$$c(TC) = [H_2CO_3] + [HCO_3^-] + [CO_3^{2-}] \tag{5-38}$$

(4) Acid-base reactions with surface hydroxyl groups on the surfaces of oxides

Oxides, especially those of Si, Al, and Fe, are common components of the solid phases in natural waters, sediments, and soils (Stumm and Morgan, 1996). The various surface hydroxyls formed on the surfaces of oxides can both associate and dissociate protons. The acid-base reactions for oxides can be written as:

$$OXOH_2^+ = OXOH + H^+ \tag{5-39}$$

$$OXOH = OXO^- + H^+ \quad (5\text{-}40)$$

Where OXOH represents a surface hydroxyl group

Similarly to carbonate species, the first and second proton dissociation constants for surface hydroxyl groups are defined as:

$$K_{ox1} = \frac{[H^+][OXOH]}{[OXOH_2^+]} \quad (5\text{-}41)$$

$$K_{ox2} = \frac{[H^+][OXO^-]}{[OXOH]} \quad (5\text{-}42)$$

The relative distribution of different functional groups of surface hydroxyl is calculated as a function of pH:

$$\beta_0 = \frac{[OXOH_2^+]}{c(TOX)} = \frac{[H^+]^2}{[H^+]^2 + K_{ox1}[H^+] + K_{ox1}K_{ox2}} \quad (5\text{-}43)$$

$$\beta_1 = \frac{[OXOH]}{c(TOX)} = \frac{K_{ox1}[H^+]}{[H^+]^2 + K_{ox1}[H^+] + K_{ox1}K_{ox2}} \quad (5\text{-}44)$$

$$\beta_2 = \frac{[OXO^-]}{c(TOX)} = \frac{K_{ox1}K_{ox2}}{[H^+]^2 + K_{ox1}[H^+] + K_{ox1}K_{ox2}} \quad (5\text{-}45)$$

Where c(TOX) is the concentration of total surface hydroxyl species:

$$c(TOX) = [OXOH_2^+] + [OXOH] + [OXO^-] \quad (5\text{-}46)$$

(5) Acid-base reactions with proton-binding groups of humic substances

Soil organic matter is a variable and complex mixture of compounds, and the detailed composition is usually unknown. It is assumed that the ‘active’ binding fraction of organic matter is composed of humic substances, so the interactions between protons,

cations and organic matter in soils can be modeled (Tipping and Hurley, 1988; Tipping, 1994).

The sites of proton-binding groups of humic substances have a range of acidities, and two types of site (denoted A and B) are recognized. Type A represents strong acid groups (mainly carboxylic acid) and Type B represents weak acid groups (mainly phenolic acid) (Stumm and Morgan, 1996; Lofts et al., 2001). It is assumed that there are half as many Type B groups as type A groups (Tipping, 1998). Carboxylic acid groups and phenolic groups have pK values between 4 and 6, and between 8 and 11, respectively (Stumm and Morgan, 1996).

The acid-base reactions with proton-binding groups of Type A and Type B are written as:

$$HA = H^+ + A^- \tag{5-47}$$

$$HB = H^+ + B^- \tag{5-48}$$

$$K_{HA} = \frac{[H^+][A^-]}{[HA]} \tag{5-49}$$

$$K_{HB} = \frac{[H^+][B^-]}{[HB]} \tag{5-50}$$

Where HA and HB represent proton-binding groups of Type A and Type B.

The relative distribution of acid and conjugate base for Type A and Type B proton-binding groups is written as:

$$\sigma_0 = \frac{[HA]}{c(THA)} = \frac{[H^+]}{[H^+] + K_{HA}} \tag{5-51}$$

$$\sigma_1 = \frac{[A^-]}{c(THA)} = \frac{K_{HA}}{[H^+] + K_{HA}} \quad (5\text{-}52)$$

$$\chi_0 = \frac{[HB]}{c(THB)} = \frac{[H^+]}{[H^+] + K_{HB}} \quad (5\text{-}53)$$

$$\chi_1 = \frac{[B^-]}{c(THB)} = \frac{K_{HB}}{[H^+] + K_{HB}} \quad (5\text{-}54)$$

Where c(THA) and c(THB) are the concentrations of total Type A and Type B proton-binding groups, respectively:

$$c(THA) = [HA] + [A^-] \quad (5\text{-}55)$$

$$c(THB) = [HB] + [B^-] \quad (5\text{-}56)$$

(6) Calcite precipitation and dissolution

Sediment usually contains minerals such as calcite, dolomite, siderite, etc. that buffer the pH of porewater in sediment (Jourabchi et al., 2005). Mineral precipitation and dissolution have an effect on sediment pH depending on concentration of minerals and kinetics of precipitation/dissolution (Van Cappellen and Wang, 1996). In this study, only calcite ($CaCO_3$) is included in the model as a typical mineral commonly found in sediment. Calcite precipitation/dissolution reaction is written as:

$$CaCO_3(s) = Ca^{2+} + CO_3^{2-} \quad (5\text{-}57)$$

The rate of this reaction can be described by a linear model as (Archer, 1996):

$$R_{calcite} = k_{diss}[CaCO_3](1 - \Omega) \quad \text{if } \Omega < 1 \quad (5\text{-}58)$$

$$R_{calcite} = k_{pctp}(\Omega - 1) \text{ if } \Omega \geq 1 \quad (5\text{-}59)$$

Where k_{diss} is dissolution rate constant, k_{pctp} is precipitation rate constant, and Ω is saturation level of calcite and defined as

$$\Omega = \frac{[Ca^{2+}][CO_3^{2-}]}{K_{sp}} \quad (5\text{-}60)$$

Where K_{sp} is the solubility product of calcite.

Other reactions, such as silicates dissolution, redox reactions, etc. are not considered in this study as their impact is negligible on pH distribution (Boudreau, 1991; Alshawabkeh and Acar, 1992).

5.3.3 Decoupling of transport and reaction processes

In the model, 14 species are considered including H^+, OH^-, H_2CO_3, HCO_3^-, CO_3^{2-}, $OXOH_2^+$, OXOH, OXO^-, HA, A^-, HB, B^-, Ca^{2+} and $CaCO_3$, so the model consists of a set of 14 PDEs of transport equations. However, the concentrations of 12 species are restricted by 7 equilibrium reactions: (5-29), (5-31), (5-32), (5-39), (5-40), (5-47), and (5-48). The whole system is a differential algebraic system (DAE) consisting of PDEs, and algebraic equations (AEs).

To decouple the differential algebraic system, it is assumed that the transport equations can be established for the following aggregate properties: total carbonate species (TC), total surface hydroxyl species (TOX), total Type A proton-binding groups (THA), and total Type B proton-binding groups (THB). Similar approaches were used in early diagenetic models and showed satisfactory results (Van Cappellen and Wang, 1996; Jourabchi et al.,2005; Archer, 1996).

Total alkalinity, acid-neutralizing capacity of water, is defined as the sum of all the titratable bases:

$$c(TA) = 2[CO_3^{2-}] + [HCO_3^-] + 2[OXO^-] + [OXOH] + [A^-] + [B^-] + [OH^-] - [H^+] \quad (5\text{-}61)$$

Where c(TA) is total alkalinity.

Apply relative distribution coefficient to (5-61):

$$c(TA) = (2\alpha_2 + \alpha_1)c(TC) + (2\beta_2 + \beta_1)c(TOX) + \sigma_1 c(THA) + \chi_1 c(THB) + \frac{K_w}{[H^+]} - [H^+] \quad (5\text{-}62)$$

The rate of total alkalinity production is derived as

$$\begin{aligned}\frac{\partial c(TA)}{\partial t} = {} & (2\alpha_2 + \alpha_1)\frac{\partial c(TC)}{\partial t} + \frac{d(2\alpha_2 + \alpha_1)}{d[H^+]} * \frac{\partial [H^+]}{\partial t} * c(TC) \\ & + (2\beta_2 + \beta_1)\frac{\partial c(TOX)}{\partial t} + \frac{d(2\beta_2 + \beta_1)}{d[H^+]} * \frac{\partial [H^+]}{\partial t} * c(TOX) \\ & + \sigma_1 \frac{\partial c(THA)}{\partial t} + \frac{d\sigma_1}{d[H^+]} * \frac{\partial [H^+]}{\partial t} * c(THA) + \chi_1 \frac{\partial c(THB)}{\partial t} \\ & + \frac{d\chi_1}{d[H^+]} * \frac{\partial [H^+]}{\partial t} * c(THB) - \frac{K_w}{[H^+]^2} * \frac{\partial [H^+]}{\partial t} - \frac{\partial [H^+]}{\partial t}\end{aligned} \quad (5\text{-}63)$$

Which is

$$\begin{aligned}&\left[\begin{matrix}\left(2\frac{d\alpha_2}{d[H^+]} + \frac{d\alpha_1}{d[H^+]}\right)c(TC) + \left(2\frac{d\beta_2}{d[H^+]} + \frac{d\beta_1}{d[H^+]}\right)c(TOX) \\ + \frac{d\sigma_1}{d[H^+]}c(THA) + \frac{d\chi_1}{d[H^+]}c(THB) - \frac{K_w}{[H^+]^2} - 1\end{matrix}\right]\frac{\partial [H^+]}{\partial t} = \\ &\frac{\partial c(TA)}{\partial t} - (2\alpha_2 + \alpha_1)\frac{\partial c(TC)}{\partial t} - (2\beta_2 + \beta_1)\frac{\partial c(TOX)}{\partial t} - \sigma_1 \frac{\partial c(THA)}{\partial t} - \chi_1 \frac{\partial c(THB)}{\partial t}\end{aligned} \quad (5\text{-}64)$$

So the rate of H^+ production can be expressed in terms of the rates of c(TA), c(TC), c(TOX) and c(THB)

$$\frac{\partial [H^+]}{\partial t} = \left[\frac{\partial c(TA)}{\partial t} - (2\alpha_2 + \alpha_1)\frac{\partial c(TC)}{\partial t} - (2\beta_2 + \beta_1)\frac{\partial c(TOX)}{\partial t} - \sigma_1 \frac{\partial c(THA)}{\partial t} - \chi_1 \frac{\partial c(THB)}{\partial t}\right]/HH \quad (5\text{-}65)$$

Where

$$HH = \left(2\frac{d\alpha_2}{d[H^+]} + \frac{d\alpha_1}{d[H^+]}\right)c(TC) + \left(2\frac{d\beta_2}{d[H^+]} + \frac{d\beta_1}{d[H^+]}\right)c(TOX) + \frac{d\sigma_1}{d[H^+]}c(THA) + \frac{d\chi_1}{d[H^+]}c(THB) - \frac{K_w}{[H^+]^2} - 1 \quad (5\text{-}66)$$

$$\frac{d\alpha_1}{d[H^+]} = \frac{-K_{a1}[H^+]^2 + K_{a1}^2 K_{a2}}{([H^+]^2 + K_{a1}[H^+] + K_{a1}K_{a2})^2} \quad (5\text{-}67)$$

$$\frac{d\alpha_2}{d[H^+]} = \frac{-K_{a1}K_{a2}(2[H^+] + K_{a1})}{([H^+]^2 + K_{a1}[H^+] + K_{a1}K_{a2})^2} \quad (5\text{-}68)$$

$$\frac{d\beta_1}{d[H^+]} = \frac{-K_{ox1}[H^+]^2 + K_{ox1}^2 K_{ox2}}{([H^+]^2 + K_{ox1}[H^+] + K_{ox1}K_{ox2})^2} \quad (5\text{-}69)$$

$$\frac{d\beta_2}{d[H^+]} = \frac{-K_{ox1}K_{ox2}(2[H^+] + K_{ox1})}{([H^+]^2 + K_{ox1}[H^+] + K_{ox1}K_{ox2})^2} \quad (5\text{-}70)$$

$$\frac{d\sigma_1}{d[H^+]} = \frac{-K_{HA}}{([H^+] + K_{HA})^2} \quad (5\text{-}71)$$

$$\frac{d\chi_1}{d[H^+]} = \frac{-K_{HB}}{([H^+] + K_{HB})^2} \quad (5\text{-}72)$$

After decoupling transport equations and equilibrium reactions, the differential algebraic system (DAE) with 14 species and 7 equilibrium reactions is converted to a nonlinear PDEs system with only 7 species, which are H^+, TC, TOX, THA, THB, calcite and Ca^{2+}.

5.3.4 Model application for sample cases

5.3.4.1 Model parameters

(1) Physical setting

The model was used to simulate an electrode enhanced capping system in vertical one dimensional domain as shown in Figure 5.7. Sediment was at the bottom from d = 4 cm to d = 30 cm, a 4-cm layer of sand was placed over the sediment (from d = 0 cm to d = 4 cm), and a 2-cm layer of overlying water was over the sand capping. Anode was

placed at the sand sediment interface (d = 4 cm) and cathode was placed at d = 0.5 cm in the sand layer. The thickness of the electrode materials was taken into consideration in the model, and it was assumed that both the anode and cathode have a thickness of 0.5 cm. The thickness of the electrodes materials defined the range of hydrogen source and sink term R_L in the governing equation (5-27) of H^+ transport and reaction. So the hydrogen source (anode reaction) located from d = 3.75 cm to d = 4.25 cm, and hydrogen sink (cathode reaction) located from d = 0.25 cm to d = 0.75 cm.

It was assumed that sand and sediment have the same solid density of 2.5 kg/L and porosity of 0.5.

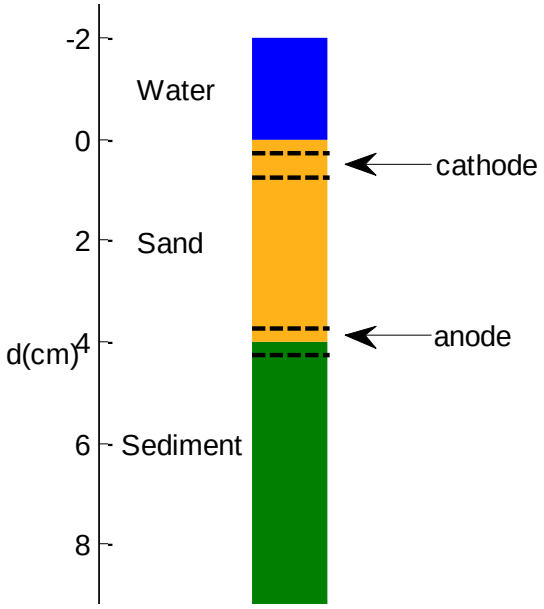

Figure 5.7 Physical setting of an electrode enhanced capping system in vertical one dimensional domain. d is the depth below the water sand interface.

(2) Electrochemical reactions

In section 4.3, the current for ElecCap2 is ~ 200 μA with an electrode area of ~ 25 cm^2, so the current density is 8 μA/ cm^2. The rate of H^+ or OH^- production with ~75%

coulombic efficiency by (5-1) is $1.55*10^{-9}$ mol/s. It is assumed that the reactions occur within $25cm^2*0.5cm$ (Area*Thickness) porous medium as a triangular rate function (Figure 5.8).

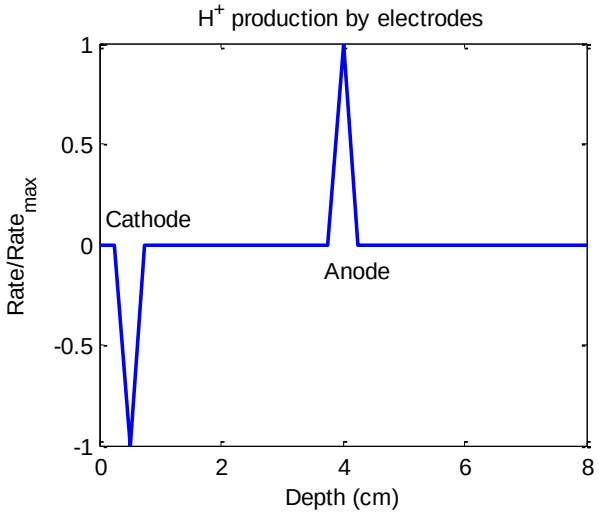

Figure 5.8 Triangular function of proton production rate by electrode reactions.

(3) Electrical potential V_{ep}

Previous studies on modeling of transport and reactions processes by electrical field showed that electrical potential gradient varied with time, but in general the electrical potential profile could be approximated by a linear relationship between two electrodes (Yu and Neretnieks, 1996). In this study, it was assumed that electrical potential V_{ep} was linear between the anode and the cathode. The difference of V_{ep} between two electrodes (i.e. ohmic loss) was estimated to be 0.2 V with an external voltage of 2 V (Figure 5.3).

(4) Transport parameters

Effective diffusion coefficient D_{ef} for aqueous species was estimated from molecular diffusion coefficient and tortuosity factor, and D_{ef} for solid species was assume

to be $1*10^{-13}$ m^2/s (Van Cappellen and Wang, 1996). There is no established method to measure the effective ionic mobility of an ion in porous medium. Effective ionic mobility u_{ef} of the ion was calibrated. Transport parameters for each simulated species in the model are listed in Table 5.2.

Table 5.2 Transport parameters for each species in the model

	D_{ef} [m^2/s]	u_{ef} [$m^2*mol/(s*C*V)$]	Charge number z
H^+	$7*10^{-9}$	$1.88*10^{-13}$	+1
TC	$1*10^{-9}$	$4.03*10^{-13}$	$-(\alpha_1+2\alpha_2)$
Ca^{2+}	$1*10^{-9}$	$4.03*10^{-13}$	+2
Calcite	$1*10^{-13}$	-	-
TOX	$1*10^{-13}$	-	-
THA	$1*10^{-13}$	-	-
THB	$1*10^{-13}$	-	-

(5) Chemical reaction parameters

Chemical reaction parameters are listed in Table 5.3. The equilibrium reaction constant of carbonate species is well studied and known, but those of surface hydroxyl groups and humic substances have a relative large uncertainty. So the parameters of surface hydroxyl groups and humic substances were obtained from literature or calibrated. Kinetic parameter of calcite dissolution and precipitation were obtained from literature. Due to the inhibiting effect of various ions on calcite growth, the onset of precipitation usually requires Ω to be much greater than unity (Zeebe and Sanyal, 2002; Zeebe, 2007). So calcite precipitation was not taken into account in the model.

Table 5.3 Chemical reaction parameters in the model

	Value	Reference
pK_w	14	Stumm and Morgan, 1996
pK_{a1}	6.35	Stumm and Morgan, 1996
pK_{a2}	10.33	Stumm and Morgan, 1996
pK_{ox1}	6.45	Hong et al., 2011
pK_{ox2}	8.96	Calibrated
pK_{HA}	5.5	Calibrated
pK_{HB}	8.8	Hong et al., 2011
K_{sp}	$3.31*10^{-9}$ M^2	Stumm and Morgan, 1996
k_{diss}	$1.16*10^{-9}$ [s^{-1}]	Slow linear model (Archer, 1996)
k_{pctp}	0	Zeebe, 2007; Jourabchi, 2005

(6) Initial concentration

Initial conditions used in the study are presented in Table 5.4. The initial condition for each species present in the system was specified based on its initial concentration in the laboratory experiments or calibrated.

Table 5.4 Initial concentrations in the model

	Water	Sand	Sediment	Unit
pH	7	7	7	-
TC	$1*10^{-5}$	$1*10^{-5}$	$1*10^{-3}$	M
Ca^{2+}		$K_{sp}/[CO_3^{2-}]$		M
Calcite	$1*10^{-10}$	$1*10^{-3}$	$1*10^{-3}$	mol/kg
TOX	$4*10^{-11}$	$4*10^{-5}$	$4*10^{-5}$	mol/kg
THA	$4*10^{-11}$	$1.6*10^{-5}$	$1.6*10^{-2}$	mol/kg
THB		[THA]/2		mol/kg

(7) Boundary conditions

As the model is one dimensional, each species needs two boundary conditions. The top boundary is the air-water interface, and the bottom boundary is modeled as the interface of sediment and rockbed. Boundary conditions used in the study are presented in Table 5.5.

Table 5.5 Boundary conditions in the model

	Air-water interface	Bottom sediment
pH	$J_{dif} + J_{mgt} = 0$	IC*
TC	$J_{dif} + J_{mgt} = 0$	IC*
Ca^{2+}	$J_{dif} + J_{mgt} = 0$	IC*
Calcite	Total flux = 0	Total flux = 0
TOX	Total flux = 0	Total flux = 0
THA	Total flux = 0	Total flux = 0
THB	Total flux = 0	Total flux = 0

* Constant concentration boundary condition:
Concentration at the boundary = initial concentration

5.3.4.2 Model application to no advection cases

The reactive transport model was implemented using COMSOL MULTIPHYSICS 3.5a. In this section, the model was applied to predict the pH profiles in stagnant sediment and sand system in electrode enhanced capping. So there is no contribution from advection flow either due to hydraulic gradient or electroosmosis.

Figure 5.9 shows the predicted pH profiles within one day and in longer time. The initial concentration of H^+ in the porewater is 10^{-7} M. Due to the water electrolysis reaction at the electrodes, H^+ is produced at the anode (d = 4 cm) and OH^- is produced at the cathode (d = 0.5 cm), respectively. An acid front is generated at the anode whereas a base front is generated at the cathode. Although the rate of increase of H^+ at the anode and that of OH^- at the cathode are identical, pH shift at the anode is less than 2 order of magnitude whereas pH increases by 2 orders of magnitude at the cathode. This is due to

the large buffer capacity of sediment around the anode. Because of diffusion and ion migration, H^+ tends to move toward the cathode, and OH^- tends to move toward the anode. The acid front drives the base front back to a zone within the last 0.5 cm of the cathode. Consequently, in most of the region in the cap and sediment, the pH condition is slightly acidic. The simulation results show that after about 50 days the pH profile reaches a steady state between the anode and the cathode, when acid front and base front meet within 0.5 cm of the cathode. Also, a sharp gradient in the pH is generated at the location where the acid and base fronts meet. The diffusion of H^+ into the deeper sediment results pH decrease in the sediment but it takes a longer time to reach steady state or quasi steady state.

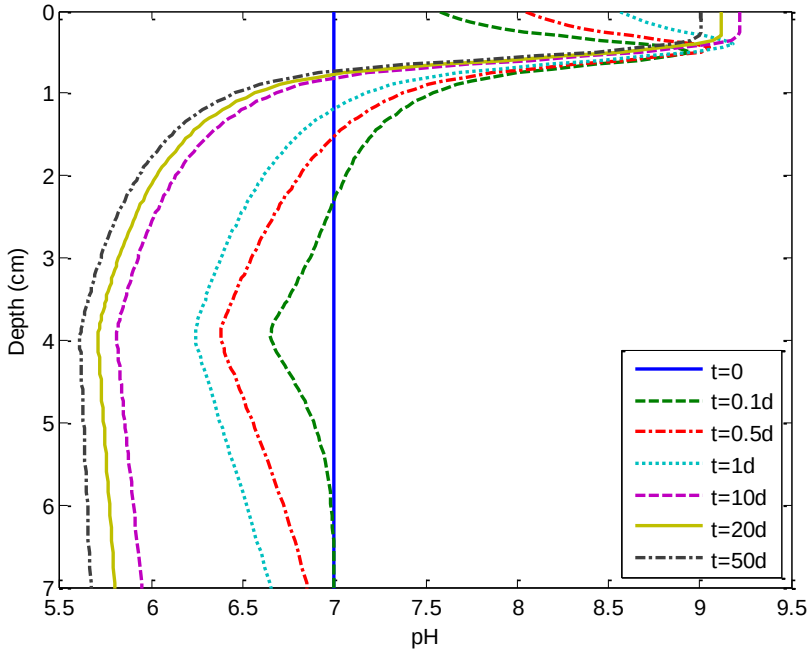

Figure 5.9 Predicted pH profiles in electrode enhanced capping at different times.

Figure 5.10 shows the pH at different depths with time. At the cathode, pH increase to 9 from 7 immediately after the application of power. Then pH at the cathode decreases slowly due to influence of acid front. Similarly, pH at the anode (d = 4 cm) and between two electrodes (d = 2 cm) decreases after the application of power. Compared with the pH changes between two electrodes, pH outside this region changes relative slowly. pH at the air-water interface increases to about 9.4 after 2-3 days and then decreases slowly. pH in the deeper sediment (d= 7 cm) also has a slower response as shown in Figure 5.10. This is because ion migration between the electrodes accelerates the movement of H^+ and other ions. However, diffusion is the only transport process affecting ion transport outside this region.

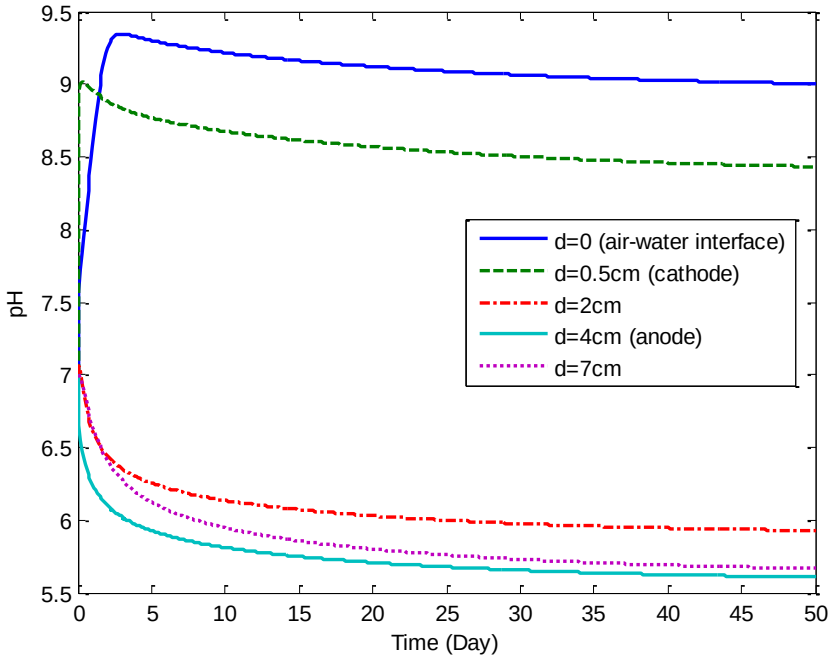

Figure 5.10 Predicted pH profiles in electrode enhanced capping at different depths.

In order to assess whether the developed model predicts pH profiles in an electrode enhanced cap, the predictions of the model were compared with experimental results from Chapter 4. Comparisons between the modeled and experimental pH profiles at different times are depicted in Figure 5.11. A reasonable agreement between the modeled and the experimental results is observed. In the deeper sediment below the anode (d > 4 cm), the model predicted the pH profile accurately with a deviation of less than 0.1. In the cathode region (d = 0 - 0.75 cm), the differences between the model and experimental data were about 0.5, which are still satisfactory results. Furthermore, the model also captured the pH decrease over time at the cathode, but with a larger rate than that in experimental data. However, the greatest difference between the model and experimental observations occurred in the region between the anode and cathode. The model underestimated the pH profiles especially for the region closed to the cathode. Both model and experimental results show a sharp gradient in pH profiles, but the gradient in the model was sharper than that in the experimental result. The sharp pH gradients have been observed in many electrokinetic experiments, and models were developed to predict the pH behaviors in the system. Similarly, pH profiles predicted by models tended to have a sharper gradient than pH observed in experiments (Shapiro and Probstein, 1993; Haran et al., 1997; Yeung and Datla, 1995; Al-Hamdan and Reddy, 2008; Alshawabkeh and Acar, 1996; Yu and Neretnieks, 1996). Because of the complex nature of sand and sediment, some reactions were not taken into account in the model, e.g. some slow reactions of H^+ and OH^- with the surface of the sediment and sand. It is very possible that the lack of slow reaction kinetics of H^+ or OH^- in the porous medium gives rise to the inaccuracy of the model developed in this study and previous electrokinetic models.

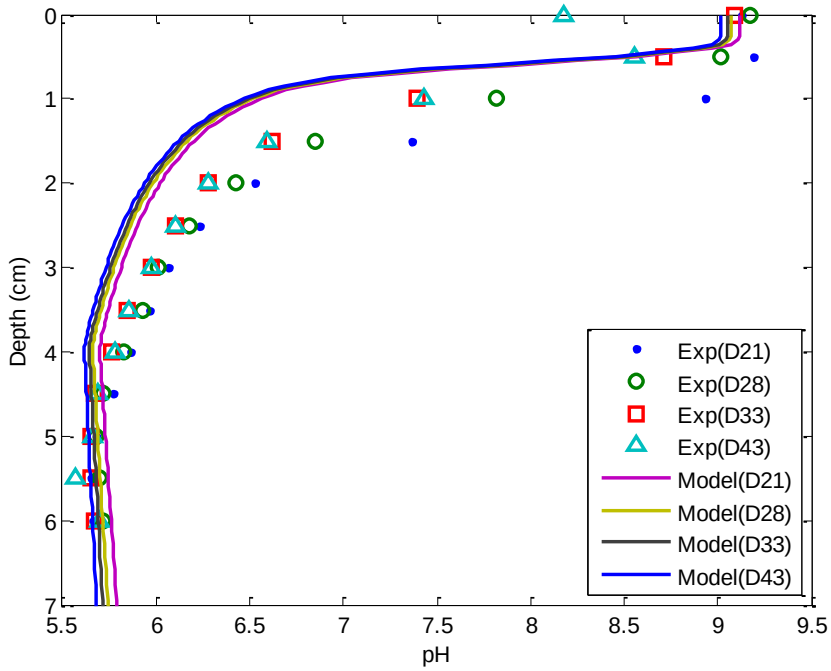

Figure 5.11 Predicted and experimental pH profiles in electrode enhanced capping at different times.

5.2.4.2 Model application to advection cases

Many contaminated sediment sites are in shallow, near-shore areas that are impacted by additional transport processes such as groundwater seepage and tidal driven movement of the flow (Burnett et al., 2003; McCoy and Corbett, 2009). So advection due to groundwater discharge and tidal movement is not uncommon and need to be addressed for electrode enhanced capping.

Electroosmosis in a pore occurs due to the drag interaction between the bulk of the liquid in the pore and a thin layer of charged fluid next to the pore wall, so liquid moves under the action of the electric field in a direction parallel to it. The thin layer of charged fluid, or electric double layer, has a typical thickness between 1 and 10 nm (Probstein and Hicks, 1993). In the application of electrode enhanced capping, sand is used as the capping material. Coarse sand is a very porous soil type and lacks capillary

capacity (Suni and Romantschuk, 2004). Furthermore, it has a very low surface charge and zeta potential, which makes electroosmosis negligible in the sand (Chen et al., 2002; Haran et al., 1997; Li et al., 1997). So electroosmotic flow was not taken into consideration in advection cases.

pH profiles for two groundwater seepage were evaluated: a low Darcy velocity of $5*10^{-8}$ m/s (4.27 mm/d) and a high Darcy velocity of $5*10^{-7}$ m/s (4.27 cm/d). As shown in Figure 5.12, after 20 days, pH at the anode was 5.7, 6.0, and 6.5 for q = 0, 4.27 mm/d, and 4.27 cm/d, respectively. At other times, the model results also show that pH was neutralized by the upflowing buffered groundwater for both advective flow cases. Although pH between two electrodes was neutralized from acidic condition by the buffered groundwater, sharp pH gradient around the cathode didn't vanish with advective flow. With high Darcy velocity (4.27 cm/d), pH profiles reach steady state within 1 day (Figure 5.13).

The simulated results for advection cases show that pH changes were less severe at the anode when upflowing buffered porewater goes into the sand cap. So the rates of PAH biodegradation at the anode may be higher with advective flow compared to stagnant sediment.

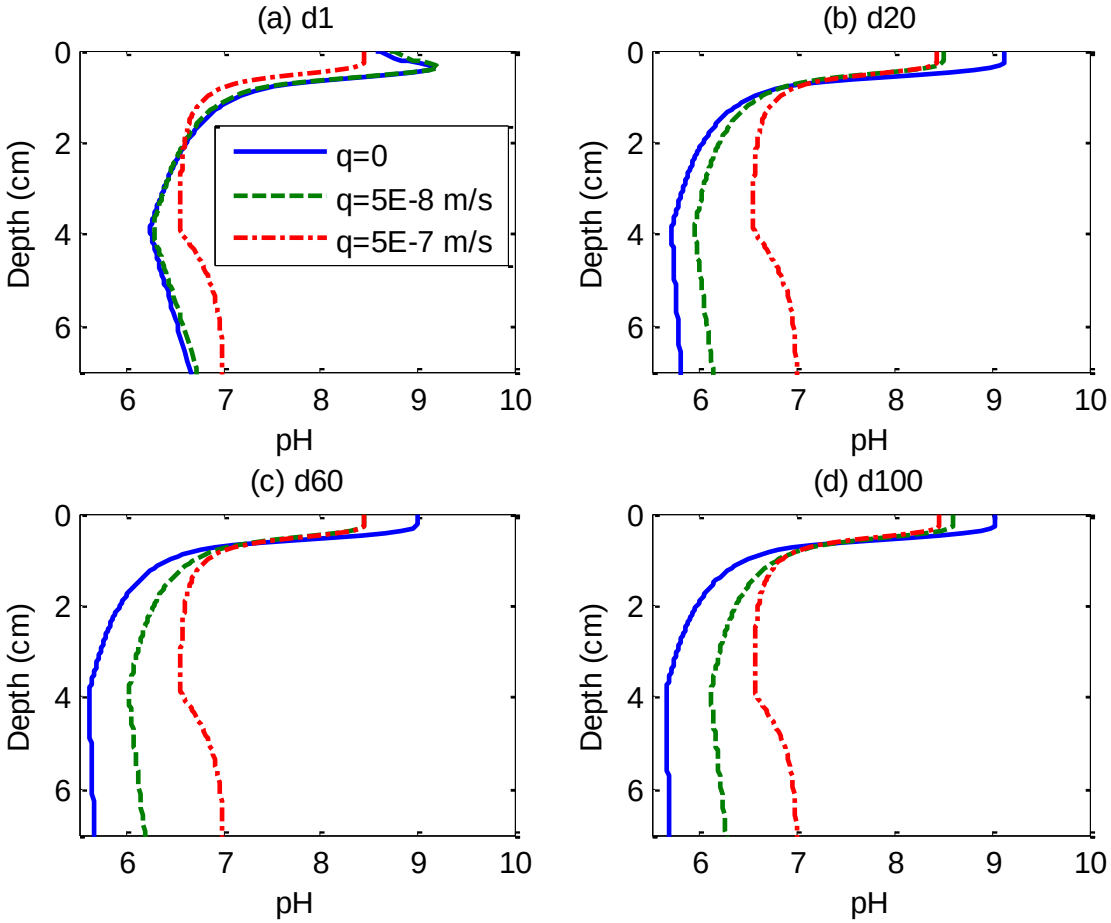

Figure 5.12 Comparison of pH profiles for different advective flow velocities (Darcy velocity q = 0, $5*10^{-7}$ and $5*10^{-8}$ m/s): (a) Day 1; (b) Day 20; (c) Day 60; (d) Day 100.

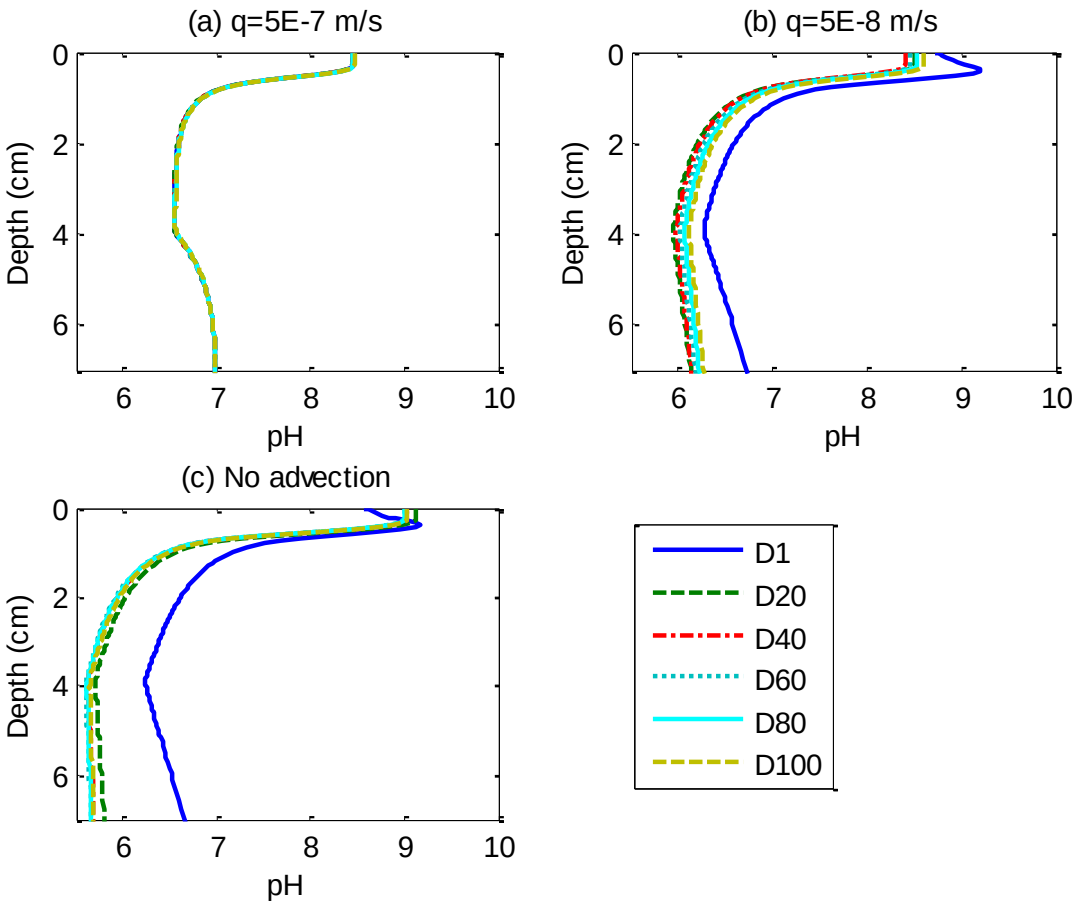

Figure 5.13 Comparison of pH profiles at different times for advection and no advection cases: (a) Darcy velocity q = $5*10^{-7}$ m/s; (b) Darcy velocity q = $5*10^{-8}$ m/s; (c) Darcy velocity q = 0.

5.4 CONCLUSIONS

In this chapter, a voltage-current relationship of electrode enhanced capping was developed and it incorporated several important parameters such as the thickness of electrode enhanced capping and the area of the electrodes. The model was calibrated by experimental dataset and empirical parameters were estimated by fitting the model to experimental data. After calibration, current could be estimated through an implicit voltage-current relationship. Voltage component analysis was performed to quantify the

contribution of thermodynamic potential of water electrolysis, overpotentials at electrodes, and ohmic loss. The model was applied in the design of electrode enhanced capping, and the effect of capping thickness was investigated. Sensitivity of current with respect to voltage changes was performed for different capping thickness.

A coupled reactive transport model was developed for multicomponent species transport focusing on pH profiles under an electric field. In this study, transport processes included: (1) advection due to the movement of groundwater under hydraulic gradient; (2) advection due to electroosmosis; (3) diffusion due to concentration gradient and (4) ion migration due to ionic movement of charged ions in response to an electric field. Chemical reactions included water electrolysis at the electrodes, self-ionization of water, equilibrium reactions of carbonate species, acid-base reactions with surface hydroxyl groups on the surfaces of oxides and with proton-binding groups of humic substances, and mineral precipitation and dissolution. The differential algebraic system (DAE) was decoupled to a nonlinear PDEs system including seven species: H^+, TC, TOX, THA, THB, calcite and Ca^{2+}.

The model successfully predicted the pH gradient in the application of electrode enhanced capping, and the model predictions reasonably agreed with the experimental results in no advection cases. pH changes under field condition with upflowing groundwater seepage were simulated and the results shows that when buffered porewater goes into cap from sediment, pH is neutralized at the anode.

The model can be a useful tool in the studies of transport and reaction processes in a porous medium in an electric field and in the design of electrode enhanced capping.

Chapter 6: Conclusions and Recommendations

6.1 CONCLUSIONS

The purpose of this research was to develop a new active capping technology – electrode enhanced capping to promote contaminant biodegradation for remediation of contaminated sediment. Laboratory scale experiments were conducted in slurry reactors and simulated sediment/cap reactors to evaluate the potential of this novel technology. Also, mathematical models were developed to describe voltage-current characteristic and the complex physical and chemical processes in electrode enhanced capping.

In Chapter 3, biodegradation of PAH under aerobic and nitrate reducing conditions shows the ability of indigenous microorganisms in Anacostia River sediment to degrade naphthalene and phenanthrene in several days or weeks. The proof of concept experiment for electrode enhanced capping was conducted in complete mix slurry reactors. An external potential of 3.5 V was applied to an anaerobic stirred slurry contaminated with naphthalene and phenanthrene. During a period of 4 days, naphthalene concentration decreased from ~1000 μg/L to ~50 μg/L, and phenanthrene was degraded from ~150 μg/L to ~30 μg /L in ElectroBio reactor. The disappearance of naphthalene was a result of both microbial degradation and electrochemical/chemical reactions, while the phenanthrene loss appeared to be solely controlled by biotic processes. By comparing with observations in aerobic and anaerobic control, it is concluded that ElectroBio reactor could accelerate biodegradation rates from anaerobic condition, and achieve almost the same rates as aerobic conditions. It is suggested that the presence of the electrodes was able to maintain aerobic degradation processes despite the initial state of the slurry as being anaerobic. qPCR analysis using PAH-RHD$_\alpha$ Gram Negative primer shows notable increases of PAH degrading genes in ElectroBio reactor and aerobic conditions, but no increase in killed control and anaerobic conditions. The detection of catabolic gene

increase provided the microbial evidence of PAH biodegradation in ElectroBio reactor and aerobic conditions.

In Chapter 4, the electrode approach was investigated in a more realistic and complicated system - microcosm with mass transfer limitation. In the sediment (no capping) microcosm study, two carbon cloth electrodes were placed horizontally in the sediment with a separation distance of 2.5 cm. In two powered reactors, the ORP around the anode was 50 – 150 mV higher than that in the control; pH around the anode dropped to ~6 from an initial value of 6.4 or 6.7. Phenanthrene vertical profile displayed a unique Z-shaped profile as the phenanthrene concentration at the anode decreased with time. These results demonstrated that the anode placed in the sediment could effectively decrease phenanthrene concentration, and create a more oxidized zone around the anode. Microcosm experiments of sediment with electrode enhanced caps were conducted to simulate a capping system. A carbon cloth anode was placed at the sediment cap interface, and the cathode was placed 3.5 cm above the anode in the capping layer. In the experiment with no bicarbonate buffer, ORP in the vicinity of the anode increased 60-100 mV compared to the control reactor, and pH decreased to 5.7 and 6 from circumneutral pH. Average phenanthrene concentrations decreased to ~ 70% of initial concentration in the 1 cm vicinity of the anode in 10 weeks whereas those in the control remained relatively constant. In the experiment with bicarbonate buffer, only a small drop of pH from 6.4 to 6 occurred due to the buffering capacity of bicarbonate. The increase in ORP was not as great with less pH changes, implying the coupled phenomenon of pH and ORP in the sediments under electrode enhanced capping. The reduction of phenanthrene concentration in the 1 cm vicinity of sediment was ~50 %, an increase from ~30% in the case of no bicarbonate buffer. Creating a biobarrier at the sediment cap interface, electrode enhanced caps could effectively prevent migration of phenanthrene from the

underlying sediment to capping layer. The increase of PAH degrading gene compared with control was detected at 0-0.5 cm sediment below the anode in the experiment with and without bicarbonate buffer.

In Chapter 5, a voltage-current relationship of electrode enhanced capping was established with the following form: $V=E_0+a+b*\log_{10}(I)+R_{rstc}*I$. Parameters a, b and R_{rstc} were estimated by fitting the model to experimental data. Current could be determined by the above implicit voltage-current function. The model was applied in the design of electrode enhanced capping, and the effect of capping thickness was investigated. A coupled reactive transport model was built for multicomponent species transport focusing on pH profiles for electrode enhanced capping. The model predictions and their comparisons with the laboratory scale experimental results demonstrate that very sharp changes in the pH profiles exist in electrode enhanced capping. The model was implemented to simulate pH profile under field condition with upflowing groundwater seepage, showing that pH is neutralized at the anode with buffered porewater.

In summary, a novel active capping technology – electrode enhanced capping was proposed and tested in this study. The consistent results from slurry and microcosm experiments demonstrated that electrode enhanced capping can be used to control redox potential in a sediment cap, provide microbial electron acceptor, and stimulate PAH degradation. The treatment demonstrated so far is one of the few successful active capping technologies for the purpose of enhancing contaminant biodegradation. In addition, this hybrid approach – coupling electrochemical process with bioremediation was seldom used for soil and groundwater remediation. This work also bridged the gap between electrochemical remediation and bioremediation in the field of soil and groundwater remediation.

6.2 RECOMMENDATIONS FOR FUTURE WORK

6.2.1 Microbial community analysis

The ability to determine the number and types of microorganisms within a community is fundamental to understanding the structure and function of an ecosystem. In this study, the copy numbers of PAH degrading genes were quantified, and it undoubtedly revealed the microbial activity of certain PAH degrading bacteria. However, there are several limitations for this approach: 1) it doesn't cover all the PAH degrading bacteria; 2) it is very difficult to distinguish the contribution of each PAH degrading gene that is amplified by the primer; 3) the shifts of microbial community in electrode enhanced capping remains unknown. To address this issue, it is beneficial to conduct exhaustive studies of bacterial community in order to determine the unique role that the bacteria play in electrode enhanced capping. This will also help understand the changes of distribution and diversity of bacteria, and ecosystem function with electrode enhanced capping. Clone libraries and/or pyrosequencing can be two powerful tools to achieve this goal.

6.2.2 Characterization of oxic zone at the anode

Oxygen produced at the anode created an oxic zone at the anode, which is considered to be the most important factor to enhance PAH biodegradation. However, several important parameters to characterize the oxic zone are still unknown. These parameters include oxygen penetration depth, the levels of dissolved oxygen, oxygen uptake rates by organic matter and other reduced species, oxygen fluxes at the anode, etc. There currently exist several techniques that can be utilized for oxygen measurement, but technical difficulties have limited their usefulness in this particular application. Under the current microcosm setup, monitoring oxygen levels in-situ, in real time, remains a

technical challenge. So it is advised to design another setup experiment focusing on the measurement of oxygen with the application of carbon cloth electrodes.

6.2.3 Capping performance under various conditions

The laboratory cap microcosm studies presented in Chapter 4 were conducted in a thin layer cap under stagnant flow conditions. It has been demonstrated that electrode enhanced capping could effectively reduce migration of contaminants into the cap in this setup. The performance of electrode enhanced capping needs to be evaluated under various conditions before scaling up to field scale. A thick-layer sand capping, which also means a large separation distance between two electrodes, is worth consideration. With a larger separation distance, it is easier to accurately control the current due to the low sensitivity of current with input voltage at large voltage. The pH and redox behaviors are also of interest when the distance between electrodes changes. Several other electrode materials and configurations can be tried with more flexibility. For instance, metal material such as copper or iron can be a quick, inexpensive and easy alternative as cathode. Another typical case need to be considered is the sediment caps under upflow conditions. With advective flow, there are benefits to PAH biodegradation due to less pH shift. But contaminant migration into the capping layer is also accelerated by advection. So the capping performance needs further investigation under upflow conditions. Ultimately, electrode enhanced capping can be scaled up to pilot scale and field scale for remediation of contaminated sediment.

6.2.4 Mineral amendment for pH control

In this study, minerals such as calcite ($CaCO_3$) and/or siderite ($FeCO_3$) were amended in the sand capping layer to serve as a solid-phase pH buffering agent. Preliminary study on using these minerals as pH buffering agent shows that they only

have very limited buffering capacity at least in short term. A possible explanation for the poor level of pH control using the mineral buffer is the slow kinetics of dissolution in stagnant sediment/cap. Mineral dissolution can be surface-controlled if the adsorption of reactant to the mineral surface is rate-limiting or transport-controlled if detached species is transported from the surface and into the bulk solution most slowly (Furrer and Stumm, 1986). Some other geochemical reactions may also prevent or slow mineral dissolution. Many metal oxides and oxyhydroxides, including iron oxides (i.e., ferrihydrite, goethite, and hematite) may form in the environment as surface coatings (Nachtegaal and Sparks, 2004; Penn et al., 2001). Organic coatings may interfere with dissolution by changing the surface characteristics, forming inner-sphere complexes, modifying the electrical properties of the kaolinite−water interface and by masking the mineral surface from reactant adsorption (Nachtegaal and Sparks, 2003). The mechanism why these minerals failed to buffer pH remained unknown at this stage and the methods to improve the dissolution kinetics needs further investigations.

Appendix A: Supporting Information for Chapter 3

A.1 PCR AMPLIFICATION OF PAH DEGRADING GENES BY PAH-RHD$_A$ GRAM NEGATIVE PRIMER

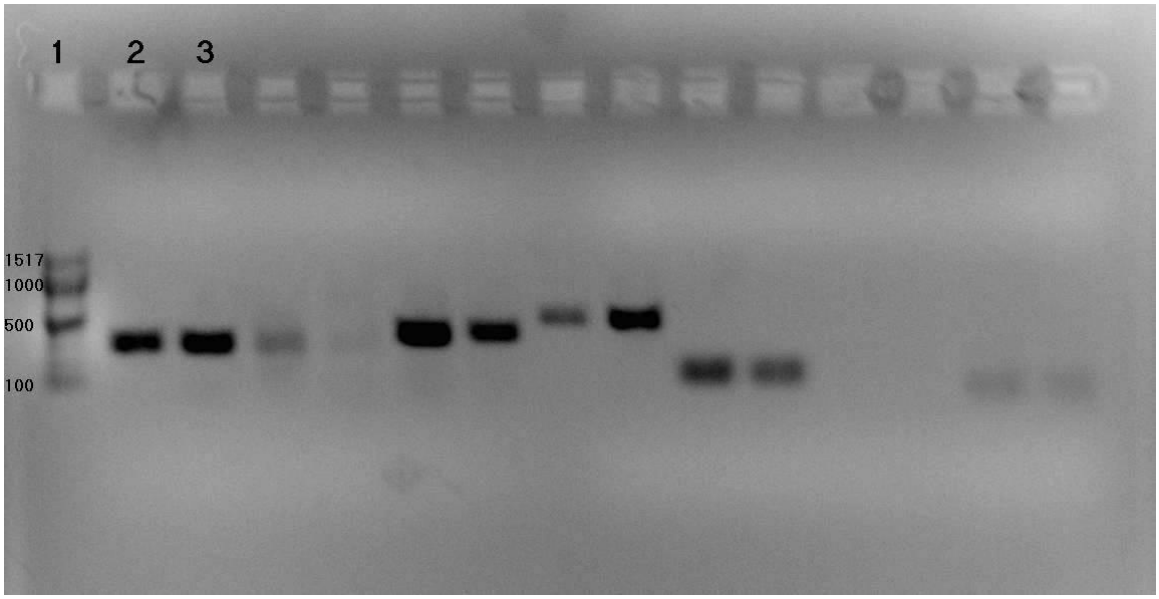

Figure A.1 Results of agarose gel electrophoresis of PCR amplicon by PAH-RHD$_\alpha$ Gram Negative (GN) primers. Lane 1 is 100bp ladder: the numbers on the left of each band represent base pairs of preload digested DNA fragments. Lane 2 and 3 are PCR amplicon (size = 306 bp) by PAH-RHD$_\alpha$ GN primer from Anacostia river sediment incubated with PAH. Bands at other lines are PCR amplicons using other primers.

Appendix B: Supporting Information for Chapter 4

B.1 Microcosm setup of PAH degradation and redox control experiments

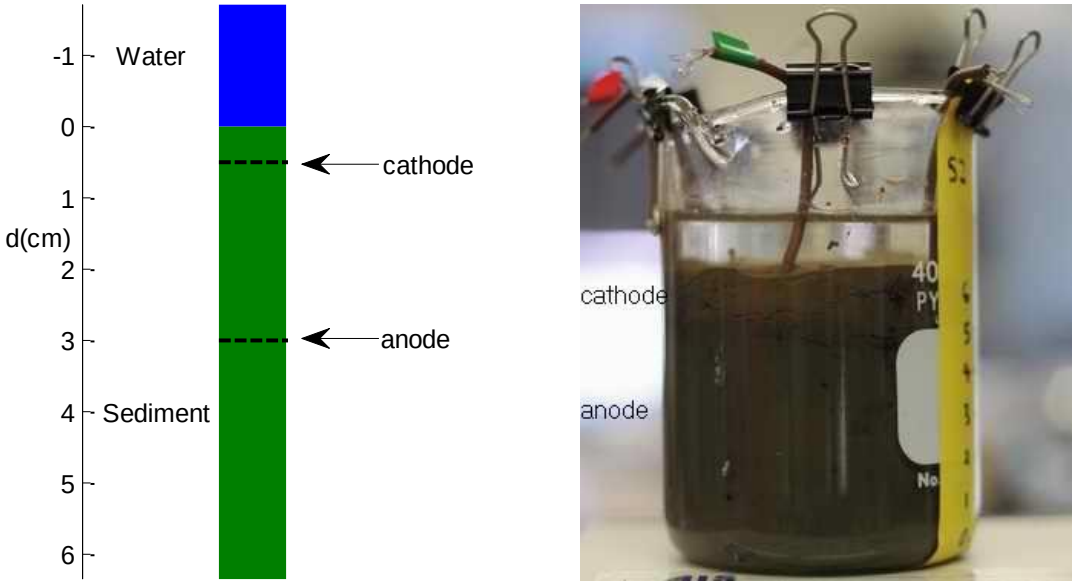

Figure B.1 Microcosm setup of PAH degradation and redox control in uncapped sediment by electrodes

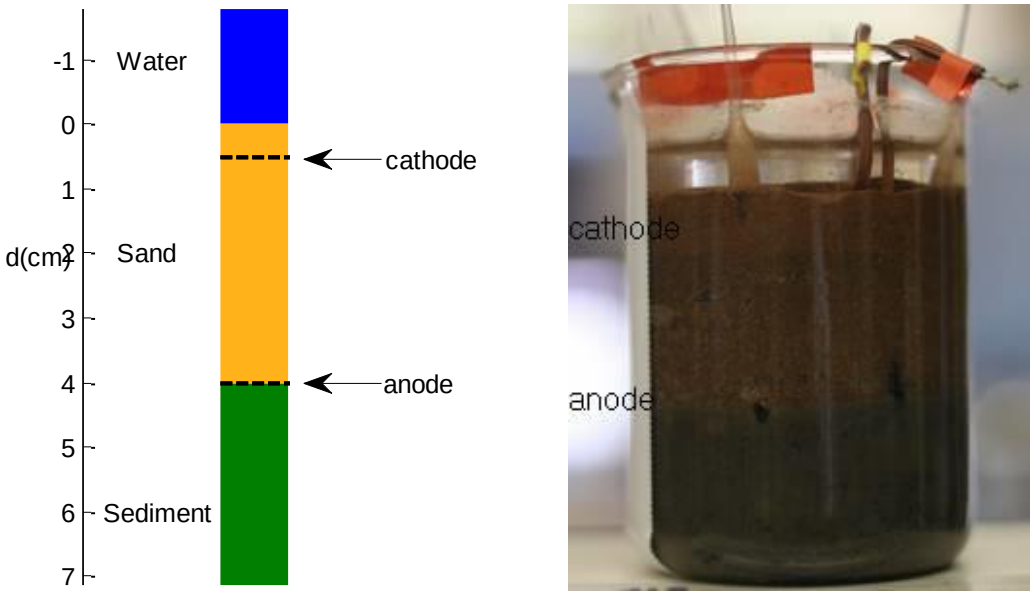

Figure B.2 Microcosm setup of PAH degradation and redox control in electrode enhanced sand caps

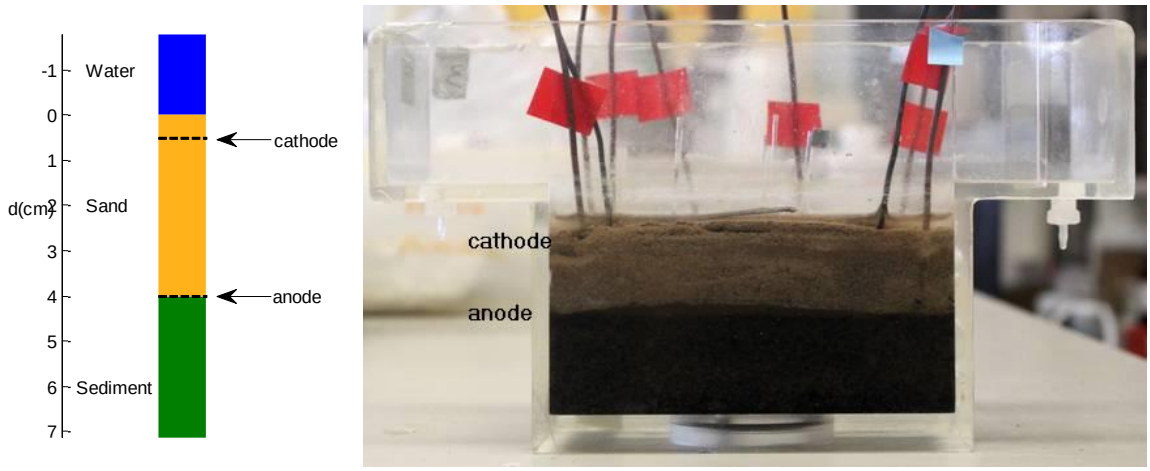

Figure B.3 Microcosm setup of PAH degradation and redox control in electrode enhanced caps with bicarbonate amendment

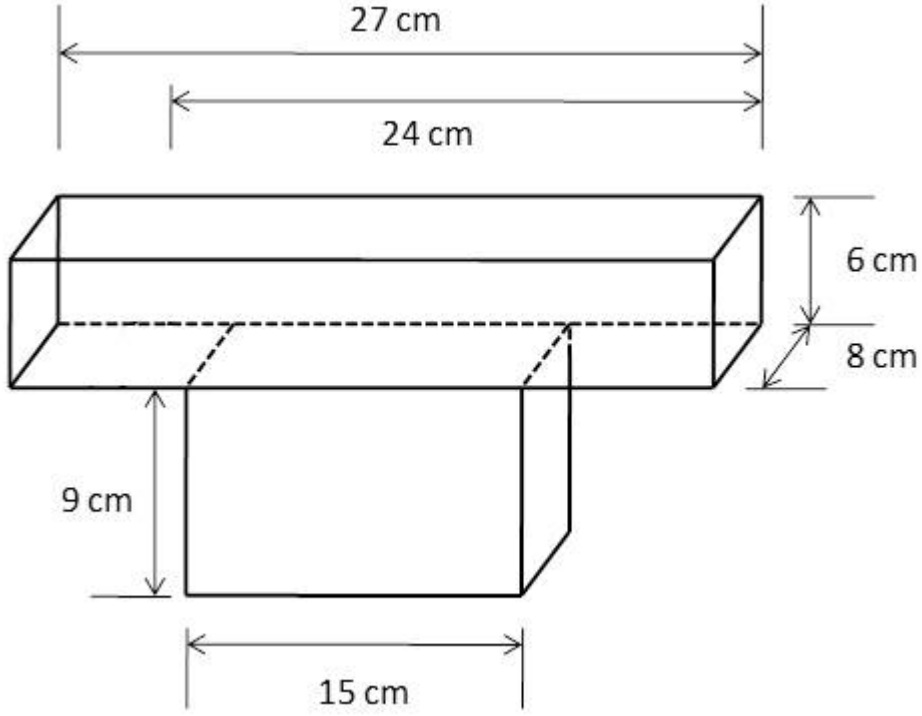

Figure B.4 T-shaped microcosm dimensions

B.2 UPTAKE KINETIC OF FIBER (210/230) FOR PHENANTHRENE

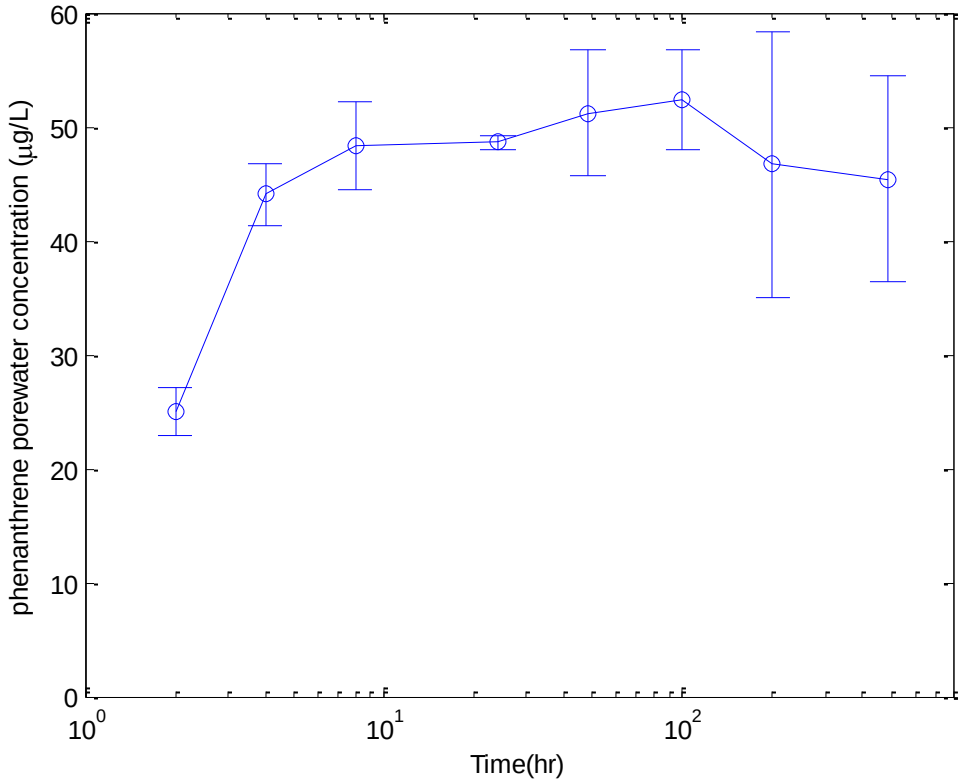

Figure B.5 Uptake kinetic of fiber (210/230) for phenanthrene. Points represent the mean of triplicate samples and error bars indicate standard deviation of triplicate data.

B.3 ORP AND pH PROFILES IN UNCAPPED SEDIMENT WITH ELECTRODES

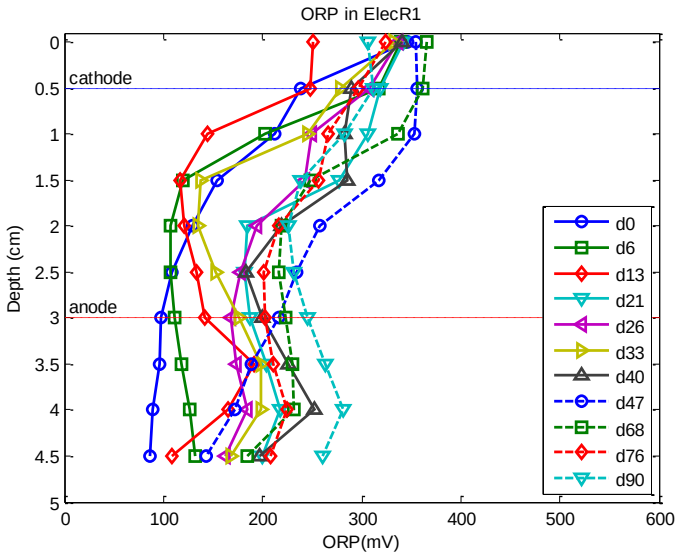

Figure B.6 Vertical profiles of ORP in ElecR1. ORP values were versus standard hydrogen electrode (SHE). Depth zero was the water-sediment interface. Cathode was at d = 0.5 cm and anode was at d = 3 cm.

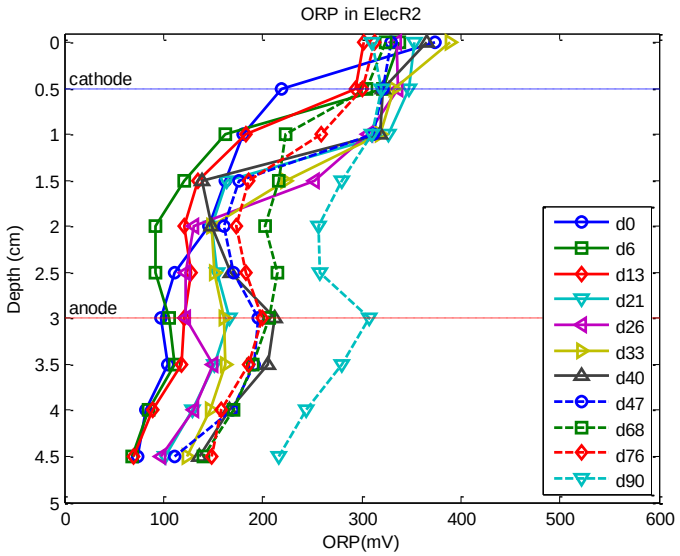

Figure B.7 Vertical profiles of ORP in ElecR2. ORP values were versus standard hydrogen electrode (SHE). Depth zero was the water-sediment interface. Cathode was at d = 0.5 cm and anode was at d = 3 cm.

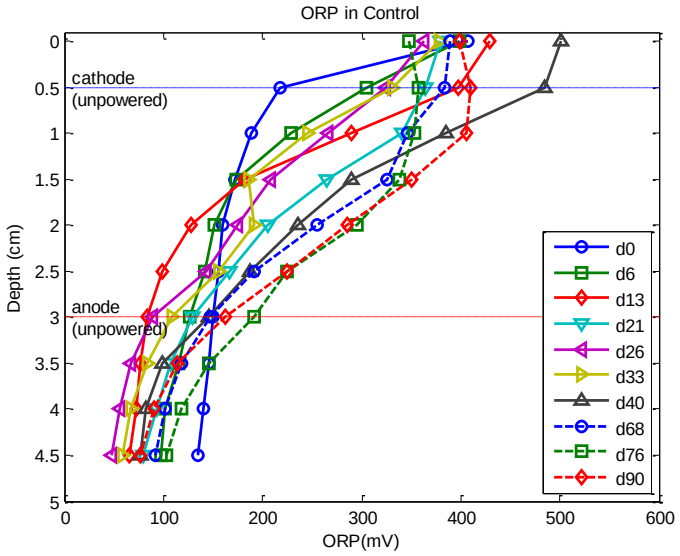

Figure B.8 Vertical profiles of ORP in Control. ORP values were versus standard hydrogen electrode (SHE). Depth zero was the water-sediment interface. Cathode was at d = 0.5 cm and anode was at d = 3 cm.

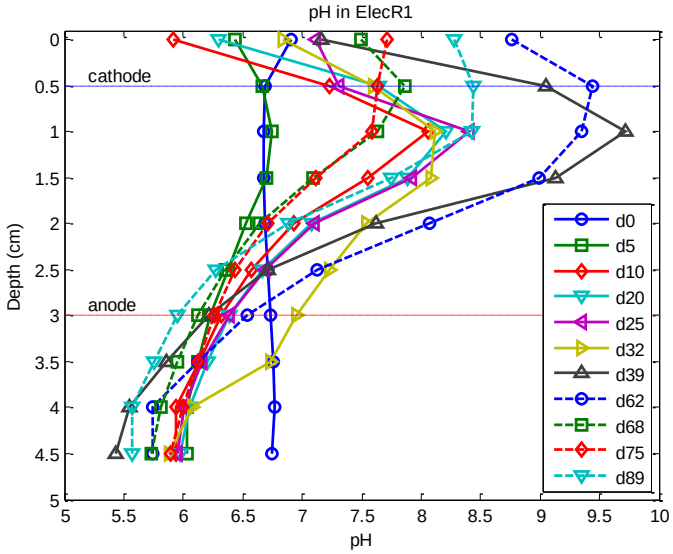

Figure B.9 Vertical profiles of pH in ElecR1. Depth zero was the water-sediment interface. Cathode was at d = 0.5 cm and anode was at d = 3 cm.

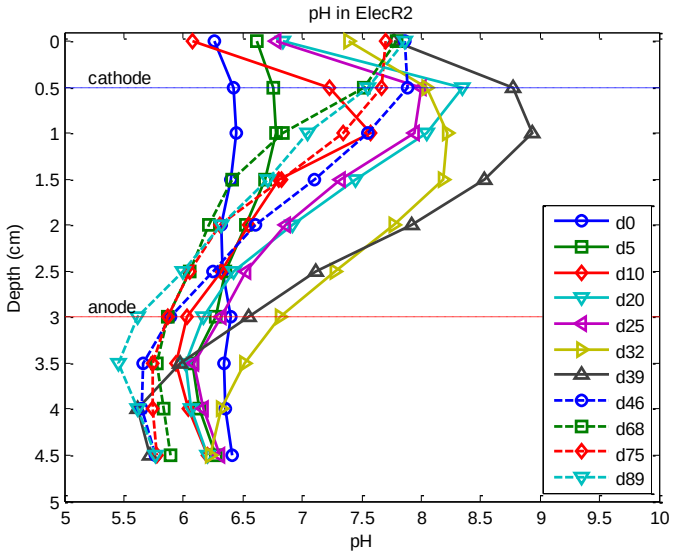

Figure B.10 Vertical profiles of pH in ElecR2. Depth zero was the water-sediment interface. Cathode was at d = 0.5 cm and anode was at d = 3 cm.

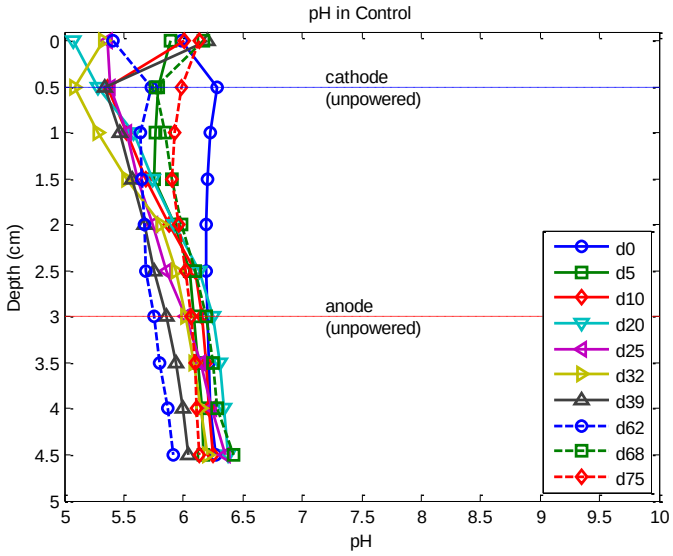

Figure B.11 Vertical profiles of pH in Control. Depth zero was the water-sediment interface. Cathode was at d = 0.5 cm and anode was at d = 3 cm.

B.4 PROFILES OF REDOX-SENSITIVE SPECIES IN UNCAPPED SEDIMENT WITH ELECTRODES

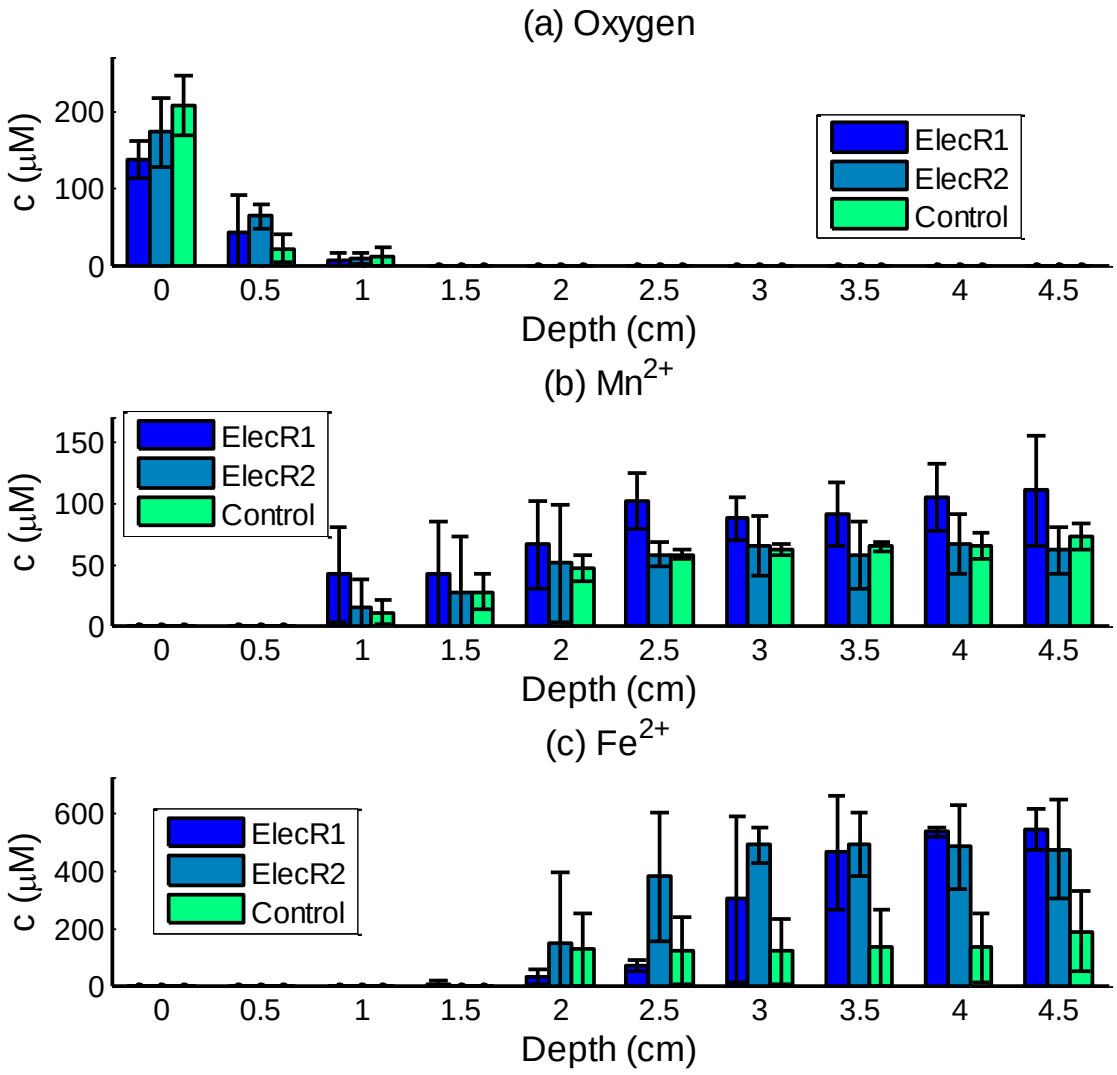

Figure B.12 Concentration of redox-sensitive species in ElecR1, ElecR2 and Control reactors: (a) Oxygen, (b) Mn^{2+} and (c) Fe^{2+}. Sulfide was not detected. Each point represents the mean of triplicate measurements from each electrode, and error bars represent standard deviations.

B.5 ORP AND pH PROFILES IN ELECTRODE ENHANCED SAND CAPS (NO BICARBONATE AMENDMENT)

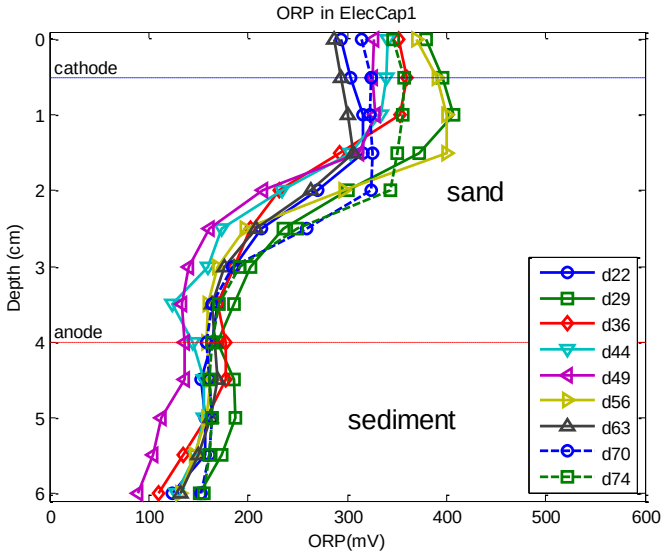

Figure B.13 Vertical profiles of ORP in ElecCap1. ORP values were versus standard hydrogen electrode (SHE). Depth zero was the water-cap interface. Cathode was at d = 0.5 cm and anode was at d = 4 cm.

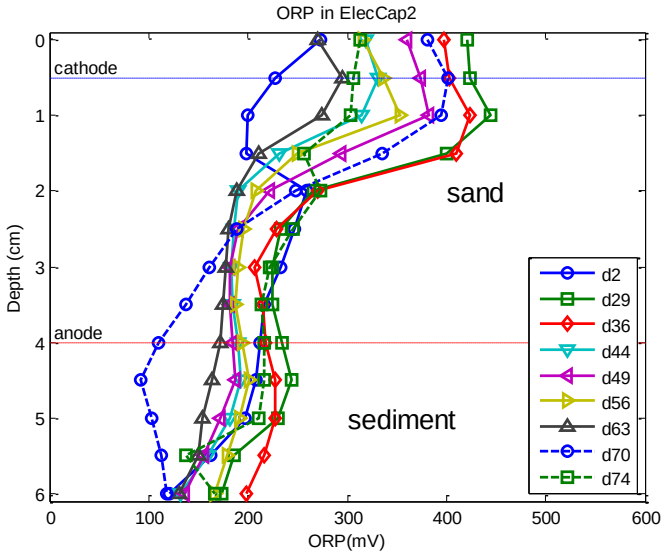

Figure B.14 Vertical profiles of ORP in ElecCap2. ORP values were versus standard hydrogen electrode (SHE). Depth zero was the water-cap interface. Cathode was at d = 0.5 cm and anode was at d = 4 cm.

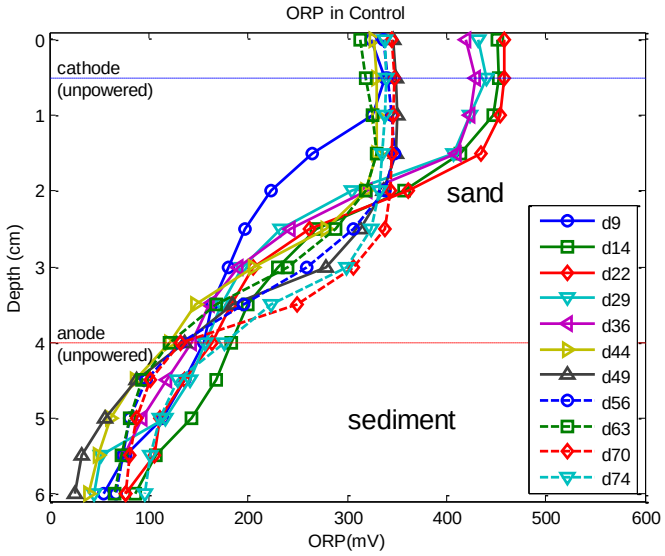

Figure B.15 Vertical profiles of ORP in Control. ORP values were versus standard hydrogen electrode (SHE). Depth zero was the water-cap interface. Cathode was at d = 0.5 cm and anode was at d = 4 cm.

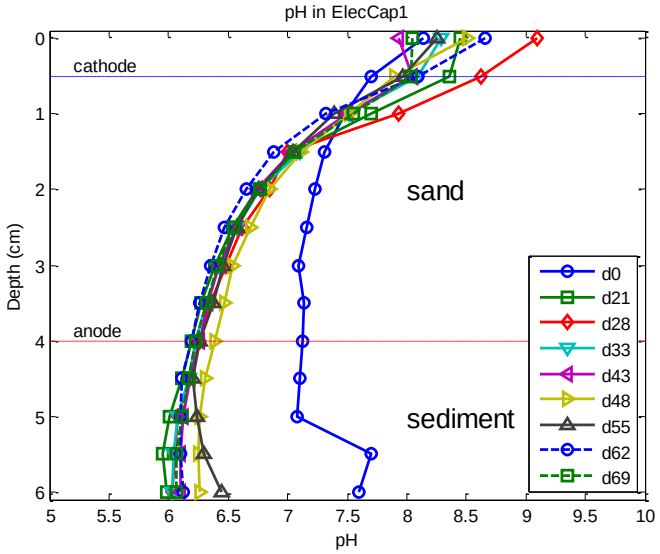

Figure B.16 Vertical profiles of pH in ElecCap1. Depth zero was the water-cap interface. Cathode was at d = 0.5 cm and anode was at d = 4 cm.

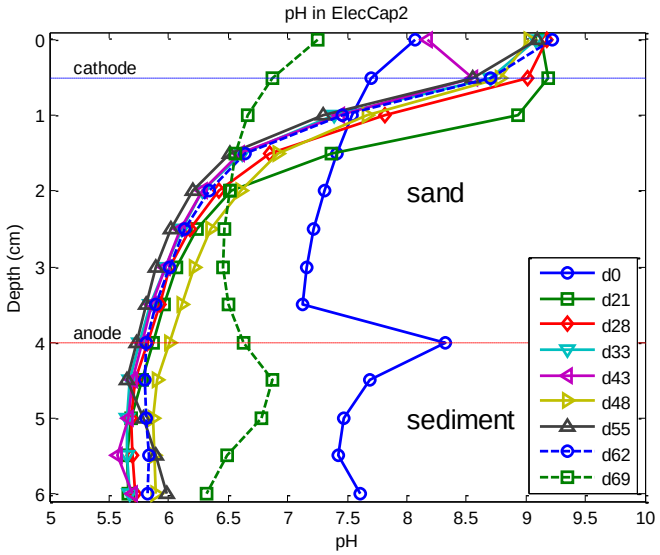

Figure B.17 Vertical profiles of pH in ElecCap2. Depth zero was the water-cap interface. Cathode was at d = 0.5 cm and anode was at d = 4 cm.

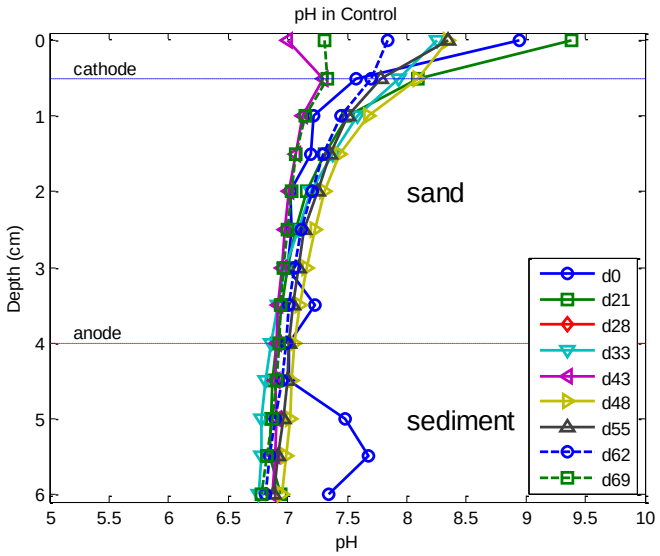

Figure B.18 Vertical profiles of pH in Control. Depth zero was the water-cap interface. Cathode was at d = 0.5 cm and anode was at d = 4 cm.

B.6 PROFILES OF REDOX-SENSITIVE SPECIES IN IN ELECTRODE ENHANCED SAND CAPS (NO BICARBONATE AMENDMENT)

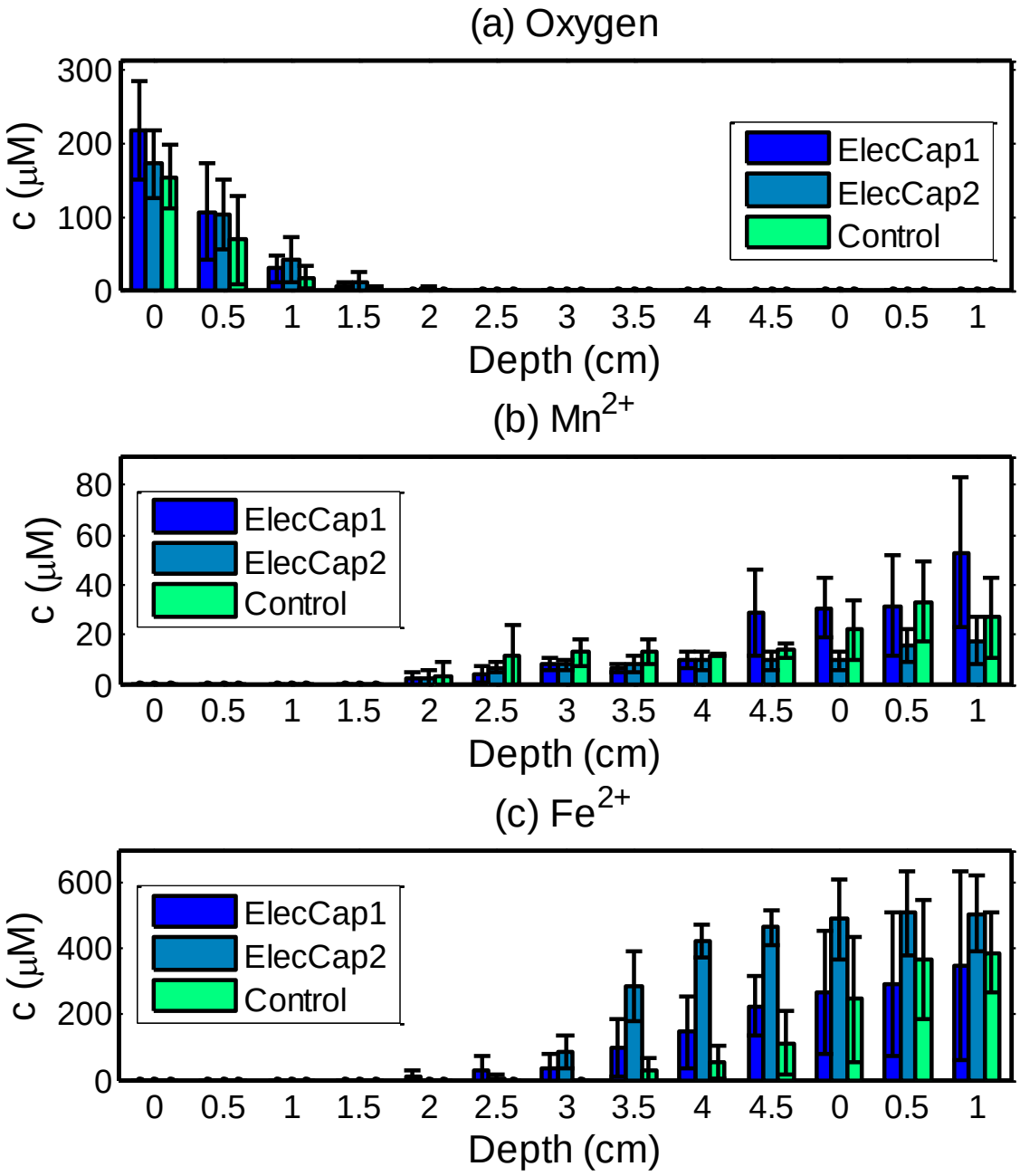

Figure B.19 Concentration of redox-sensitive species in ElecCap1, ElecCap2 and Control reactors: (a) Oxygen, (b) Mn^{2+} and (c) Fe^{2+}. Sulfide was not detected. Each point represents the mean of triplicate measurements from each electrode, and error bars represent standard deviations.

B.7 ORP AND pH PROFILES IN ELECTRODE ENHANCED CAPS WITH BICARBONATE AMENDMENT

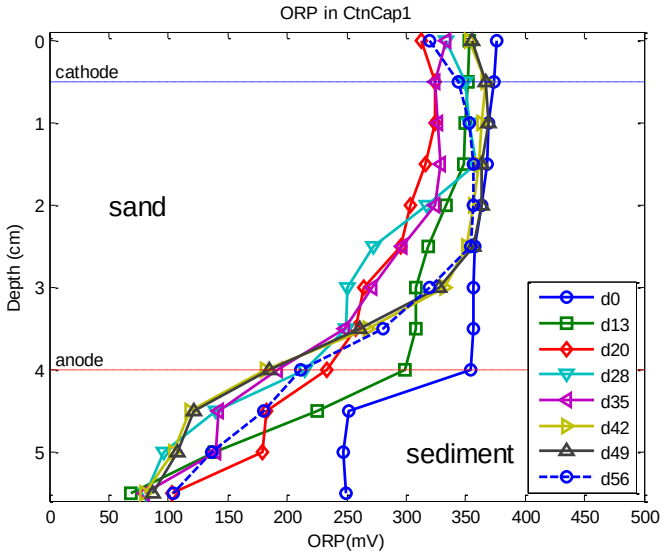

Figure B.20 Vertical profiles of ORP in CtnCap1. ORP values were versus standard hydrogen electrode (SHE). Depth zero was the water-cap interface. Cathode was at d = 0.5 cm and anode was at d = 4 cm.

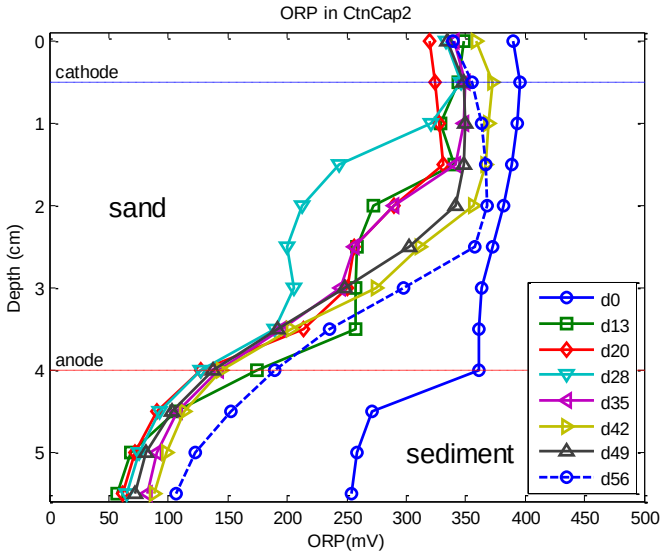

Figure B.21 Vertical profiles of ORP in CtnCap2. ORP values were versus standard hydrogen electrode (SHE). Depth zero was the water-cap interface. Cathode was at d = 0.5 cm and anode was at d = 4 cm.

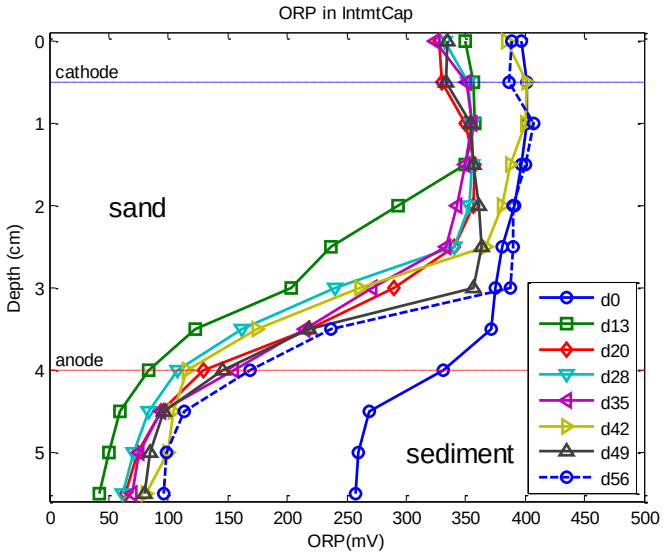

Figure B.22 Vertical profiles of ORP in IntmtCap. ORP values were versus standard hydrogen electrode (SHE). Depth zero was the water-cap interface. Cathode was at d = 0.5 cm and anode was at d = 4 cm.

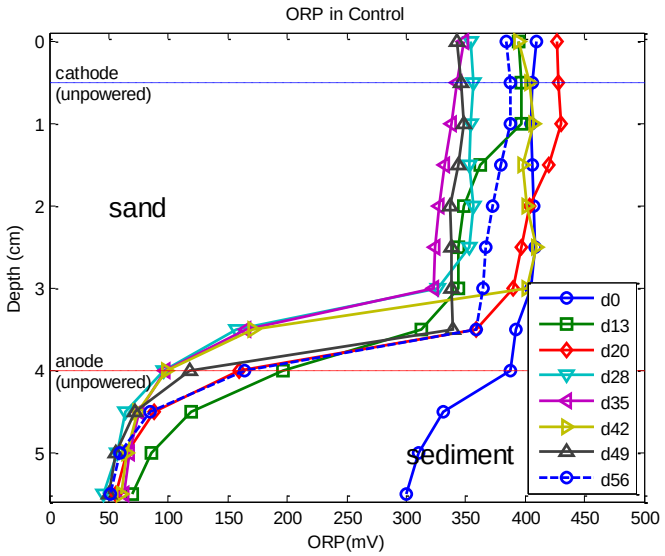

Figure B.23 Vertical profiles of ORP in Control. ORP values were versus standard hydrogen electrode (SHE). Depth zero was the water-cap interface. Cathode was at d = 0.5 cm and anode was at d = 4 cm.

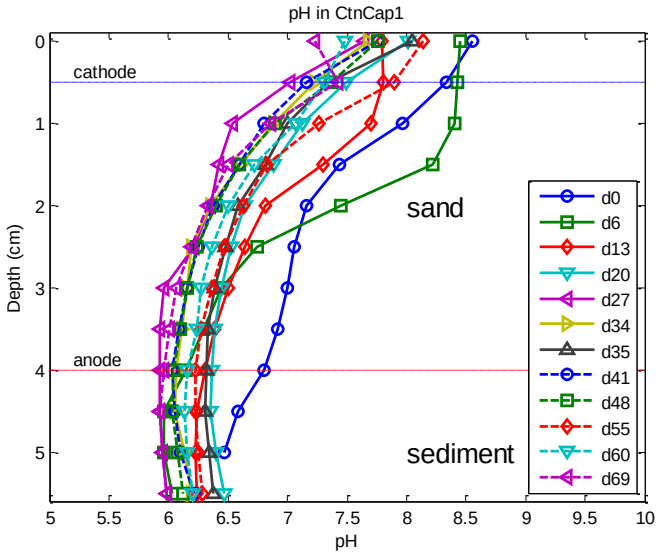

Figure B.24 Vertical profiles of pH in CtnCap1. Depth zero was the water-cap interface. Cathode was at d = 0.5 cm and anode was at d = 4 cm.

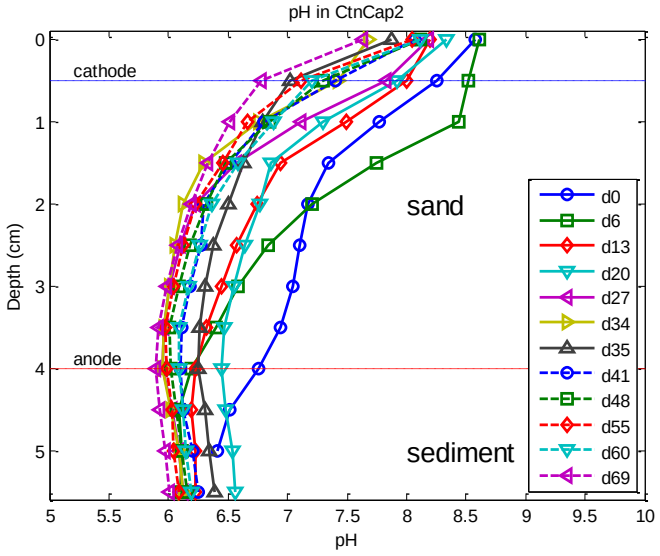

Figure B.25 Vertical profiles of pH in CtnCap2. Depth zero was the water-cap interface. Cathode was at d = 0.5 cm and anode was at d = 4 cm.

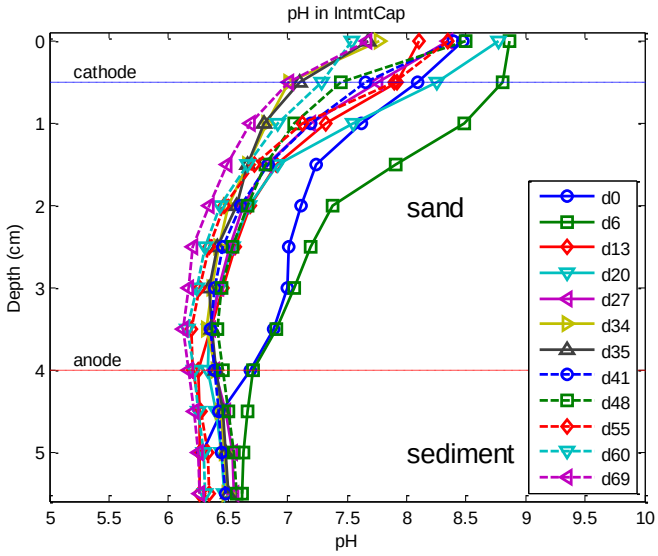

Figure B.26 Vertical profiles of pH in IntmtCap. Depth zero was the water-capinterface. Cathode was at d = 0.5 cm and anode was at d = 4 cm.

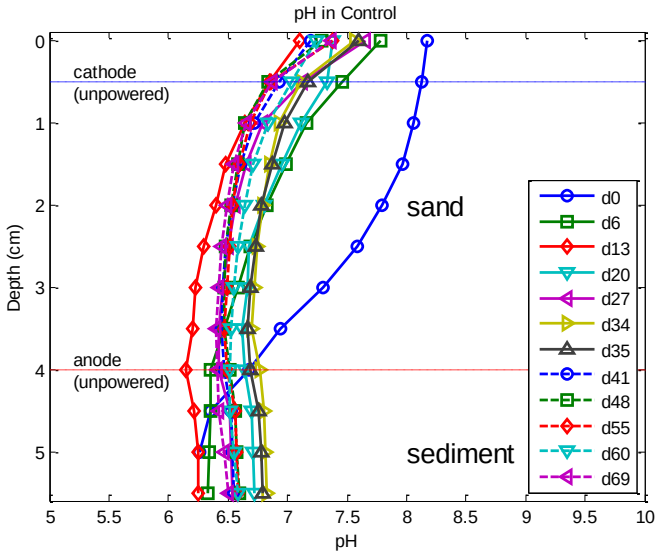

Figure B.27 Vertical profiles of pH in Control. Depth zero was the water-cap interface. Cathode was at d = 0.5 cm and anode was at d = 4 cm.

B.8 PROFILES OF REDOX-SENSITIVE SPECIES IN ELECTRODE ENHANCED CAPS WITH BICARBONATE AMENDMENT

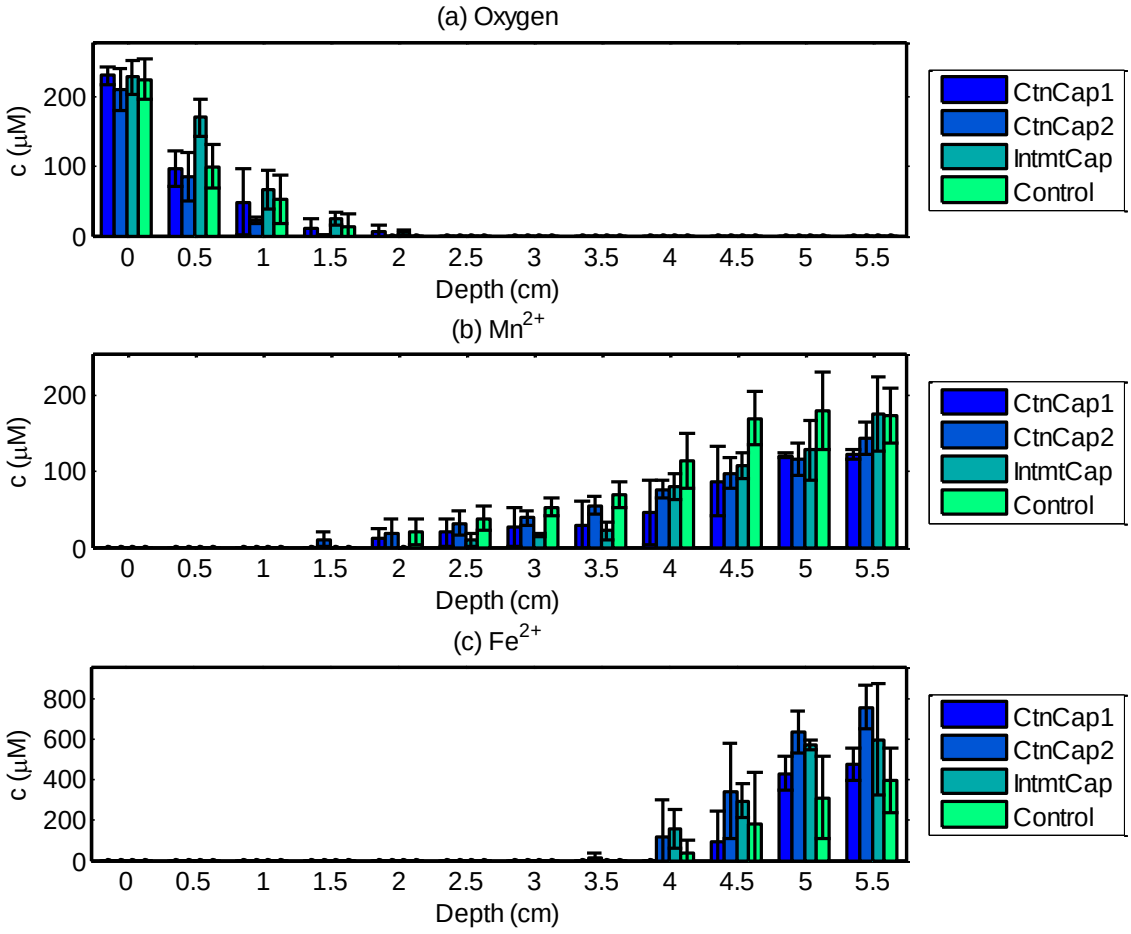

Figure B.28 Concentration of redox-sensitive species in CtnCap1, CtnCap2, IntmtCap and Control reactors: (a) Oxygen, (b) Mn^{2+} and (c) Fe^{2+}. Sulfide was not detected. Each point represents the mean of triplicate measurements from each electrode, and error bars represent standard deviations.

B.9 VOLTAGE AND CURRENT IN THE EXPERIMENT OF ELECTRODE ENHANCED CAPS WITH BICARBONATE AMENDMENT

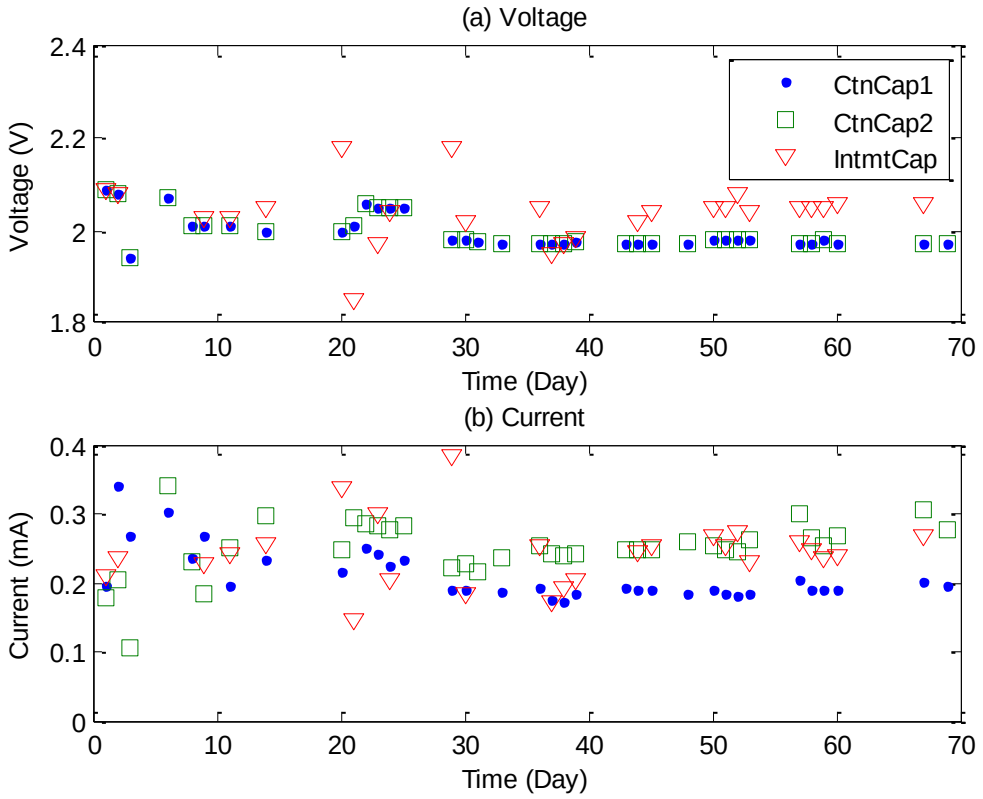

Figure B.29 Voltage and current in CtnCap1, CtnCap2 and IntmtCap reactors in the experiment of electrode enhanced capping with bicarbonate amendment.

Appendix C: Supporting Information for Chapter 5

C.1 Derivation of overpotential and current density relationship

Theoretically, the relationship between the current at the electrode and the overpotential follows Butler-Volmer expressions as follows (Newman and Thomas-Alyea, 2004):

$$I = Ai_0 \left[\exp\left(\alpha_a \frac{F}{RT}\eta\right) - \exp\left(-\alpha_c \frac{F}{RT}\eta\right)\right] \quad \text{(C-1)}$$

Where I is current, A is electrode active surface area, i_0 is exchange current density, F is Faraday constant, R is ideal gas constant, T is absolute temperature, η is overpotential, α_a and α_c are apparent transfer coefficients.

For large value of positive η, i.e. at the anode, the second term in Equation (C-1) is negligible.

$$\exp\left(\alpha_a \frac{F}{RT}\eta\right) \gg \exp\left(-\alpha_c \frac{F}{RT}\eta\right) \quad \text{(C-2)}$$

So Equation (C-1) becomes

$$I_A = Ai_0 \left[\exp\left(\alpha_a \frac{F}{RT}\eta_A\right)\right] \quad \text{(C-3)}$$

Or

$$\eta_A = \frac{RT}{\alpha_a F}[\ln(I_A) - \ln(Ai_0)] \quad \text{(C-4)}$$

Where I_A is current at the anode ($I_A > 0$), and η_A is overpotential at the anode ($\eta_A > 0$).

Similarly, for large value of negative η, i.e. at the cathode, the first term in Equation (C-1) is negligible, so Equation (C-1) becomes

$$I_C = -Ai_0\left[\exp\left(-\alpha_c \frac{F}{RT}\eta_C\right)\right] \tag{C-5}$$

Or

$$\eta_C = -\frac{RT}{\alpha_c F}[\ln(-I_C) - \ln(Ai_0)] \tag{C-6}$$

Where I_C is current at the cathode ($I_C < 0$), and η_C is overpotential at the cathode ($\eta_C < 0$).

The current at the anode has to match the current at the cathode, so $|I_A| = |I_C|$. Furthermore, assume both oxygen and hydrogen generation reactions have apparent transfer coefficients of 0.5 for α_a and α_c, then

$$|\eta_A| + |\eta_C| = \frac{2RT}{\alpha_a F} * [\ln(I_A) - \ln(Ai_0)] = a' + b' * \log_{10} I \tag{C-7}$$

Equation (C-7) is the simplified Tafel equation including both anode and cathode reactions.

References

Acar YB, Alshawabkeh AN. 1993. Principles of electrokinetic remediation. Environmental Science & Technology 27:2638-2647.

Acar YB, Gale RJ, Alshawabkeh AN, Marks RE, Puppala S, Bricka M, Parker R. 1995. Electrokinetic remediation - basics and technology status. Journal of Hazardous Materials 40:117-137.

Al-Hamdan AZ, Reddy KR. 2008. Electrokinetic remediation modeling incorporating geochemical effects. Journal of Geotechnical and Geoenvironmental Engineering 134:91-105.

Alshawabkeh AN, Acar YB. 1992. Removal of contaminants from soils by electrokinetics - a theoretical treatise. Journal of Environmental Science and Health Part a-Environmental Science and Engineering & Toxic and Hazardous Substance Control A27:1835-1861.

Alshawabkeh AN. 1994. Theoretical and experimental modeling of removing contaminants from soils by an electric field. (Doctoral dissertation). The Louisiana State University, Baton Rouge, LA.

Alshawabkeh AN, Acar YB. 1996. Electrokinetic remediation .2. Theoretical model. Journal of Geotechnical Engineering-Asce 122:186-196.

Alshawabkeh AN, Sarahney H. 2005. Effect of current density on enhanced transformation of naphthalene. Environmental Science & Technology 39:5837-5843.

Amann RI, Ludwig W, Schleifer KH. 1995. Phylogenetic identification and in-situ detection of individual microbial-cells without cultivation. Microbiological Reviews 59:143-169.

Annweiler E, Michaelis W, Meckenstock RU. 2002. Identical ring cleavage products during anaerobic degradation of naphthalene, 2-methylnaphthalene, and tetralin indicate a new metabolic pathway. Applied and Environmental Microbiology 68:852-858.

Archer D. 1996. A data-driven model of the global calcite lysocline. Global Biogeochemical Cycles 10:511-526.

Archie GE.1942. The Electrical resistivity log as an aid in determining some reservoir characteristics. Trans AIME 146: 54-62.

Atlas RM. 2010. Handbook of microbiological media. 4th Ed. CRC Press, Boca Raton, FL.

Baldwin BR, Nakatsu CH, Nebe J, Wickham GS, Parks C, Nies L. 2009. Enumeration of aromatic oxygenase genes to evaluate biodegradation during multi-phase

extraction at a gasoline-contaminated site. Journal of Hazardous Materials 163:524-530.

Baudo R, Muntau H. Lesser known in-place pollutants and diffuse source problems. In: Baudo R, Giesy JP, Muntau H(eds). Sediments: Chemistry and Toxicity of In-Place Pollutants. Lewis Publishers, Ann Arbor. pp1-14

Bard AJ, Faulkner LR. 2001. Electrochemical Methods: Fundamentals and Applications, 2nd ed..Wiley, New York.

Bauer JE, Capone DG. 1985. Degradation and mineralization of the polycyclic aromatic-hydrocarbons anthracene and naphthalene in intertidal marine-sediments. Applied and Environmental Microbiology 50:81-90.

Baumard P, Budzinski H, Michon Q, Garrigues P, Burgeot T, Bellocq J. 1998. Origin and bioavailability of PAHs in the Mediterranean sea from mussel and sediment records. Estuarine Coastal and Shelf Science 47:77-90.

Bender ML, Heggie DT. 1984. Fate of organic-carbon reaching the deep-sea floor - a status-report. Geochimica Et Cosmochimica Acta 48:977-986.

Boudreau BP. 1991. Modeling the sulfide-oxygen reaction and associated pH gradients in porewaters. Geochimica Et Cosmochimica Acta 55:145-159.

Boyd TJ, Montgomery MT, Steele JK, Pohlman JW, Reatherford SR, Spargo BJ, Smith DC. 2005. Dissolved oxygen saturation controls PAH biodegradation in freshwater estuary sediments. Microbial Ecology 49:226-235.

Brendel PJ, Luther GW. 1995. Development of a gold amalgam voltammetric microelectrode for the determination of dissolved Fe, Mn, O_2, and S(II) in porewaters of marine and fresh-water sediments. Environmental Science & Technology 29:751-761.

Brezna B, Khan AA, Cerniglia CE. 2003. Molecular characterization of dioxygenases from polycyclic aromatic hydrocarbon-degrading Mycobacterium spp. FEMS Microbiology Letters 223:177-183.

Burdige DJ. 2007. Preservation of organic matter in marine sediments: Controls, mechanisms, and an imbalance in sediment organic carbon budgets. Chemical Reviews 107:467-485.

Burnett WC, Bokuniewicz H, Huettel M, Moore WS, Taniguchi M. 2003. Groundwater and pore water inputs to the coastal zone. Biogeochemistry 66:3-33.

Cebron A, Norini MP, Beguiristain T, Leyval C. 2008. Real-Time PCR quantification of PAH-ring hydroxylating dioxygenase (PAH-RHD_α) genes from Gram positive and Gram negative bacteria in soil and sediment samples. Journal of Microbiological Methods 73:148-159.

Cerniglia CE. 1992. Biodegradation of polycyclic aromatic hydrocarbons. Biodegradation 3: 351-368.

Chang BV, Shiung LC, Yuan SY. 2002. Anaerobic biodegradation of polycyclic aromatic hydrocarbon in soil. Chemosphere 48:717-724.

Chen JL, Al-Abed S, Ryan J, Roulier M, Kemper M. 2002. Effects of electroosmosis on soil temperature and hydraulic head. II: Numerical simulation. Journal of Environmental Engineering-ASCE 128:596-603.

Chin DT, Cheng CY. 1985. Oxidation of phenol with ac electrolysis. Journal of the Electrochemical Society 132:2605-2611.

Choi H, Agarwal S, Al-Abed SR. 2009. Adsorption and Simultaneous Dechlorination of PCBs on GAC/Fe/Pd: Mechanistic Aspects and Reactive Capping Barrier Concept. Environmental Science & Technology 43:488-493.

Choi YS, Lui R. 1995. A mathematical-model for the electrokinetic remediation of contaminated soil. Journal of Hazardous Materials 44:61-75.

Chung WK, King GM. 2001. Isolation, characterization, and polyaromatic hydrocarbon degradation potential of aerobic bacteria from marine macrofaunal burrow sediments and description of Lutibacterium anuloederans gen. nov., sp nov., and Cycloclasticus spirillensus sp nov. Applied and Environmental Microbiology 67:5585-5592.

Cornelissen G, Pfttersen A, Broman D, Mayer P, Breedveld GD. 2008. Field testing of equilibrium passive samplers to determine freely dissolved native polycyclic aromatic hydrocarbon concentrations. Environmental Toxicology and Chemistry 27:499-508.

Dagher F, Deziel E, Lirette P, Paquette G, Bisaillon JG, Villemur R. 1997. Comparative study of five polycyclic aromatic hydrocarbon degrading bacterial strains isolated from contaminated soils. Canadian Journal of Microbiology 43:368-377.

Davies JI, Evans WC. 1964. Oxidative metabolism of naphthalene by soil pseudomonads. Biochem J 91: 251-261.

Das N, Chandran P. 2011. Microbial Degradation of Petroleum Hydrocarbon Contaminants: An Overview. Biotechnology Research International 2011, doi:10.4061/2011/941810.

Ding GC, Heuer H, Zuhlke S, Spiteller M, Pronk GJ, Heister K, Kogel-Knabner I, Smalla K. 2010. Soil Type-Dependent Responses to Phenanthrene as Revealed by Determining the Diversity and Abundance of Polycyclic Aromatic Hydrocarbon Ring-Hydroxylating Dioxygenase Genes by Using a Novel PCR Detection System. Applied and Environmental Microbiology 76:4765-4771.

Foght J. 2008. Anaerobic biodegradation of aromatic hydrocarbons: Pathways and prospects. Journal of Molecular Microbiology and Biotechnology 15:93-120.

Franz JA, Williams RJ, Flora JR, Meadows ME, Irwin WG. 2002. Electrolytic oxygen generation for subsurface delivery: effects of precipitation at the cathode and an assessment of side reactions. Water Research 36:2243-2254.

Friedman SP. 2005. Soil properties influencing apparent electrical conductivity: a review. Computers and Electronics in Agriculture 46:45-70.

Furrer G, Stumm W. 1986. A Coordination Chemical Approach to the Kinetics of Weathering: I. Dissolution of d-Al_2O_3 and BeO. Geochimica et Cosmochimica Acta 50: 1847-1860.

Gent DB, Wani AH, Davis JL, Alshawabkah A. 2009. Electrolytic Redox and Electrochemical Generated Alkaline Hydrolysis of Hexahydro-1,3,5-trinitro-1,3,5 triazine (RDX) in Sand Columns. Environmental Science & Technology 43:6301-6307.

Gibson DT, Subramanian V. 1984. Microbial degradation of aromatic hydrocarbons. In Microbial degradation of organic compounds. Marcel Dekker, New York. pp181-252.

Gidley PT, Kwon S, Yakirevich A, Magar VS, Ghosh U. 2012. Advection Dominated Transport of Polycyclic Aromatic Hydrocarbons in Amended Sediment Caps. Environmental Science & Technology 46:5032-5039.

Gilbert DM, Sale TC. 2005. Sequential electrolytic oxidation and reduction of aqueous phase energetic compounds. Environmental Science & Technology 39:9270-9277.

Goel RK, Flora JRV, Ferry J. 2003. Mechanisms for naphthalene removal during electrolytic aeration. Water Research 37:891-901.

Goldman R, Enewold L, Pellizzari E, Beach JB, Bowman ED, Krishnan SS, Shields PG. 2001. Smoking increases carcinogenic polycyclic aromatic hydrocarbons in human lung tissue. Cancer Research 61:6367-6371.

Gomes NCM, Borges LR, Paranhos R, Pinto FN, Krogerrecklenfort E, Mendonca-Hagler LCS, Smalla K. 2007. Diversity of ndo genes in mangrove sediments exposed to different sources of polycyclic aromatic hydrocarbon pollution. Applied and Environmental Microbiology 73:7392-7399.

Gregory KB, Bond DR, Lovley DR. 2004. Graphite electrodes as electron donors for anaerobic respiration. Environmental Microbiology 6:596-604.

Hambrick GA, Delaune RD, Patrick WH. 1980. Effect of estuarine sediment ph and oxidation-reduction potential on microbial hydrocarbon degradation. Applied and Environmental Microbiology 40:365-369.

Hamed J, Acar YB, Gale RJ. 1991. Pb(II) removal from kaolinite by electrokinetics. Journal of Geotechnical Engineering-Asce 117:241-271.

Haran BS, Popov BN, Zheng GH, White RE. 1997. Mathematical modeling of hexavalent chromium decontamination from low surface charged soils. Journal of Hazardous Materials 55:93-107.

Hart JK, Martinez K. 2006. Environmental Sensor Networks: A revolution in the earth system science? Earth-Science Reviews 78:177-191.

Hedlund BP, Staley JT. 2006. Isolation and characterization of Pseudoalteromonas strains with divergent polycyclic aromatic hydrocarbon catabolic properties. Environmental Microbiology 8:178-182.

Heitkamp MA, Cerniglia CE. 1987. Effects of chemical-structure and exposure on the microbial-degradation of polycyclic aromatic-hydrocarbons in fresh-water and estuarine ecosystems. Environmental Toxicology and Chemistry 6:535-546.

Hicks RE, Tondorf S. 1994. Electrorestoration of metal-contaminated soils. Environmental Science & Technology 28:2203-2210.

Himmelheber DW, Pennell KD, Hughes JB. 2011. Evaluation of a laboratory-scale bioreactive in situ sediment cap for the treatment of organic contaminants. Water Research 45:5365-5374.

Hong YS, Kinney KA, Reible DD. 2011. Acid volatile sulfides oxidation and metals (Mn, Zn) release upon sediment resuspension: laboratory experiment and model development. Environmental Toxicology and Chemistry 30:564-575.

Jacobs PH, Forstner U. 1999. Concept of subaqueous capping of contaminated sediments with active barrier systems (ABS) using natural and modified zeolites. Water Research 33:2083-2087.

Johnsen AR, de Lipthay JR, Reichenberg F, Sorensen SJ, Andersen O, Christensen P, Binderup ML, Jacobsen CS. 2006. Biodegradation, bioaccessibility, and genotoxicity of diffuse polycyclic aromatic hydrocarbon (PAH) pollution at a motorway site. Environmental Science & Technology 40:3293-3298.

Johnson K, Ghosh S. 1998. Feasibility of anaerobic biodegradation of PAHs in dredged river sediments. Water Science and Technology 38:41-48.

Johnston N, Sadler R, Shaw GR, Connell DW. 1993. Environmental modification of PAH composition in coal-tar containing samples. Chemosphere 27:1151-1158.

Jourabchi P, Van Cappellen P, Regnier P. 2005. Quantitative interpretation of pH distributions in aquatic sediments: A reaction-transport modeling approach. American Journal of Science 305:919-956.

Juhasz AL, Naidu R. 2000. Bioremediation of high molecular weight polycyclic aromatic hydrocarbons: a review of the microbial degradation of benzo[a] pyrene. International Biodeterioration & Biodegradation 45:57-88.

Juhasz AL, Stanley GA, Britz ML. 2000. Microbial degradation and detoxification of high molecular weight polycyclic aromatic hydrocarbons by Stenotrophomonas maltophilia strain VUN 10,003. Letters in Applied Microbiology 30:396-401.

Kanaly RA, Harayama S. 2000. Biodegradation of high-molecular-weight polycyclic aromatic hydrocarbons by bacteria. Journal of Bacteriology 182:2059-2067.

Kaplan DI, Knox AS. 2004. Enhanced contaminant desorption induced by phosphate mineral additions to sediment. Environmental Science & Technology 38:3153-3160.

Kastner M, Breuer-Jammali M, Mahro B. 1998. Impact of inoculation protocols, salinity, and pH on the degradation of polycyclic aromatic hydrocarbons (PAHs) and survival of PAH-degrading bacteria introduced into soil. Applied and Environmental Microbiology 64:359-362.

Kastner M, Breuerjammali M, Mahro B. 1994. Enumeration and characterization of the soil microflora from hydrocarbon-contaminated soil sites able to mineralize polycyclic aromatic-hydrocarbons (PAH). Applied Microbiology and Biotechnology 41:267-273.

Knox AS, Paller MH, Roberts J. 2012. Active Capping Technology - New Approaches for In Situ Remediation of Contaminated Sediments. Remediation 22: 93-117

Lageman R. 1993. Electroreclamation. Environmental Science & Technology 27:2648-2650.

Lampert DJ. 2010. An Assessment of the Design of In Situ Management Approaches for Contaminated Sediments. (Doctoral dissertation). The University of Texas at Austin, Austin, TX.

Lampert DJ, Sarchet WV, Reible DD. 2011. Assessing the Effectiveness of Thin-Layer Sand Caps for Contaminated Sediment Management through Passive Sampling. Environmental Science & Technology 45:8437-8443.

Laurie AD, Lloyd-Jones G. 1999. The phn genes of Burkholderia sp. strain RP007 constitute a divergent gene cluster for polycyclic aromatic hydrocarbon catabolism. Journal of Bacteriology 181:531-540.

Leduc R, Samson R, Albashir B, Alhawari J, Cseh T. 1992. Biotic and abiotic disappearance of 4 PAH compounds from flooded soil under various redox conditions. Water Science and Technology 26:51-60.

Li ZM, Yu JW, Neretnieks I. 1997. Removal of Pb(II), Cd(II) and Cr(III) from sand by electromigration. Journal of Hazardous Materials 55:295-304.

Lloyd-Jones G, Laurie AD, Hunter DWF, Fraser R. 1999. Analysis of catabolic genes for naphthalene and phenanthrene degradation in contaminated New Zealand soils. FEMS Microbiology Ecology 29:69-79.

Lofts S, Woof C, Tipping E, Clarke N, Mulder J. 2001. Modelling pH buffering and aluminium solubility in European forest soils. European Journal of Soil Science 52:189-204.

Logan BE. 2009. Exoelectrogenic bacteria that power microbial fuel cells. Nature Reviews Microbiology 7:375-381.

Lovley DR. 2008. The microbe electric: conversion of organic matter to electricity. Current Opinion in Biotechnology 19:564-571.

Lu XX, Reible DD, Fleeger JW. 2006. Bioavailability of polycyclic aromatic hydrocarbons in field-contaminated Anacostia River (Washington, DC) sediment. Environmental Toxicology and Chemistry 25:2869-2874.

Lu XX, Skwarski A, Drake B, Reible DD. 2011. Predicting bioavailability of PAHs and PCBs with porewater concentrations measured by solid-phase microextraction fibers. Environmental Toxicology and Chemistry 30:1109-1116.

Luther GW, Reimers CE, Nuzzio DB, Lovalvo D. 1999. In situ deployment of voltammetric, potentiometric. and amperometric microelectrodes from a ROV to determine dissolved O_2, Mn, Fe, S(-2), and pH in porewaters. Environmental Science & Technology 33:4352-4356.

Mastrangelo G, Fadda E, Marzia V. 1996. Polycyclic aromatic hydrocarbons and cancer in man. Environmental Health Perspectives 104:1166-1170.

Mayer P, Vaes WHJ, Wijnker F, Legierse K, Kraaij RH, Tolls J, Hermens JLM. 2000. Sensing dissolved sediment porewater concentrations of persistent and bioaccumulative pollutants using disposable solid-phase microextraction fibers. Environmental Science & Technology 34:5177-5183.

McCoy CA, Corbett DR. 2009. Review of submarine groundwater discharge (SGD) in coastal zones of the Southeast and Gulf Coast regions of the United States with management implications. Journal of Environmental Management 90:644-651.

McDonough KM, Murphy P, Olsta J, Zhu Y, Reible D, Lowry GV. 2007. Development and placement of a sorbent-amended thin layer sediment cap in the Anacostia River. Soil & Sediment Contamination 16:313-322.

Menzie CA, Potocki BB, Santodonato J. 1992. Exposure to carcinogenic PAHs in the environment. Environmental Science & Technology 26:1278-1284.

Mihelcic JR, Luthy RG. 1988. Degradation of polycyclic aromatic hydrocarbon compounds under various redox conditions in soil-water systems. Applied and Environmental Microbiology 54:1182-1187.

Mueller JG, Chapman PJ, Pritchard PH. 1989. Creosote-contaminated sites - their potential for bioremediation. Environmental Science & Technology 23:1197-1201.

Murphy P, Marquette A, Reible D, Lowry GV. 2006. Predicting the performance of activated carbon-, coke-, and soil-amended thin layer sediment caps. Journal of Environmental Engineering-Asce 132:787-794.

Nachtegaal M, Sparks DL. 2003. Nickel sequestration in a kaolinite-humic acid complex. Environmental Science & Technology 37:529-534.

Nachtegaal M, Sparks DL. 2004. Effect of iron oxide coatings on zinc sorption mechanisms at the clay-mineral/water interface. Journal of Colloid and Interface Science 276:13-23.

Nakamura A, Hirano K, Iji M. 2005. Decomposition of trichlorobenzene with different radicals generated by alternating current electrolysis in aqueous solution. Chemistry Letters 34:802-803.

Newman J, Thomas-Alyea KE. 2004. Electrochemical Systems, 3rd ed., John Wiley & Sons, New York.

Page DS, Boehm PD, Douglas GS, Bence AE, Burns WA, Mankiewicz PJ. 1999. Pyrogenic polycyclic aromatic hydrocarbons in sediments record past human activity: A case study in Prince William Sound, Alaska. Marine Pollution Bulletin 38:247-260.

Palermo M, Maynord S, Miller J, Reible D. 1998. Guidance for In-Situ Subaqueous Capping of Contaminated Sediments," EPA 905-B96-004, Great Lakes National Program Office, Chicago, IL.

Park H, Vecitis CD, Hoffmann MR. 2008. Solar-powered electrochemical oxidation of organic compounds coupled with the cathodic production of molecular hydrogen. Journal of Physical Chemistry A 112:7616-7626.

Penn RL, Zhu C, Xu H, Veblen DR. 2001. Iron oxide coatings on sand grains from the Atlantic coastal plain: High-resolution transmission electron microscopy characterization. Geology 29:843-846.

Perelo LW. 2010. Review: In situ and bioremediation of organic pollutants in aquatic sediments. Journal of Hazardous Materials 177:81-89.

Petersen MA, Sale TC, Reardon KF. 2007. Electrolytic trichloroethene degradation using mixed metal oxide coated titanium mesh electrodes. Chemosphere 67:1573-1581.

Pletcher D, Walsh FC. 1990. Industrial Electrochemistry. Chanpmand and Hall Ltd, New York.

Probstein RF. 1989. Physicochemical Hydrodynamics.Wiley, New York.

Probstein RF, Hicks RE. 1993. REMOVAL OF CONTAMINANTS FROM SOILS BY ELECTRIC-FIELDS. Science 260:498-503.

Reddy KR, Parupudi US. 1997. Removal of chromium, nickel and cadmium from clays by in-situ electrokinetic remediation. Journal of Soil Contamination 6:391-407.

Reible D, Hayes D, Lue-Hing C, Patterson J, Bhowmik N, Johnson M, Teal J. 2003. Comparison of the long-term risks of removal and in situ management of contaminated sediments in the Fox River. Soil & Sediment Contamination 12:325-344.

Reible D. 2004. Cost and Feasibility of Conventional and Active Sediment Capping. Presented at the Technology Benchmarking Workshop For Sediment and Floodplain Remediation, Ann Arbor, MI, March 25-26.

Reible DD, Lu XX, Blishke H. 2005. Organoclay for the Control of NAPLs in Sediments. Society of Environmental Toxicology and Chemistry 26th Annual Meeting, Baltimore, MD.

Reible DD, Lambert D, Constant DW, Mutch RD, Zhu Y. 2007. Active capping demonstration in the Anacostia River, Washington, DC. Remediation 17: 39-53.

Renaud PC, Probstein RF. 1987. Electroosmotic control of hazardous wastes. Physicochemical Hydrodynamics 9:345-360.

Rockne KJ, Chee-Sanford JC, Sanford RA, Hedlund BP, Staley JT, Strand SE. 2000. Anaerobic naphthalene degradation by microbial pure cultures under nitrate-reducing conditions. Applied and Environmental Microbiology 66:1595-1601.

Rockne KJ, Strand SE. 1998. Biodegradation of bicyclic and polycyclic aromatic hydrocarbons in anaerobic enrichments. Environmental Science & Technology 32:3962-3967.

Rockne KJ, Strand SE. 2001. Anaerobic biodegradation of naphthalene, phenanthrene, and biphenyl by a denitrifying enrichment culture. Water Research 35:291-299.

Rothermich MM, Hayes LA, Lovley DR. 2002. Anaerobic, sulfate-dependent degradation of polycyclic aromatic hydrocarbons in petroleum-contaminated harbor sediment. Environmental Science & Technology 36:4811-4817.

Sabate J, Grifoll M, Vinas M, Solanas AM. 1999. Isolation and characterization of a 2-methylphenanthrene utilizing bacterium: identification of ring cleavage metabolites. Applied Microbiology and Biotechnology 52:704-712.

Saichek RE, Reddy KR. 2005. Electrokinetically enhanced remediation of hydrophobic organic compounds in soils: A review. Critical Reviews in Environmental Science and Technology 35:115-192.

Sakakibara Y, Nakayama T. 2001. A novel multi-electrode system for electrolytic and biological water treatments: Electric charge transfer and application to denitrification. Water Research 35:768-778.

Schafer AI, Broeckmann A, Richards BS. 2007. Renewable energy powered membrane technology. 1. Development and characterization of a photovoltaic hybrid membrane system. Environmental Science & Technology 41:998-1003.

Shapiro AP, Probstein RF. 1993. Removal of contaminants from saturated clay by electroosmosis. Environmental Science & Technology 27:283-291.

Shapiro AP, Renaud PC, Probstein RF. 1989. Preliminary studies on the removal of chemical-species from saturated porous-media by electroosmosis. Physicochemical Hydrodynamics 11:785-802.

Shennan, JL. 1984. Hydrocarbons as substrates in industrial fermentation. In Petroleum Microbiology Atlas. Macmillan R.M.ed. pp. 643-683.

Shuttleworth KL, Cerniglia CE. 1995. Environmental aspects of PAH biodegradation. Applied Biochemistry and Biotechnology 54:291-302.

Sparks DL. 1996, Methods of soil analysis. Part 3, Chemical methods. Soil Science society of America and Ameican Society of Agronomy, Madison, WI 53711.

Stumm W, Morgan JJ. 1996. Aquatic Chemistry, 3rd ed. John Wiley & Sons, New York.

Sun HW, Xu XY, Gao GD, Zhang ZZ, Yin PJ. 2010. A novel integrated active capping technique for the remediation of nitrobenzene-contaminated sediment. Journal of Hazardous Materials 182:184-190.

Sun M, Yan F, Zhang RL, Reible DD, Lowry GV, Gregory KB. 2010. Redox Control and Hydrogen Production in Sediment Caps Using Carbon Cloth Electrodes. Environmental Science & Technology 44:8209-8215.

Suni S, Romantschuk M. 2004. Mobilisation of bacteria in soils by electro-osmosis. FEMS Microbiology Ecology 49:51-57.

Thibodeaux LJ, Bosworth WS. 1990. A Theoretical Evaluation of the Effectiveness of Capping PCB Contaminated New Bedford Harbor Bed Sediment, Final Report. Hazardous Waste Research Center, Louisiana State University, Baton Rouge, LA.

Thoma GJ, Reible DD, Valsaraj KT, Thibodeaux LJ. 1993. Efficiency of capping contaminated sediments in-situ .2. Mathematics of diffusion adsorption in the capping layer. Environmental Science & Technology 27:2412-2419.

Thrash JC, Van Trump JI, Weber KA, Miller E, Achenbach LA, Coates JD. 2007. Electrochemical stimulation of microbial perchlorate reduction. Environmental Science & Technology 41:1740-1746.

Tipping E. 1998. Humic ion-binding model VI: An improved description of the interactions of protons and metal ions with humic substances. Aquatic Geochemistry 4:3-48.

Tipping E, Hurley MA. 1988. A model of solid-solution interactions in acid organic soils, based on the complexation properties of humic substances. Journal of Soil Science 39:505-519.

US DOE. 2011. Energy savers - How small solar electric systems work. February 2011

US EPA. 1998. Contaminated Sediment Management Strategy, Office of Water, EPA-823-R-98-001.

US EPA. 2005. Contaminated Sediment Remediation Guidance for Hazardous Waste Sites, Office of Solid Waste and Emergency Response, EPA-540-R05-012.

US EIA. 2012. Electric Power Monthly June 2012. U.S. Energy Information Administration, Office of Electricity, Renewables & Uranium Statistics, U.S. Department of Energy, Washington, DC.

VanCappellen P, Wang YF. 1996. Cycling of iron and manganese in surface sediments: A general theory for the coupled transport and reaction of carbon, oxygen, nitrogen, sulfur, iron, and manganese. American Journal of Science 296:197-243.

Wang XQ, Thibodeaux LJ, Valsaraj KT, Reible DD. 1991. Efficiency of capping contaminated bed sediments in situ .1. Laboratory-scale experiments on diffusion adsorption in the capping layer. Environmental Science & Technology 25:1578-1584.

Watanabe T, Hashimoto S, Kuroda M. 2002. Simultaneous nitrification and denitrification in a single reactor using bio-electrochemical process. Water Science and Technology 46:163-169.

Widada J, Nojiri H, Kasuga K, Yoshida T, Habe H, Omori T. 2002. Molecular detection and diversity of polycyclic aromatic hydrocarbon-degrading bacteria isolated from geographically diverse sites. Applied Microbiology and Biotechnology 58:202-209.

Wilson MS, Bakermans C, Madsen EL. 1999. In situ, real-time catabolic gene expression: Extraction and characterization of naphthalene dioxygenase mRNA transcripts from groundwater. Applied and Environmental Microbiology 65:80-87.

Wilson SC, Jones KC. 1993. Bioremediation of soil contaminated with polynuclear aromatic-hydrocarbons (PAHs) - a review. Environmental Pollution 81:229-249.

Yeung AT, Datla S. 1996. Fundamental formulation of electrokinetic extraction of contaminants from soil: Reply. Canadian Geotechnical Journal 33:682-684.

Yu JW, Neretnieks I. 1996. Modelling of transport and reaction processes in a porous medium in an electrical field. Chemical Engineering Science 51:4355-4368.

Zeebe RE. 2007. Modeling CO_2 chemistry, delta C-13, and oxidation of organic carbon and methane in sediment porewater: Implications for paleo-proxies in benthic foraminifera. Geochimica Et Cosmochimica Acta 71:3238-3256.

Zeebe RE, Sanyal A. 2002. Comparison of two potential strategies of planktonic foraminifera for house building: Mg^{2+} or H^{+} removal. Geochimica Et Cosmochimica Acta 66:1159-1169.

Zhang T, Gannon SM, Nevin KP, Franks AE, Lovley DR. 2010. Stimulating the anaerobic degradation of aromatic hydrocarbons in contaminated sediments by providing an electrode as the electron acceptor. Environmental Microbiology 12:1011-1020.

Zimmerman JR, Ghosh U, Millward RN, Bridges TS, Luthy RG. 2004. Addition of carbon sorbents to reduce PCB and PAH bioavailability in marine sediments: Physicochemical tests. Environmental Science & Technology 38:5458-5464.

Vita

Fei Yan was born in Shanxi, China and attended high school in Taiyuan, Shanxi, China. He received the degrees of Bachelor and Master from Tsinghua University, and received the degree of Master of Engineering from the University of Florida. In 2007, he entered the Graduate School at The University of Texas at Austin.

Permanent Address: Taiyuan, Shanxi, China

This manuscript was typed by the author.